Mechatronic, electrical energy, and dynamic systems (MEED)
Institute of Mechanics, Materials and Civil Engineering (iMMC)
Université Catholique de Louvain (UCL)

Autonomous microgrids for rural electrification: joint investment planning of power generation and distribution through convex optimization

Benoît Martin
Electromechanical Engineer

Thesis submitted in partial fulfillment of the requirements
for the degree of Doctor in Engineering Sciences

7 February 2018

Jury

Pr.	T. Pardoen	UCL - iMMC	President
Pr.	E. De Jaeger	UCL - iMMC	Supervisor
Pr.	F. Glineur	UCL - ICTEAM	Supervisor
Pr.	F. Vallée	UMONS	
Pr.	A. Papavasiliou	UCL - IMMAQ	
Pr.	F. Pilo	UNICA (Italy)	
Dr.	E. Haesen	Ecofys	
Dr.	N. Leemput	Tractebel Engie	

Acknowledgements

No one can whistle a symphony. It takes a whole orchestra to play it
– H.E. Luccock

A PhD thesis is often seen as solitary work, however this is only partly true. Even though I had to steer my ship during these four years, I could count on numerous persons who acted as lighthouses that helped me find my way throughout this journey. Not only would this work have been more limited without their help, but it would also have been boring and burdensome. I wish to thank them all for the valuable exchange on a technical as well as personal level.

First, I want to express my gratitude to my two supervisors, Emmanuel De Jaeger and François Glineur who have been very supportive throughout my research work. Emmanuel has always provided me sound advice thanks to his *lourd passé* and broad knowledge of the electric power sector. Furthermore, he contributed to install a very pleasant and informal working environment in our research team. François kindly and patiently introduced me to the fascinating world of optimization and has always helped me in bridging the gap between my power systems background and convex programming, which was very stimulating.

Then, I want to thanks the Power Systems Consulting team at Tractebel Engie who proposed the topic of this thesis and introduced me to their existing tools. More specifically, I would like to thank Niels Leemput, Parvathy Chittur and Stéphane Rapoport who closely followed my work and gave me sound advice and guidance along the way.

I also want to thank warmly Frederik Geth who gave me a lot of support both at Tractebel Engie and at KULeuven, introduced me to the topic of convex optimization in power systems and gave me a lot of good advice.

Outside of Belgium, I want to thanks the team of the Center for Non-linear Stud-

ies (CNLS) at the Los Alamos National Laboratory (LANL) for welcoming me during three weeks. A particular thanks to Line Roald and Sidhant Misra who were very good hosts for my first stay in the USA. Line was not only a host but also introduced me to stochastic optimization which really helped me for my work.

I would also like to express my gratitude to Carleton Coffrin (CNLS) for the discussions, the great help, the kind advice and the proofreading of some parts of my work.

Thank you to Daniel Molzahn from Argonne National Laboratory for sharing with me his excellent work, knowledge and advice.

Now coming back to Europe, I want to thank warmly the members of my jury who kindly accepted to evaluate this work and gave a lot of sound advice during these four years: François Vallée (UMons), Edwin Haesen (Ecofys), Fabrizio Pilo (Unica), Anthony Papavasiliou (UCL), Niels Leemput (Tractebel Engie) and Thomas Pardoen (UCL).

Thanks to David Vangulick (ORES) for the advice and interesting discussions.

Thanks to Fernando de Cuadra (Universidad Pontificia Comilla) for sharing the data about the Michiquillay test case and answering my questions.

Thanks to Philippe De Rua, who voluntarily spent a few summer weeeks after his graduation working with me on a really interesting topic, it was a nice and fruitful collaboration.

I would also like to thank two people who helped me with technical matters, mostly related to computer and computational issues: Bob Fourer (AMPL) and Etienne Huens (UCL).

Then, I have to thank warmly all my colleagues at the MEED department for making it a really nice working environment, and more specifically the *Nuggets* team for all the discussions, exchanges and advices.

A warm thank to Georges Lognay for the detailed proofreading of this manuscript and the sound advice.

Then, I have to thank my family and friends whose for their presence and careful listening during these four years. A special thanks to my dad who transmitted to me his interest for energy and sustainability matters.

At last, I would like to thank the *Fonds National pour la Recherche Scientique - FNRS* for the funding of this research work.

Abstract

Rural electrification in developing countries is a significant challenge. In 2016, 1.1 billion people still lacked access to electricity worldwide, 84% of them located in rural areas [48]. Alongside central grid expansion and standalone home energy systems, microgrids are expected to play an important role towards universal electricity access [48]. The investment planning of microgrids is a constrained optimization problem that has to account for both distribution and generation assets in a green field context. Furthermore, it is subject to uncertainty, notably related to the power consumption of newly connected users or to the intermittency of renewable power production.

In this work, we propose an original approach to tackle the joint planning of distribution and generation from the viewpoint of mathematical optimization. The non-convex power flow equations and integer investment decision variables give rise to a mixed-integer and non-convex optimization problem. Due to the inherent complexity of such problems, we propose a hierarchy of planning models with increasing precision, based on convex relaxations of power flow equations. We assess the performances of these models in terms of power flow modelling accuracy, feasibility of the solutions and computational tractability. The tests, performed on a real-world use case, highlight how the feasibility of planning solutions heavily relies on the accuracy of power flows modelling. Among the proposed models, the Convex DistFlow-based formulation proves to be successful in providing adequate microgrid design solutions for all the operating conditions considered.
In a second phase, we extend this model with the aim of integrating load-related uncertainty. To this end, we propose a robust planning approach that delivers microgrid design solutions which operate successfully in both nominal and worst anticipated loading conditions. This approach is shown to present a reasonable increase in runtime compared with the deterministic planning method on which it is based.

This work investigates in detail the performances of microgrid planning models based on convex relaxations of power flow equations. Hence, it constitutes a first step towards leveraging the recent advances of power flow modelling in a microgrid planning context.

Contents

Introduction and background

1

1.1 Electrification of rural areas

1.1.1 Energy access

Humankind has always relied on energy to survive. From the mastering of fire (cooking, lighting, heating, crafting) to the harvesting of wind and water energy (irrigation, food processing, load lifting), energy has been a key enabler for human civilizations in terms of major technological, and, thereby, societal advances [13]. A further step was taken with the invention of steam machines that allowed to turn heat into mechanical work [13]. Coupled with the exploitation of high energy density fossil fuels, it dramatically increased the energy amount available to humans and allowed to exploit natural resources more than ever before, giving birth to our modern industrialized, fossil fuel-based economy [13].
However, even if the average French citizen's total energy consumption[1] equates the mechanical energy of more than 400 permanently available human slaves [51], there are significant disparities between regions of the world regarding energy access. This concerns both the energy use per capita and the energy mix, as shown on Fig. 1.1. As a matter of fact, it highlights that:

(i) High income countries inhabitants use roughly ten times more energy than those living in low income countries

(ii) Low income countries heavily rely on biomass for their energy needs, among which cooking and heating [35].

[1] Direct and indirect use, i.e. the so called *grey energy* of all consumed products and services

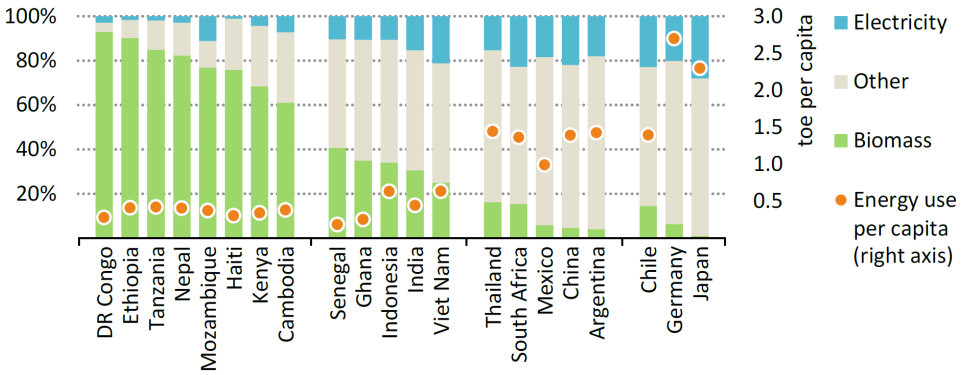

Fig. 1.1: Final energy use per capita and fuel mix in selected low, middle and high-income countries, 2015 (toe: ton of oil equivalent). Adapted from [48]

Yet, it is widely acknowledged that energy access is a necessary condition to improve living conditions in developing countries and for the development process at large [8, 48]. In particular, the United Nations included energy access as one of their 17 Sustainable Development Goals (SDGs) for 2030 [8]. Indeed, it is considered as essential to other SDGs covering amongst others education, poverty reduction, gender equality, fight against climate change, economic development and health. With respect to this last point, one third of world's population depends on solid biomass (wood, animal dung, etc.) for cooking, which is often done in rudimentary installations, thereby creating health threatening smokes [48].

1.1.2 From grid expansion to individual power generation systems

The access to "modern energy services" [48] is largely achieved through the access to electricity. In this regard, there are large disparities between different parts of the world (Fig.1.2). In 2016, 1.1 billion people (14% of the world's population) still lacked electricity access, the vast majority of them being located in sub-Saharan Africa. At global scale, 84% of people lacking electricity access lived in rural areas in 2016 [48]. Hence, universal electricity access is first and foremost a rural electrification issue.

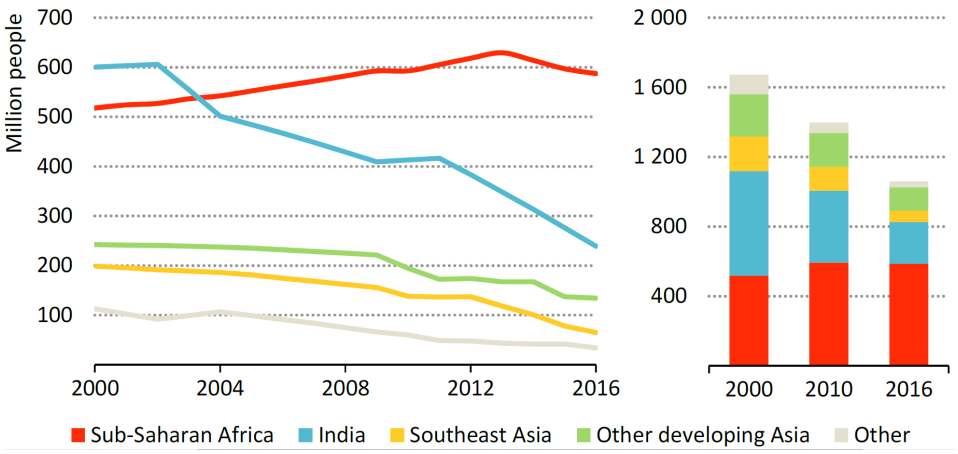

Fig. 1.2: Population without access to electricity by region. Adapted from [48]

The various options for rural electrification may be divided in three main categories:

(i) **Grid expansion**: the considered area is connected to the existing grid at distribution or transmission level depending on the estimated power demand
(ii) **Microgrid**: A local power network that is limited to the considered area and not connected to any other existing network
(iii) **Standalone systems**: Integrated systems that are not connected to any network, typically delivering power to a single household, most of them being diesel generators or solar systems including batteries [48]

Grid expansion versus decentralized electrification

Option (i) corresponds to classical power system expansion, while options (ii) and (iii) are decentralized solutions, not relying on any existing infrastructure. The former has traditionally been the way to electrify new areas and still represents 97% of the new connections realized since 2000 [48]. Nonetheless, grid expansion in rural areas suffers from several drawbacks. Indeed, the distance between these rural areas on one side and existing power infrastructures on the other side may be very long. The cost of building new lines to interconnect them may thus quickly become prohibitive, more specifically under circumstances of capital scarcity. Furthermore, these remote locations may be located in rough terrain, adding technical constraints to economical ones.
Decentralized options, i.e. microgrids and standalone systems, usually have lower upfront costs than grid expansion and provide viable alternatives. The International Energy Agency (IEA) foresees that they will play a significant role in providing power to unelectrified areas from now to 2030. Indeed, in its *Energy For All* scenario,

where the universal electricity access is reached by 2030, IEA expects about 550 million new connections to be made via grid expansion , 450 million via microgrids and 330 million via standalone systems [48]. In this scenario, decentralized systems will thus roughly account for 60% of new connections, with 35% for microgrids alone.

Microgrids versus standalone systems

The choice for one or another decentralized option is highly dependent on the geographical and demographical context. Microgrids are generally the cheapest option for densely populated remote areas, while standalone systems may be economically more attractive in remote areas with sparse populations [48].
Microgrids do nonetheless present advantages over standalone systems. First, they allow to use electricity generation means more efficiently thanks to their pooling between a larger amount of users [30]. Then, they can accommodate larger capacity generation units which in turn allows for supplying larger loads, e.g. for industrial or commercial applications [30]. This is illustrated on Fig. 1.3. Finally, unlike standalone systems, microgrids are scalable solutions which, in time, may be connected to the central grid if this one is extended to the area covered by these microgrids [48].

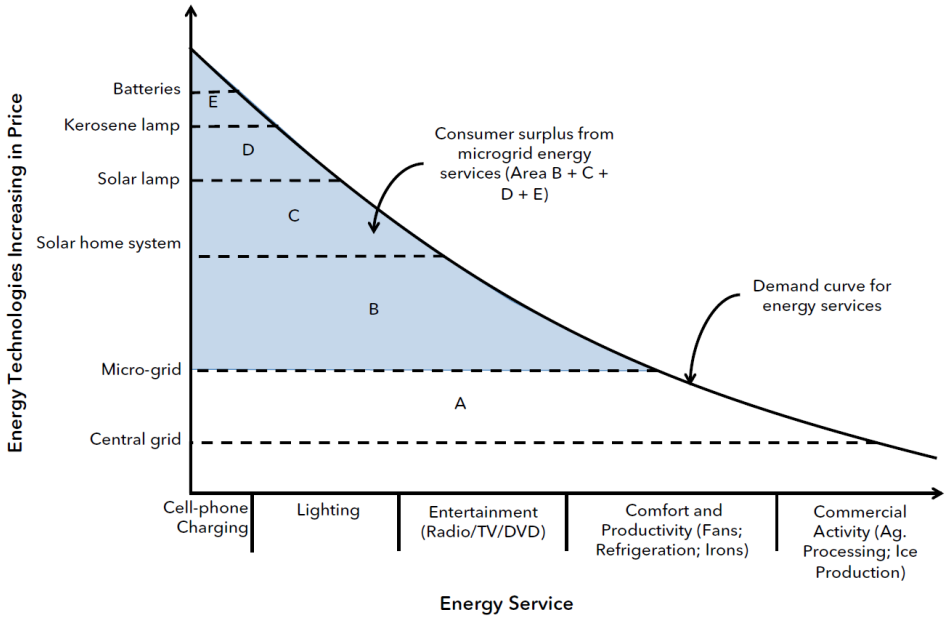

Fig. 1.3: Price of Energy Services Provided by Energy Fuels and Technologies. Adapted from [87]. The range of energy services made available by microgrids not only includes residential but also productive applications

1.1.3 Challenges in microgrids development

Among the spectrum of available options for rural electrification, this work addresses the investment planning of microgrids on the basis of engineering and optimization. However, there are also numerous and important socio-economic challenges to deal with when implementing microgrids, parts of which are illustrated below.

A first challenge is related to the affordability of microgrids. Indeed, even though the unit cost of energy might be lower when switching from traditional means, e.g. candles, to electricity supplied through the microgrid, upfront connexion costs can be a barrier to the poorest inhabitants [48]. Then, the microgrid financial viability itself may be a challenge as well in the case of low payment capacity. The tariffs should be designed accordingly to the business model (for profit, partly or fully subsidised by authorities or donators), depending on the costs these tariffs are supposed to cover, e.g. capital, operation, maintenance costs [87]. A badly designed tariff could result in vicious circles where the lack of payments from newly connected users results in insufficient incomes for the microgrid owner. This translates into poor maintenance, hence a low system reliability and frequent outages that contribute to lower the value of the microgrid for customers who are thus willing to pay less and less for it [87].

Operators training and adequate maintenance expenses are of paramount importance as well. Indeed, cases are reported in India where the failure to meet these requirements led to microgrids becoming inoperational even though sufficient investments had been made for their implementation [87]. Finally, cultural factors play a role, the will to keep traditions being a potential obstacle for the acceptance of modern energy sources by local populations [48].

1.2 Joint investment planning of autonomous microgrids

1.2.1 Characterization of the problem

Definition of planning

As exposed in section 1.1, the present work focuses on the investment planning of microgrids for the electrification of rural and remote areas. In this context, we define the concept of planning as follows:

> ***Planning:*** Procedure that delivers an investment plan for the considered system over the planning horizon. It consists in determining **which** assets are to be placed, **when** and **where** they should be placed. These investment decisions must be made in a way that is **optimal** regarding the **planning objectives** while being compliant with the problem **constraints**.

Autonomous microgrids

A majority of authors define a microgrid as a grouping of generators and loads operated in a coordinated way, connected to the main grid as a unique entity and capable of functioning in islanding mode [47, 81, 80]. As we address the problem of electrifying remote areas, we will only consider autonomous microgrids, i.e. that are not physically connected to a central network and are thus operated in standalone. As stated in section 1.1, these systems might eventually be connected to the main grid if it is expanded at a later state, but they are initially planned to be able to function by their own.
This means that an autonomous microgrid should include enough generation capacity to cover the consumption of all connected users. It is a major paradigm shift compared to usual low voltage distribution networks that only route the energy produced by larger plants connected to higher voltage levels. When implementing an autonomous microgrid, both distribution and generation assets have to be built. Planning them separately, in a sequential way, might be suboptimal. We thus choose to address the problem in a joint way by considering both types of assets simultaneously in the planning process. The drawback of this approach is that it increases the computational burden.
Distribution planning encompasses the design of all elements, i.e. lines, transformers and switches, that interconnect the nodes of the network. This includes:

(i) **Feeder routing**: determine the optimal layout of electrical lines, i.e. the graph

of the network (including potential sectionalizing switches). The graph of the network is almost always required to be connected (no islanding) and is very often radial in distribution context. Geographical obstacles have to be considered when performing feeder routing.

(ii) **Line sizing**: choose the appropriate type and size of conductor for each line section, that will determine its current carrying capacity or thermal rating.

(iii) **Transformer/substation siting**: select the nodes where new transformers should be located

(iv) **Transformer/substation sizing**: determine the rating of new transformers or substations

Generation planning consists in designing generation units integrated in the system, which involves:

(i) **Generation siting**: select the nodes where new generators should be located

(ii) **Energy source**: choose the appropriate generation technology and energy source, e.g. oil, gas, biomass, PV (Photovoltaic systems) or WT (Wind Turbines). There may be a cap on the share of RES (Renewable Energy Sources)-based generation in the electricity mix to account for the intermittency related to it.

(iii) **Generation sizing**: determine the rating of new generators

(iv) **Batteries siting and sizing**: Autonomous systems including intermittent generation often integrate storage systems in order to compensate for the variability of intermittent resources

The planning of autonomous microgrids generally concerns areas with no existing infrastructure, which is referred to as green field planning approach.

Multistage planning

As mentioned above, the planning process should not only determine the assets type and siting but also the timing of investments over the planning horizon. Indeed, the electrical consumption of the microgrid users may increase in time, particularly in newly electrified areas where the improvement of living conditions can lead to a demand for more sophisticated electrical appliances, e.g. for increasing comfort and entertainment. It is thus necessary to be able to reinforce the microgrid capacity in time to account for an increasing load. The phasing of investments has furthermore an economic interest as it may be profitable to delay investments in time to lower their net present value and thereby reduce the global cost of the project. Finally, the project initiator may be subject to budgetary constraints preventing him to realize all needed investments at once, which necessitates a progressive phasing of investments. This progressive phasing is from here on referred to as multistage planning.
Some authors do not implement this phasing and consider all investments at once (static planning). Other works determine the phasing in an approximate way by

solving a sequence of static planning problems each covering a single timestep of the planning horizon , which may be suboptimal as each subproblem only considers a single timestep and is blind to the future condition (pseudodynamic planning [32]). Finally, a dynamic planning problem considers all timesteps at once to account for the whole planning horizon when phasing investments.

Operational feasibility

Even though the problem at hand concerns long term investments, it is also necessary to incorporate the operation of the microgrid to the planning procedure as both are strongly interrelated [75]. As a matter of fact, the microgrid must be able to operate properly for all foreseeable conditions that may arise during its lifetime. These are notably determined by the evolution of the microgrid users electric consumption, that is observed both at intraday (rhythm of daily activities, lighting needs at different times of the day) and long term timescales (increasing amount of connected users and/or electrical appliances).
Incorporating intraday load variations to the planning problem, even on a hourly basis, represents significant computational challenges as the planning horizon of microgrids is typically in the order of several decades, which represents hundreds of thousands of hours, hence as many timesteps to consider in the planning process.
Operational feasibility of a microgrid and, more generally, of a power system, can be assessed through four criteria:

(i) **Adequacy**: the capacity of the system to cover the whole electrical energy consumption of customers while ensuring reliable and safe system operation [49]. Spinning reserve requirements may be considered in order to compensate generation outages
(ii) **Reliability:** the ability to guarantee the continuity of supply in case of contingencies. It is measured by a series of performance indices, for example related to the duration and frequency of outages
(iii) **Power Quality:** set of standards defining the allowed value range for quality indices related to the frequency, waveform, amplitude and balance of the three-phase voltage supply
(iv) **Equipment limits:** operating range in which assets should be and for which their lifetime is determined, including: line thermal rating, generator capability curve, transformer rating, battery minimum and maximum State Of Charge (SOC), battery maximum charge and discharge rate

Power flow equations

AC power systems are governed by Power Flow (PF) equations that relate nodal quantities, i.e. bus voltages and power injections, and branch quantities, i.e. power

flows. These equations, that are at the heart of every AC power system optimization related problem, represent a computational challenge as they are non-convex. This implies that corresponding optimization problems are generally NP-hard and may present several local optima [74], which greatly complicates the search for a global optimum.
The distribution system planning related works may incorporate an exact version (AC PF), a relaxation or an approximation of these equations (see chapter 3 for more details about relaxations and approximations).

Mixed-Integer problem

The autonomous microgrid planning includes variables representing both investment decisions and operational setpoints. The former are intrinsically discrete as they relate to a discrete and finite set of investment options (there are only so many lines and generators types and sizes) while the latter are continuous quantities, e.g. voltage and active power.
Mixed-integer problems are known to be hard to solve due to their partially combinatorial character. As a matter of fact, the discrete nature of the solution space implies that its size grows exponentially with the size of the problem, which is known as the 'curse of dimensionality'. As a simple illustration, the number of possible radial networks connecting n nodes (in graph theory, the number of spanning trees) is equal to n^{n-2}. This already makes around 2.7×10^{23} different possibilities of building a 20 node-network, without even considering the sizing of branches nor the siting and sizing of generators.

Uncertainty

There are three major sources of stochasticity in the microgrid planning problem. The first one is the inherent uncertainty in load forecasting. Then, microgrids incorporating intermittent generation, such as PhotoVoltaïc (PV) installations or Wind Turbines (WT), are also subject to forecast errors regarding their output power. At last, contingencies , whether due to climatic conditions or human errors, introduce another degree of unpredictability in the planning problem.
Uncertainty also affects interconnected power systems, for the same reasons exposed above. However, microgrids do not benefit from the sophisticated Supervisory Control And Data Acquisition (SCADA) systems nor the level of redundancy characteristic of larger power systems, which makes them more vulnerable to uncertainty.

Planning objectives

The planner's objectives may be multiple as they depend on the underlying business

model. They can relate to economical considerations, e.g. minimizing investment and/or operational costs, minimizing losses or maximizing profits. Technical criteria can also be addressed, e.g. by minimizing bus voltage deviations from their nominal values, minimizing equipment loading or maximizing the reliability. Finally, environmental criteria may come into play, by maximizing the share of renewable energy in the generation mix or minimizing the emissions of greenhouse gases.
From a computational point-of-view, multi-objective optimization obviously presents an additional challenge.

Optimization methods

A large variety of optimization methods have been employed in the field of power system planning. They can be divided into two broad categories: mathematical optimization and heuristic methods. The former exploit the mathematical structure of the problem to get a provably optimal solution to the problem while the latter rely on predefined rules to explore the feasibility space of the problem and do not guarantee the optimality of a solution. Mathematical optimization problems are classified according the type of variables (continuous and/or discrete) , constraints and objectives (linear, quadratic, conic, positive semi-definite, polynomial, posynomial, non-linear) they include. Heuristics vary widely depending on the implemented rules. A large proportion of heuristics employed in the power system planning literature belong to the class of Evolutionary Algorithms (EA) that mimic the functioning of natural systems when looking for an optimal solution, e.g. Genetic Algorithms (GA), Particle Swarm Optimization (PSO), Ant Colony Algorithm (ACA) or Simulated Annealing (SA).

1.2.2 Related work

Evolution of distribution systems planning

The majority of works related to autonomous microgrids planning originate from distribution systems planning in the context of conventional power systems, i.e. centralized and interconnected networks with different voltage levels. This topic has been the subject of a growing attention during the last fifteen years or so. This is due to the massive increase of Decentralized Generation (DG) units, mainly PVs and WTs, installed both at medium and low voltage level in a context of energy decarbonization and strongly supported by incentive measures [100, 81]. As a matter of fact, distribution networks were traditionally passive in the way that they routed the electrical energy, produced by large power plants connected to the transmission grid, to the end-users. Hence, they were designed for unidirectional flow patterns,

with a 'Fit and Forget' approach where the distribution network sizing was performed such that it would be able to accomodate the expected peak loading conditions, given the expected load growth, with little or no additional actions needed during its operation[81].
This approach is not suitable anymore for the Distribution System Operators (DSO) in the presence of numerous DG units as these can radically change the flow patterns, increase current levels, cause overvoltage and blind protection systems [3]. There are two options for DSOs to cope with DG units. The first is to reinforce their network by investing in new larger capacity lines and transformers , which quickly becomes expensive. The second option is to increase the observability and controllability of distribution networks (e.g. smart metering and smart substations) to implement operational strategies aiming at relieving the aforementioned constraints, hence delaying costly investments. These strategies, referred to as Active Distribution Network (ADN) management include Demand Side Management (DSM), DG dispatch and curtailment, network reconfiguration through line switching, Volt/Var control and battery operation [81].

In the previous section, we characterized the autonomous microgrid planning problem by presenting its main features. We now undertake a (non-exhaustive) literature review to identify the gaps and remaining open questions from which we infer relevant research axes for the present work. We only review references explicitly dealing with distribution system planning in the current section, while the literature more specifically related to subparts of the problem will be introduced in the relevant chapters. The reviewed references are grouped hereafter depending on the degree to which they include DG in the planning process. A more detailed characterization of these works according to the features identified in section 1.2.1 is given in tables 1.1 and 1.2.

Passive distribution systems planning

As mentioned above, distribution systems traditionally supplied passive loads and hosted little or no generation units injecting power on the network. Hence, these systems were designed as tree-like feeder structures originating from distribution transformers, being reinforced in time to account for load growth. Most of these passive approaches aim at minimizing reinforcement costs. A dynamic programming approach (DP) is proposed in [78] for the multistage expansion planning of an existing distribution system facing load growth through reconductoring (replacing existing lines by higher capacity ones), transformer uprating or installation of new ones. A separable linear approach is presented in [34] to perform distribution expansion planning with feeder routing and sizing and substation siting. A similar problem is tackled with a specifically designed heuristic approach mimicing expert

judgement and accouting for real geographical obstacles in [83]. A heuristic network reinforcement algorithm is presented in [31] to optimally select conductor sizes in a distribution system facing load growth. Reliability costs,representing the cost of outages and unserved energy, are accounted for in [22] where feeder routing and sizing is performed in a green field context using a GA (Genetic Algorithm). A similar problem is tackled in [20] using an AIS (Artificial Immune System) algorithm. A complete distribution system planning method where feeder routing and sizing as well as substation siting and sizing are treated is developed in [54] using a GA and in [84] using an ICA (Imperalist Competitive Algorithm). The same problem is formulated for the simultaneous planning of Low Voltage (LV) and Medium Voltage (MV) distribution networks including reliability costs and solved with a PSO (Particle Swarm Optimization) algorithm in [101].

Distribution systems expansion planning accounting for distributed generation

A second facet of the distribution system planning literature approaches the expansion planning of such systems in cases where DG units are installed at various nodes of the network by consumers, with little or no control from the DSO, which thus needs to accommodate them as best it can. A multistage joint expansion planning of lines and transformers accounting for DG units present at different nodes of the network is presented in [45] and [46], using a DC load flow model and considering load shedding and DG curtailment as planning alternatives. A heuristic approach aiming at improving the hosting capacity of distribution networks for DG units is implemented in [4] where feeder routing and switch location are done in such a way as balancing the expected curtailed power during line contingencies over the set of feeders. References [37] and [38] deal with both green field and expansion planning of feeders, switches and transformers in networks hosting DG units with a multi-objective approach aiming at maximizing the reliability of the system and minimizing its total cost simultaneously, using PSO and DP approaches respectively. In reference [63], the authors approach the switch investment planning in order to be able to reconfigure the network topology with the goal of reducing DG units curtailment. A graph approach is implemented in [56] to evaluate in the planning procedure the reliability of a distribution network hosting DG units. In a similar context , the feeder routing and sizing problem is first exactly formulated as a MINLP, then gradually relaxed in a tractable MILP in [89].

Joint planning of distribution and generation

The last category of works presented in this section goes a step further as these refer-

ences include DG units as a planning alternative, meaning that these are now considered to be installed by the DSO that has now control over their siting and size. The HOMER (Hybrid Optimization of Multiple Energy Resources) software [1] is used in [57] to design a multi-energy microgrid supplying heat and power in a remote context, choosing among different generation and storage technologies and using a single node representation gathering all electrical appliances (no consideration of network graph). A similar problem is treated with a PSO algorithm in [61], where both environmental and economic factors are aggregated in a single objective function and the operational management of storage and generation units is accounted for. Reference [76] presents a full version of the multistage joint expansion planning problem dealing with the siting and sizing of feeders, DG units and transformers. The authors of [32] follow a similar approach while also integrating reliability costs. Reference [88] deals with a comparable formulation, further adds socio-environmental costs to the objective function and considers yearly budget limits. Finally, a multi-objective approach is developed in [102] that aims at minimizing both gas emissions and total system costs in the joint expansion planning of distribution and generation assets, using a GA and including load- and intermittent generation-related uncertainty.

			References											
			[78]	[34]	[83]	[31]	[22]	[20]	[54]	[84]	[101]	[45]	[4]	[37]
Objective	Minimize	Losses	x	x	x	x	x	x	x	x	x		x	x
		OPEX	x	x	x	x	x	x	x		x	x		x
		CAPEX	x	x	x	x	x	x	x	x	x	x	x	x
		Voltage deviations												x
		Gas emissions												
	Maximize	Reliability	x				x	x			x	x	x	x
		DG penetration											x	x
Constraints	Network	Connectivity		x	x		x	x	x	x		x	x	x
		Radiality		x	x		x	x	x	x	x			
		Geographical obstacles			x									
	Lines	Thermal rating	x	x	x	x	x	x	x	x	x	x	x	x
	Generation	Capability curve										x		
		Maximum RES share												
	Transformer	Thermal rating	x						x	x		x		
	Voltage	Amplitude	x	x	x	x	x	x	x	x	x	x		x
	Battery	(Dis)charge rate and SOC												
	Reliability	Spinning reserve												
		Outage duration/frequency												
Investment decisions	Generator / Transformers	Siting	x	x						x	x	x		x
		Capacity		x					x			x		x
		Technology												
	Lines	Routing		x	x		x	x	x	x	x	x	x	x
		Conductor type	x	x	x	x	x	x	x		x	x	x	x
	Batteries	Siting												
		Capacity												
	Switches	Siting											x	x
Operational decisions	Generation dispatch / curtailment											x		
	Line switching						x					x		
	Battery dispatch													
	DSM/load shedding											x		
Multistage	Static					x	x	x	x		x		x	x
	Pseudo dynamic			x	x					x				
	Dynamic		x									x		
Uncertainty	Load							x						x
	Generation												x	
	Contingencies							x						x
Power flow modelling	AC			x	x	x			x		x			
	Relaxation													
	Approximation		x							x		x	x	x
Method	Mathematical optimization		DP	MILP								MILP	MILP	
	Heuristic				x	x	GA	AIS	GA	ICA	PSO	x	x	PSO

Table 1.1: Classification of reviewed works following the identified criteria

			References								
			[63]	[56]	[89]	[57]	[61]	[76]	[32]	[88]	[102]
Objective	Minimize	Losses	x	x	x		x	x	x		x
		OPEX	x	x	x	x	x	x	x	x	x
		CAPEX	x	x	x	x	x	x	x	x	x
		Voltage deviations									
		Gas emissions	x				x			x	x
	Maximize	Reliability						x			
		DG penetration	x				x				
Constraints	Network	Connectivity			x			x		x	x
		Radiality	x	x	x			x	x		x
		Geographical obstacles									
	Lines	Thermal rating	x	x	x			x	x	x	x
	Generation	Capability curve			x	x	x	x	x	x	
		Maximum RES share						x			x
	Transformer	Thermal rating		x	x			x	x		x
	Voltage	Amplitude	x	x				x	x	x	x
	Battery	(Dis)charge rate and SOC				x	x				
	Reliability	Spinning reserve				x		x			
		Outage duration/frequency				x	x				
Investment decisions	Generator / Transformers	Siting		x				x	x	x	x
		Capacity			x	x	x	x	x		x
		Technology				x	x	x		x	x
	Lines	Routing	x	x	x			x	x	x	
		Conductor type	x		x			x	x		x
	Batteries	Siting									
		Capacity				x	x				
	Switches	Siting	x								
Operational decisions	Generation dispatch / curtailment		x		x	x	x		x	x	
	Line switching		x								x
	Battery dispatch					x	x				
	DSM/load shedding					x	x			x	
Multistage	Static		x		x		x				
	Pseudo dynamic		x			x			x		
	Dynamic							x		x	x
Uncertainty	Load		x							x	x
	Generation		x								x
	Contingencies			x					x		
Power flow modelling	AC		x	x					x		x
	Relaxation				x						
	Approximation							x		x	
Method	Mathematical optimization				MILP			MILP	MINLP	MILP	
	Heuristic		x	x		x	PSO		GA		GA

Table 1.2: Classification of reviewed works following the identified criteria (cont'd)

Existing tools

In addition to the aforementioned research works, software tools have been developed to address the planning of microgrids. We focus on two of them, which have been used to lay out the design of microgrids in real-world cases.
The first one, HOMER is a commercially available software that helps the microgrid planner to optimally design a decentralized generation system. It allows to choose among a wide range of generation and storage technologies and sizes, and to simulate numerous operational strategies and scenarios related to battery operation, RES generation production profile, fuel costs, etc. Nonetheless, HOMER aggregates all system components on a single bus, hence it does not account for the layout of the network. It optimizes the generation system design by exhaustively enumerating all possible combinations of system components and sizes. This optimization approach does not scale for larger search spaces, e.g. in the case of feeder routing. As a matter of fact, there exist n^{n-2} different radial layouts for a network connecting a set of n nodes, which means that there are 10^8 possible ways to connect 10 nodes with a radial network for example. This precludes the use of exhaustive search space exploration for such problems.
The second tool is the Reference Electrification Model/Reference Network Model (REM/RNM), developed in the framework of the Low-cost energy technologies for Universal Access, a research project jointly led by the Massachusetts Institute of Technology (MIT, USA) and the IIT Comillas University (Spain). This tool aims at determining, for every load point in an unelectrified area, the least-cost electrification mode (grid extension, microgrid or individual home energy system) and the layout and size of both distribution and generation assets. The determination of the optimal electrification mode is performed by the REM part of the tool with a clustering procedure. The detailed generation and network design is then made by the RNM. The main advantage of this tool is that it allows to handle very large areas including several millions of customers and delivers a large scale target architecture for the electrification of these areas. On the other side, the local generation and distribution designs are performed separately, through heuristic approaches [60].

Current limitations

The analysis of tables 1.1 and 1.2 allows to highlight the limitations of the existing literature regarding the problem at hand.
First, it can be observed that only few references tackle the joint planning of distribution and generation [61, 76, 32, 88, 102].
Then, the majority of reviewed works do not incorporate any representation of the different uncertainty sources, which is limiting in high RES potential contexts. Furthermore, a lot of these works are based on approximated representations of PF

equations. More precisely, mathematical optimization approaches neither include exact nor relaxed version of these equations at the exception of [89]. Some heuristic approaches do rely on exact AC equations since these approaches perform the optimization of discrete variables and the verification of constraints (here, PF equations) separately. In this case, the constraint satisfaction problem is only a Non-Linear (NL) one. However, the objective and constraints cannot be handled separately in mathematical optimization. Hence, AC PF equations make the problem MINLP in this framework, which is computationally challenging even for a limited amount of decision variables. Yet, it is important to accurately represent PF equations in a planning problem to guarantee the operational feasibility of the optimal solution. As a matter of fact, inaccuracies regarding the computation of power flows and voltage may lead to an overoptimistic assessment of constraints satisfaction and deliver a planning solution which is not feasible in reality.
We also observe that most presented works are based on heuristics rather than mathematical optimization. The former allow to treat large problems, a priori too computationally intensive for a mathematical optimization approach. However, heuristics suffer from several shortcomings:

(i) The optimality of solutions delivered by heuristic approaches may not be proved
(ii) In cases where the optimization is stopped before convergence to a solution due to a limited computation budget, heuristics do not provide any measure of the distance to optimality (the optimality gap)
(iii) Some of these approaches(EA for example) are based on random operators and may thus deliver different solutions from one run to another
(iv) They often rely on a significant amount of optimization parameters that need to be fine-tuned to obtain adequate results and do not benefit from widely adopted commercial implementations
(v) Mainly academic approaches, not often implemented in the industry

On the contrary, a mathematical optimization approach presents several advantages:

(i) It delivers provably optimal solutions and determines the optimality gap if it is stopped before converging to an optimal solution
(ii) It is deterministic and, for the same problem, it will deliver the same results run after run
(iii) There are many commercially available, off-the-shelf solvers dedicated to the different classes of mathematical optimization problems, which allows to focus on the model of the problem rather than implementing an algorithm or tuning an existing one
(iv) It is widely adopted in the industry
(v) There is a growing interest and community in power systems research around the relaxations of PF equations, partly due to significant performance im-

provements of commercial solvers during the last decade or so. They are now very well studied for various operational problems, e.g. Optimal Power Flow (OPF) problems

This comparison between analytical (mathematical optimization) and heuristic methods should nonetheless be nuanced as analytical methods also present disadvantages, the most critical one being the computational burden. Indeed, the guarantee of optimality may come at the cost of a larger computational burden, depending on the underlying model. Typically, the planning problem presented above is computationally challenging for real size problems and analytical approaches based on accurate power flow representations might not be applicable as they could fail to converge. Heuristics and approximations, even though they do not guarantee exact results nor an exhaustive exploration of the search space, can thus be helpful to find 'good' solutions for real-world problems and might be necessary in this context.

Besides the above considerations, we observed that comparing the methods and results originating from various references was not an easy task. As a matter of fact, there is a growing amount of benchmarks and databases available to compare the results of different methods developed for operational problems such as OPF or Unit Commitment (UC). Yet, we could not find similar resources for planning problems. We believe this is due to the complex nature of such problems, but also to the wide variety of constraints, objectives, models and algorithms that are considered by the different authors.

Bearing the above elements in mind, we chose to direct this work towards the mathematical optimization framework by using various relaxations of power flow equations. The goal is to make the most of these potentially very accurate approaches and to identify the extent to which they can be applied to real-size problems.

We also deliberately chose not to address flexibility (storage or demand response) in this work. The reason for this is that we aim at assessing the performances and applicability of various mathematical programming formulations for the considered planning problem. Yet, as it is shown in chapter 4, the problem is already challenging when only considering distribution lines and generators, hence we do not want to further increase the computational burden. Nonetheless, there is no modelling restriction that prevents from integrating storage or demand response in the chosen mathematical programming framework and the models presented in this work can directly be expanded to include such elements.

1.3 Open questions

When comparing the characterization of autonomous microgrid planning with the existing approaches to solve it, we observe that these approaches do not capture all of its features. For that reason, this thesis aims at investigating the following open questions:

- How does the accuracy of power flow modelling, and more precisely the use of convex relaxations of power flow equations , impact the quality of planning solutions?
- Is it possible to devise scalable (that remain computationally tractable for a growing problem size) and accurate joint planning methods that leverage the strength of mathematical optimization?
- How to account for the uncertainty inherent to the planning of autonomous microgrids in a scalable way?

1.4 Document structure

The rest of the document is structured as follows. We begin to tackle the problem from a network planning perspective using a dynamic programming approach in chapter 2. This method relies on an exact representation of the three-phase, unbalanced, AC power flow problem to check the feasibility of a network planning solution. The optimal investment plan is determined as the lightest path in a graph representing all possible investment trajectories. Such an approach is already computationally challenging for the sole network planning problem due to the explicit enumeration of the different possible combinations of investment decisions. In order to be able to tackle the whole joint planning problem, including generation planning, we decide to shift from this graph-based optimization approach to a convex optimization-based framework. A brief introduction to convex optimization is given in chapter 3. In chapter 4, we present a deterministic and non-convex formulation of the autonomous microgrid planning problem. Then, we study the existing convex relaxations of power flow equations on the basis of which we propose a hierarchy of growing accuracy, convex relaxations of the planning problem. These are based on the Network Flow, Taylor-Hoover and Convex DistFlow relaxations of power flow equations respectively. The proposed models are tested on a real-world planning case in order to compare their computing needs, the quality of their respective solutions, and their modelling accuracy, taking the Convex DistFlow-based planning model as

a reference. Chapter 5 addresses in more detail the accuracy of the Convex Dist-Flow relaxation of power flow equations in the context of an Optimal Power Flow problem. We then consider the inclusion of load related uncertainty in the planning problem in chapter 6 and we propose a stochastic planning approach, built upon the previous deterministic method, that delivers a robust planning solution in the context of imperfect load forecasting. Finally, we summarize the main results obtained with both deterministic and stochastic planning approaches and conclude this work with future perspectives and avenues of research.

1.5 List of publications

Conference papers

B. Martin, E. De Jaeger, F. Glineur, and A. Latiers. **A dynamic programming approach to multi-period planning of isolated microgrids**. In *Advances in Energy System Optimization*, pages 123–137. Springer, 2017. [65]

B. Martin, P. De Rua, E. De Jaeger, and F. Glineur. **Loss reduction in a windfarm participating in primary voltage control using an extension of the Convex Dist-Flow OPF** (Forthcoming). In *20th Power Systems Computation Conference*, Dublin, 2018. [66]

B. Martin, E. De Jaeger, and F. Glineur. **Comparison of convex formulations for the joint planning of microgrids**. *CIRED - Open Access Proceedings Journal*, 2017(1):2174–2178, 2017. [68]

B. Martin, E. De Jaeger, and F. Glineur. **A robust convex optimization framework for autonomous network planning under load uncertainty**. In *2017 IEEE Manchester PowerTech*, pages 1–6, 2017. [69]

A. Latiers, F. Glineur, B. Martin, and E. De Jaeger. **On Decentralized Control of Small Loads and Energy Rebound within Primary Frequency Control**. In *19th Power Systems Computation Conference*, Genoa, 2016. [59]
I contributed to the discussion of the methodology and the results and presented the paper at the conference.

Journal paper

B. Martin, B. Feron, A. Monti, E. De Jaeger, and F. Glineur. **Peak shaving: a planning alternative to reduce investment costs in distribution systems?** Submitted to *Energy Systems*, Springer, 2018. [67]

Code

AMPL and *Matlab* codes developed during this work are freely available online at https://github.com/bemartinucl (distributed under GNU General Public License)

A dynamic programming approach to network planning

2

This chapter is an adaptation of: B. Martin, E. De Jaeger, F. Glineur, and A. Latiers. A dynamic programming approach to multi-period planning of isolated microgrids. In *Advances in Energy System Optimization*, pages 123–137. Springer, 2017

2.1 Problem definition

2.1.1 Graph formulation of the problem

Formally, the problem of distribution planning may be expressed using graph theory. The aim is to connect a set of vertices or nodes $\mathcal{E}$(the loads) with a set of edges $\mathcal{V}$(network lines). Those two sets form an the graph $\mathcal{G} = (\mathcal{V}, \mathcal{E})$. Graph $\mathcal{G}$ is undirected as power may flow in both directions. An important planning choice is to decide whether to build a meshed network or a radial one. Meshed networks, if well planned, may reduce losses, voltage constraints [5] and enhance reliability by providing alternative feeding routes in case of contigencies [23]. However, they are more complex to plan [5]. Furthermore, they require more sophisticated protection schemes, which renders the DSO's (Distribution system operators) reluctant to implement them. In this chapter, we will only focus on radial distribution network. Hence, graph $\mathcal{G}$ is a tree, where there is only one path from one vertex to another.

2.1.2 Objective function and constraints

The objective is to minimize the Net Present Value of the system over the planning horizon T as expressed by (**1**).

$$\min_{u_{t,b,i,j}} \sum_{t=1}^{T} \sum_{i,j \in \mathcal{V}} \sum_{b \in \mathcal{B}} \frac{1}{(1+r)^t} (\, u_{t,b,i,j} \cdot l_{i,j} \cdot c_b \; + E^{loss}_{i,j,t} \cdot C_{en}) \tag{1}$$

There are two cost components: investments costs (CAPEX) to build new lines or reinforce existing ones and operational costs (OPEX) related to losses. Investments in lines are chosen among a set $\boldsymbol{\mathcal{B}}$ of available branches. The discount rate is r, the decision variable $u_{t,b,i,j}$ is 1 if a line of type b is placed between nodes i and j at timestep t and is 0 otherwise. The length of the line beween nodes i and j is $l_{i,j}$ $[km]$, the cost of a type b branch is $c_b[\$/km]$. The second term in the equation is the cost of losses, where $E^{loss}_{i,j,t}$ represent the losses in the line between nodes i and j during timestep t $[kWh]$ and C_{en} the cost of energy $[\$/kWh]$. There are three types of constraints. First, the graph must be a connected tree (**2**), meaning that every node is supplied at all times by a unique route. n is the amount of nodes to be supplied, with $n = |\boldsymbol{\mathcal{V}}|$

$$|\boldsymbol{\mathcal{E}}| = n - 1 \tag{2}$$

The following constraints are related to power flows, node voltages and branch currents. At first, balance of active and reactive power injections must be respected at all nodes, as stated by (**3**). P_k and Q_k are the active and reactive power injections at node k (positive if power is consumed) and $P_{l,k}$ and $Q_{l,k}$ are active and reactive power flows from node l to node k. For the rest of the paper, the complex power notation is used for more convenience: $\overline{S}_{t,k} = P_{t,k} + jQ_{t,k}$.

$$\overline{S}_k = \sum_{l \neq k} \overline{S}_{l,k} \qquad \forall k, l \in \mathcal{V} \tag{3}$$

Then, nodal voltages should be bound as in (**4**), V_n being the nominal voltage and V_i the voltage phasor at node i.

$$0.9 \cdot V_n \leqslant |V_i| \leqslant 1.1 \cdot V_n \qquad \forall i \in \mathcal{V} \tag{4}$$

Finally, branch currents are limited by the thermal rating of lines (**5**), $I_{max,b}$ being the ampacity of conductors of type b and $I_{i,j}$ the current flowing from node i to node j in phasor form with $b_{i,j}$ the type of the branch linking i and j.

$$|I_{i,j}| \leqslant I_{max,b_{i,j}} \qquad \forall i, j \in \mathcal{V} \tag{5}$$

The last type of constraints concerns investment trajectory. The load is considered to grow through the planning horizon. Voltage and ampacity constraints can thus only become worse with time with growing power flows on the same network. This

implies that investments cannot be unmade and the size of the lines may only be growing (**6**).

$$Size_{i,j,t} \leqslant Size_{i,j,t+1} \qquad \forall i,j \in \mathcal{V}, t = 1,...,T-1 \tag{6}$$

A power flow problem is solved to verify that constraints (**3**) to (**5**) are satisfied. The choice is made for a three-phase backward forward sweep algorithm. The main modelling features are the following:

(i) Loads are represented as one, two or three current sources depending on whether they are single-, two- or three-phase. They are considered as constant-power loads.
(ii) Generators are considered as negative loads (i.e. they consume a negative current which is equivalent to inject a positive current)
(iii) Voltage drops (or rises in case of positive current injection towards the grid) on the three phases of a line are computed with the full impedance matrix and the three-phase currents, taking into account the mutual impedances effect
(iv) Only series impedances are considered, not shunt capacitances. This hypothesis is valid for short lines in distribution networks. Methodologically, it would not add any difficulty to the problem to consider shunt capacitances. It only necessitates to slightly adapt the power flow algorithm.
(v) The network is considered balanced but the loads are not, hence a full three-phase power problem is solved

Comparative tests have been carried out to assess the loss of accuracy when using a single-phase load flow instead of a three-phase one to compute voltages on a distribution network with only single-phase loads. For this comparison, single-phase loads are replaced by three-phase loads with the same total power but evenly distributed on the three phases. Furthermore, intrinsic unbalance of the line impedances is neglected. These 2 hypotheses allow to draw an equivalent single-line diagram on which a single-phase load flow is run. It has been found that voltages relative errors up to 4% are introduced when using this single-phase approximation. Hence, it justifies the use of a full three-phase load flow calculation for distribution systems where there are many single-phase loads and generators. The backward forward sweep algorithm is proven to be faster than traditional Newton-Raphson or Gauss-Seidel methods for radial networks [28]. It is an iterative method in which currents (backward sweep) and voltages (forward sweep) are successively computed and updated with the result of previous iterations until convergence. The interested reader can refer to [28] for more details on this algorithm. The modelling of branches and loads, based on the work of [103] and [28], has been slightly adapted to explicitly model 4-wires networks.

2.1.3 Input data

There are three types of data for this planning study. First, there is the set of n cartesian coordinates (X, Y) $[km]$ for each node. Then, the load consumption is given for each node and each timestep t of the planning horizon $\{\overline{S}_{t,1}, ..., \overline{S}_{t,n}\}$ $[kVA]$. Finally, there is the set of available electric conductors $\mathcal{B}$, with their respective impedance matrices Z_b and costs c_b, $b \in 1, ..., n_{\mathcal{B}}$ with $n_{\mathcal{B}}$ the amount of different available conductor types .

2.2 Problem decomposition and tool structure

The goal is to solve (**1**) subject to constraints (**2**) - (**6**) while having an existing and feasible power flow solution. In (**1**), the decision variables $u_{t,b,i,j}$ aggregate three different decisions: place a line between nodes i and j, give it the size b and build it at timestep t. All these decisions are discrete by nature, making the problem subject to the curse of dimensionality. If 15 nodes are to be connected in a radial way with 3 different branch sizes available, there are $2 * 10^{15}$ possible trees connecting the nodes. For each of them, there are $5 * 10^6$ different possibilities for branch sizes. There are thus 10^{22} different possible networks, without even taking investment timing into account. To avoid this computational intractability, decision making is separated in four. Firstly, the architecture is determined. Then, all possible combinations of branch sizes are generated and constraints are evaluated for each alternative. The timing of investments is finally decided. The following subsections are dedicated to each subproblem.

2.2.1 Network routing

In (**1**), OPEX and CAPEX are simultaneously minimized, which are conflicting objectives as the cheapest lines (the ones with smallest cross-sections) are also the ones that generate the highest losses. Nevertheless, preliminary tests have shown that the cost of losses is always an order of magnitude below the cost of investments. Investment minimization may thus be considered alone in first approximation. Cost of investment in new lines or reinforcement of existing ones depends on the cross-section of the conductor and the length of the line. As network sizing has not been done yet, only the total length of the lines can be minimized . The problem is thus reduced to a Minimum Spanning Tree (MST) problem. The Kruskal algorithm is used to find the MST [14]. First, the $n * (n-1)/2$ possible branches between n nodes are defined. Then, the Kruskal algorithm chooses the routes in a greedy way [14]. The center of the graph is defined as the node with the smallest eccentricity, that is, with

the smallest maximum distance to any other node of the network. This node will be the feeding node of the network, i.e. where the necessary generation is placed. It is further called the source node. This heuristic decision is motivated by the fact that this node is likely to be a good position for a generator as it minimizes the distance between this generator and any load point, hence reducing voltage drops and losses. In an expansion planning, the feeding node of the network is already existing and we have to consider it as the source node, whether it is the center of the graph or not. Data about graph connectivity is stored in a connectivity matrix $\mathcal{C}$ $[n \times n]$, which is the output of the 'Network routing' subproblem (see Fig. 2.2). Node i is said to be the feeding node of node j if there is a branch between both and i is upstream from j relative to the source node. $\mathcal{C}$ is a defined as follows (0.7):

$$\mathcal{C}_{i,j} = \begin{cases} 1 & \text{if } i \text{ is the feeding node of } j \\ -1 & \text{if } j \text{ is the feeding node of } i \\ 0 & \text{otherwise} \end{cases} \tag{0.7}$$

2.2.2 Network sizing

The goal here is to enumerate the different possible network alternatives with branch sizes chosen among a set $\mathcal{B}$ of branches. Let $n_{\mathcal{B}}$ be the cardinality of this set. With $n-1$ branches, there are $n_{\mathcal{B}}^{n-1}$ choices for network sizing, which rapidly grows with an increase in the amount of available conductors or nodes. Again, a decomposition technique is proposed to reduce computational burden, which consists of three steps:

- Feeder decomposition
- Decreasing size of branches
- Section decomposition

First, the radial nature of the network can be exploited. Indeed, power flows on one feeder neither influence power flows nor voltage plan on adjacent feeders. Feeders can thus be considered as independent networks that can be optimized separately. Then, as generation is located at the center of the network, power flows are always directed from the center to the extreme nodes of the network. This means that current flowing in the branches may only increase when getting closer to the center. This implies that a particular branch size should always be greater than or equal to the size of any branch located downstream. Finally, the search space is further reduced by specifying that branches located on the same section should have the same size. A section of a feeder is defined as a set of branches of this feeder with no junction. In the network shown on Fig. 3, there are 2 feeders. The 2 feeders connect the nodes $[1{-}10{-}11{-}12{-}13{-}14{-}15{-}16{-}17{-}18{-}19{-}20]$ and $[1{-}8{-}6{-}7{-}5{-}4{-}3{-}2{-}9]$

respectively. One section is for example $[1-8-6]$. The output of this subblock is a set $\boldsymbol{\mathcal{S}}$ of n_{alt} matrices B_k , each one representing the branch size of each network alternative (see Fig. 2.2).

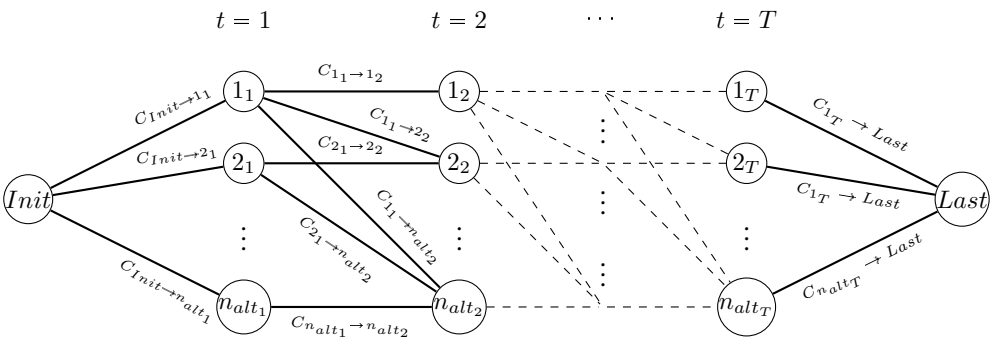

Fig. 2.1: Graph $\boldsymbol{\mathcal{T}}$ of the transition costs between different network alternatives at successive timesteps

2.2.3 Constraints verification and transition costs

There is now a set of n_{alt} network alternatives. A network alternative is characterized by its connectivity matrix, common to all alternatives, and its matrix B, which differs from one alternative to another. Constraint (**2**) is always respected with the Kruskal algorithm presented above. Remaining constraints may be divided in two types. *Static* constraints (**3**) to (**5**), related to power flows and equipment limits, must be ensured *at each timestep* while the *transition* constraint (**6**) must hold *between each two successive timesteps*. Let alternative k be considered at timestep t and alternative l at timestep t+1, $k, l \in 1, ..., n_{alt}$. This particular transition is written $k_t \to l_{t+1}$. There are three verifications to make:

1. Constraints (**3**) to (**5**) hold for alternative k at t
2. Constraints (**3**) to (**5**) hold for alternative l at $t+1$
3. Constraint(**6**) holds from k to l

If these three steps are respected, $i_t \to j_{t+1}$ is assigned a finite transition cost $C_{k_t\to l_{t+1}}$. It includes the reinforcement cost from i to j and the operational cost during timestep $t+1$. The former is the cost of additional conductor. The latter is the cost of losses on network l with particular load consumptions at all nodes during timestep $t+1$,$\{\overline{S}_{t+1,1}, ..., \overline{S}_{t+1,n}\}$. If one of the three steps is not respected, $C_{k_t\to l_{t+1}} = \infty$.

The output of this subblock is the transition graph $\mathcal{T}$ (see Fig. 2.2) .On this graph $\mathcal{T}$, each node represents a network alternative at a given timestep. An edge between nodes k_t and l_{t+1} has a weight equal to $C_{k_t \to l_{t+1}}$, thus representing the evolution from alternative k to alternative l for branches sizes. Two additional nodes are defined: $Init$ corresponds to the initial situation before the beginning of planning horizon (timestep 0) when there is no network. $C_{Init \to k_1} \quad k \in 1, ..., n_{alt}$ thus comprises the total cost of building particular alternative k plus the cost of losses on this particular network at first timestep. Node $Last$ represents the situation after timestep T. $C_{k_T \to Last}$ is set to zero as there are no further investments considered after the end of planning horizon.

2.2.4 Investment timing with dynamic programming

As mentioned in the introduction, the goal of this planning is to determine not only a network able to supply power demand at the beginning of the planning horizon, but also to decide the reinforcements that will be made afterwards to cope with a growing demand from the nodes.
Once the transition graph has been defined, the least-cost sequence of investment is still to be found. As mentioned in the beginning of this paper, a dynamic programming approach is chosen to handle this multistage problem, in a similar way to [78]. This approach is adapted to problems to which Bellman's principle of optimality applies. This principle states that at any timestep of a multistage decision making problem, the optimal decision policy for future timesteps should not depend on previously made decisions but only on the current state of the system [15]. This is the case for this problem as future investment and operational costs only depend on the current state of the system, not on the way it got at this current state. In this case, the state variables x_t of the system are the set of branches sizes at a given timestep $t \in 1, ..., T$ and the decision variables are the reinforcement decisions u_t. The state equation can be written in a compact form [79] (7).

$$x_t = x_{t-1} + u_t; \tag{7}$$

The minimization objective may be written as follows (8), with $C_{opt}(x_0)$ the optimal solution cost for the whole planning horizon given the initial state x_0 for which there is no network yet.

$$C_{opt}(x_0) = \min_{u_1,...,u_T} \sum_{t \in 1,...,T} \text{Cost}(u_t) \tag{8}$$

The idea behind dynamic programming is to make use of Bellman's principle of optimality to rewrite (8) in a recursive way by defining the function $f_{min}(x_t)$ as the optimal solution cost for all $\tau \geqslant t$ given the state x_t (9). This form is called *Bellman Optimality Equation* [79]. It can be interpreted as follows: at each timestep,

the optimal solution cost for future timesteps is the minimum of the sum of current decision cost and the optimal solution cost at the next timestep given the state in which current decision will bring the system. x_{t+1} is obtained from state x_t and decision u_{t+1} with the state equation (7). $C_{x_t \to x_{t+1}}$ is the transition cost defined in subsection 2.2.3. At the last timestep, $f_{min}(x_T) = 0$.

$$f_{min}(x_t) = \min_{u_{t+1}} [\ C_{x_t \to x_{t+1}} + f_{min}(x_{t+1})\ ] \tag{9}$$

The problem is thus solved in an iterative way. To do that, Dijkstra's algorithm [14] is applied to the previously defined transition graph $\mathcal{T}$. As a matter of fact, this algorithm is based on the same recursive principle as Bellman Optimality Equation. The output of this subblock is the set $\mathcal{U}$ of investment decisions with their respective timing (see Fig. 2.2).
It might be objected that a simpler, blind policy could be applied to decide the timing of investments. Such policy consists in making investments as late as possible, i.e. when constraints are not satisfied and investments are needed to relieve constraint violations. This accounts for the fact that the net present value of a particular investment is decreasing with the time of investment. Nonetheless, anticipating line reinforcements can help reduce losses, hence operational costs, even when constraints are not yet violated. There might thus be a trade-off between these two opposite effects. Dynamic programming is suited to find such a trade-off thanks to the consideration of the simultaneous impact of present and future decisions on the global net present value.

2.2.5 Global structure of the planning tool

In previous subsections, the four different subblocks of the planning tool have been defined. The following diagram (Fig. 2.2) summarizes the articulation of these subblocks, the three types of input data they use and the information they exchange. The output is the set $\mathcal{U}$ of investment decisions. As mentionned in section (2.1), an investment decision mentions the reinforcement (conductor size increase), the line being concerned by this reinforcement and the timestep at which the investment is made.

2.3 Case-study

The planning tool presented in section (2.2) is applied to a 20-node dataset used in [22]. This dataset, including cartesian coordinates of nodes, power consumptions and conductor data, can be found in [21]. Network upgrading can be realized either by reconductoring or reinforcement. In the former case, the existing conductor is

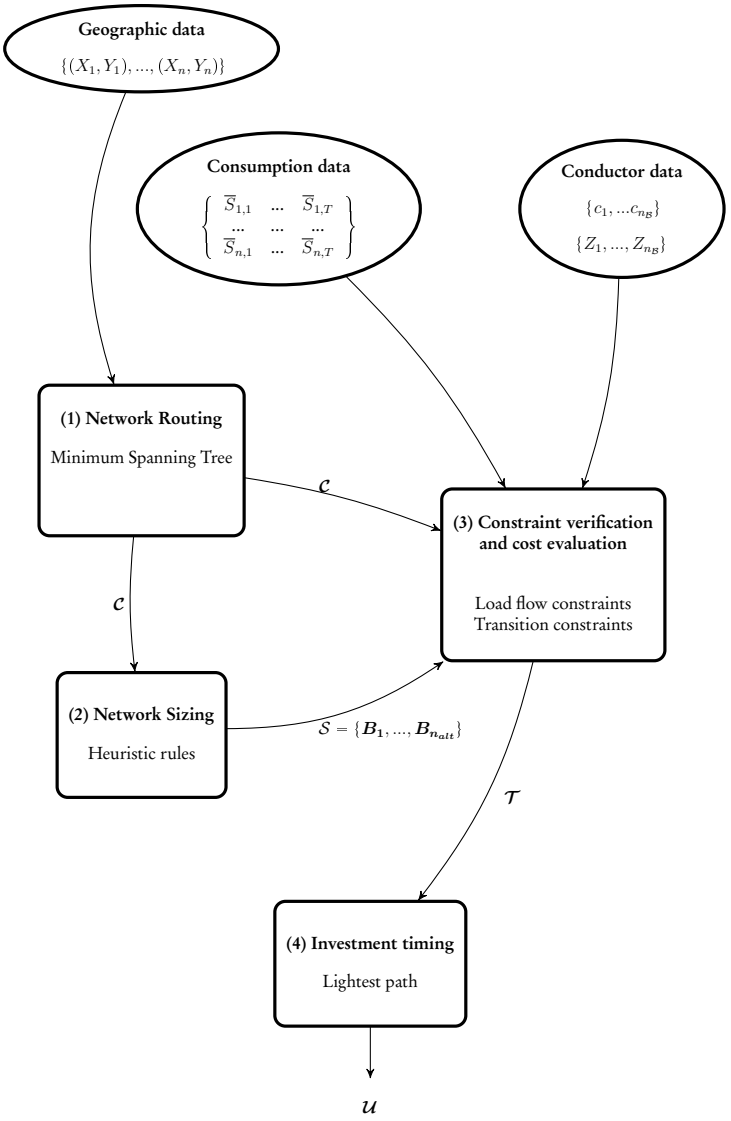

Fig. 2.2: The problem has 3 different types of data. There are 4 subblocks that perform the following functions: (1) Network routing, (2) Network sizing, (3) Constraint verification and cost evaluation and (4) Investment timing. The output is the set $\boldsymbol{\mathcal{U}}$ of investment decisions with their respective timing.

removed and replaced by a conductor of bigger capacity. In the latter case, a conductor is added in parallel to the existing one to reduce the total impedance of the line and increase its ampacity. In this study, only reinforcement is considered. A single conductor type is used, and up to three such conductors can be placed in parallel, which gives three possible branch sizes, named hereafter 1, 2 and 3. In this case,

the impedance of size 2 and 3 lines is thus half and a third of size 1 lines impedance respectively. In subsection 2.2.2, a rule has been introduced to limit the size of the search space: every branch of a section of a feeder should have the same size. For this case study, the relevance of this rule is tested by running 2 planning studies, one with this rule (case 1) and the other one without (case 2). The planning horizon is set to 20 years. Load consumption is growing at at constant and uniform yearly rate of 10%, with consumptions at the beginning of the planning horizon being the same as in [21], for a total initial load of 4.9 $[MVA]$. Relevant parameters for the planning study are presented in Table 2.1. The cost of lines is made of two components. The first one is a fixed one, called the building cost of line in Table 2.1. It is common to all lines and corresponds to pole installation. The second component is the cost of conductors. If is obtained by multiplying the unit conductor cost by the amount of lines in parallel (1,2 or 3). Both cases have been run on a 2.7Ghz Intel Core i7 processor with 8Go memory.

Planning horizon	20	$[Years]$
Interest rate	10%	
Cost of losses	60	$[\$/MWh]$
Yearly load growth	10%	
Base voltage	13.8	$[kV]$
Conductor resistance	0.64	$[\Omega/km]$
Conductor reactance	0.45	$[\Omega/km]$
Conductor ampacity	214	$[A]$
Building cost of line	23000	$[\$/km]$
Unit conductor cost	8220	$[\$/km]$

Table 2.1: Parameters used for the planning study

Initial and final network (year 1 and year 20) are presented for cases 1 and 2 in Table 2.4. Tables 2.2 and 2.3 illustrate the differences in the sequences of investment for cases 1 and 2, with the third line of these tables representing the upgrade in the line size. Fig. 2.3 shows the final network for case 2, with network graph and branch sizes.

Branch	2-4	4-5	5-6	2-9	2-9
Year	6	6	6	9	10
Reinf.	$2 \rightarrow 3$	$2 \rightarrow 3$	$2 \rightarrow 3$	$1 \rightarrow 2$	$2 \rightarrow 3$

Table 2.2: Investment sequence: case 1

B	2-4	6-8	5-6	4-5	2-9	2-4	2-9
Y	2	2	3	5	6	8	12
R	$1 \rightarrow 2$	$2 \rightarrow 3$	$2 \rightarrow 3$	$2 \rightarrow 3$	$1 \rightarrow 2$	$2 \rightarrow 3$	$2 \rightarrow 3$

Table 2.3: Investment sequence: case 2

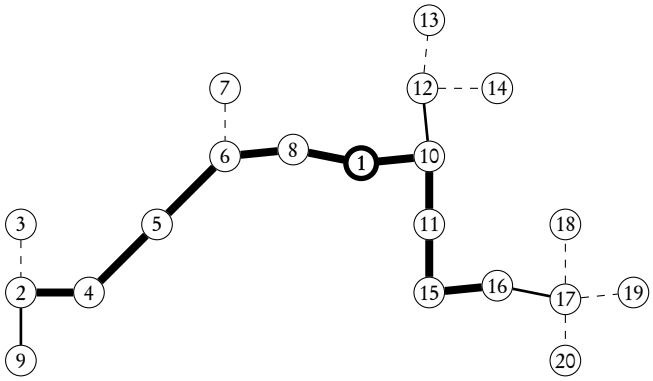

Fig. 2.3: Final network for case 2. Thick lines represent branches of size 3, normal lines branches of size 2 and dashed lines branches of size 1. Node 1 is the center of the network, where generation is placed.

Several observations can be made for results in Table 2.4. First, initial and final solutions are very close for both cases. Then, branch (16-17) can have a lower size by relaxing the aforementioned rule. Furthermore, the removal of this rule allows to have a more progressive investment sequence (Tables 2.3 and 2.4) for case 2. This means that some costs happen later in time. These costs thus contribute less to the total NPV of the system because of the time value of money. The cost for case 1 is 1393 $[k\$]$ while it is 1385 $[k\$]$ for case 2, which makes a 0.6% difference. Execution times are respectively $200[s]$ and $467[s]$ for cases 1 and 2. This comparative case study thus shows that the rule that has been imposed to limit computational burden does not yield a significant error while substantially reducing execution time. However, it has to be confirmed for bigger problems with more nodes and longer feeder sections.

	Case 1		Case 2	
Branch	Year 1	Year 20	Year 1	Year 20
1-8	3	3	3	3
8-6	3	3	2	3
6-7	1	1	1	1
6-5	2	3	2	3
5-4	2	3	2	3
4-2	2	3	1	3
2-3	1	1	1	1
2-9	1	3	1	3
1-10	3	3	3	3
10-11	2	2	2	2
11-15	2	2	2	2
15-16	2	2	2	2
16-17	2	2	1	1
17-18	1	1	1	1
17-19	1	1	1	1
17-20	1	1	1	1
10-12	1	1	1	1
12-13	1	1	1	1
12-14	1	1	1	1

Table 2.4: Branches size at the beginning of years 1 and 20 where reinforcements take place. Gray cells show differences between the 2 cases

2.4 Discussion

The proposed approach has introduced some simplifications. As a matter of fact, network sizing and network routing have been decoupled to limit the computational burden. However, it may introduce a loss of optimality because the behaviour of a network depends not only on its graph but also on the size of its branches. By defining the graph first, other topologies are dismissed that may lead, with appropriate branch sizing, to better solutions.

Limiting factors for the problem are mainly the amount of nodes and the amount of available conductors. The duration of the planning study is less critical regarding problem size as the number of evaluations to make grows linearly with the amount of planning steps, while a growing amount of nodes or available conductors produces a combinatorial explosion of the amount of network alternatives to evaluate at each timestep. For example, adding an extra conductor type (four instead of three types) multiplies the amount of network alternatives by a factor 5 in the case-study presented in the previous section.

Hence, the biggest limitation concerns the size of the problems that can be solved: this approach, in its current form, did not converge in less than one day for a 40-node

network. Furthermore, we did not consider generation planning yet.
A last limitation is the fact that the proposed approach is not suited for meshed distribution networks. Indeed, the Backward-Forward Sweep Algorithm form used in the present case only works with radial networks. However, it can be extended to weakly meshed network as described in [103].
The field of approximate dynamic programming gathers a set of approximation methods to cope with the traditional curse of dimensionality encountered in dynamic programming. Further research might thus be oriented towards the investigation of such methods to cope with problems of bigger size. However, for the rest of this work, we decide to focus on convex optimization-based formulations to tackle the joint planning problem. Indeed, recent developments in convex power flow formulations offer interesting perspectives for the joint planning of microgrids.

Convex optimization background

3

Convex optimization presents two major advantages over non-convex optimization. First, every optimum is necessarily a global one. Then, there are efficient algorithms allowing to solve large convex problems, which has been made possible by the development of polynomial-time interior-point methods for linear, second order cone and semidefinite problems [93]. However, the autonomous microgrid planning problem is not convex. Hence, its needs to be *convexified* in order to make use of the powerful convex optimization tools.
This chapter aims at providing an introduction to the mathematical optimization tools used in the subsequent chapters in order to make the present document self-contained. It is by no means intended to be an exhaustive treatment of such a wide-ranging topic as convex optimization. The developments presented in this chapter are partly based on reference [16], to which the interested reader is referred for in-depth coverage of the subject.

3.1 Constrained optimization

3.1.1 Problem formulation

Solving a constrained optimization problem consists in selecting, among a set of possible *decisions* (or actions), those that result in the *best possible outcome* given predefined *limitations*. Depending on the context, we may want to *maximize* or *minimize* a certain quantity that is function of the aforementioned decisions. For the rest of this chapter, we will focus on minimization problems.
A constrained minimization problem can be mathematically formulated as follows, with $\mathbf{x} \in \mathbb{R}^n$ a vector of n real-valued variables, $f(\mathbf{x})$ a real valued function,

$g(\mathbf{x}) : \mathbb{R}^n \mapsto \mathbb{R}^E$ and $h(\mathbf{x}) : \mathbb{R}^n \mapsto \mathbb{R}^I$ vector-valued functions of $\mathbf{x}$:

$$\begin{aligned} &\min_{\mathbf{x}} f(\mathbf{x}) \\ &\text{s.t.} \\ &g_i(\mathbf{x}) = 0 \quad i = 1, ..., E \\ &h_i(\mathbf{x}) \leqslant 0 \quad i = 1, ..., I \end{aligned} \tag{10}$$

The set of possible decisions is represented by the variables $\mathbf{x}$, the outcome of the problem is the objective function $f(\mathbf{x})$ whose value depends on $\mathbf{x}$ and the context and the limitations are modelled by equality and inequality constraints, respectively $g(\mathbf{x})$ and $h(\mathbf{x})$. Optimization problems are characterized by the form of their objective and constraint functions, hence there is a rich variety of classes: linear optimization, non-linear optimization, quadratic optimization, non-convex optimization, polynomial optimization, etc. We will focus on the distinction between convex and non-convex problems.

3.1.2 Feasible set

Constraints $g(\mathbf{x}) = 0$ and $h(\mathbf{x}) \leqslant 0$ in (10) define the *feasible set* $\mathcal{F}$ of the problem, i.e. a subset of $\mathbb{R}^n$ containing the allowed values for $\mathbf{x}$, as expressed hereunder

$$\mathcal{F} = \{\mathbf{x} \in \mathbb{R}^n | g_i(\mathbf{x}) = 0 \quad i = 1, ..., E \wedge h(\mathbf{x}) \leqslant 0 \quad i = 1, ..., I\} \tag{11}$$

The problem (10) may thus be rewritten as

$$\min_{\mathbf{x} \in \mathcal{F}} f(\mathbf{x}) \tag{12}$$

An example of feasible set is given on Fig. 3.1 in the case of a two-dimensional problem with variables $\mathbf{x} = [x_1 \ x_2]$, no equality constraints and a set of linear inequality constraints.

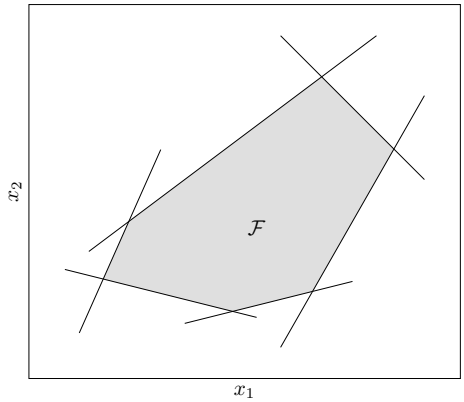

Fig. 3.1: Example of a 2-D feasible set determined by linear inequalities

3.1.3 Objective function minima

In general, an objective function $f(\mathbf{x})$ may present several minima on a given feasible set $\mathcal{F}$. We can distinguish *local minima* and *global minima*.
A local minimum $\mathbf{x}_l^*$ is a point belonging to $\mathcal{F}$ such that $\exists \delta > 0 : \|(\mathbf{x} - \mathbf{x}_l^*)\| \leqslant \delta \Rightarrow f(\mathbf{x}_l^*) \leqslant f(\mathbf{x})$ for $\mathbf{x} \in \mathcal{F}$, i.e. there exists a neighbourhood of $\mathbf{x}_l^*$ in which $f(\mathbf{x}_l^*)$ is the smallest value of $f(\mathbf{x})$.
A global minimum $\mathbf{x}_g^*$ is a point of $\mathcal{F}$ that corresponds to the smallest value of $f(\mathbf{x})$ on its whole feasible set, i.e. $f(\mathbf{x}_g^*) \leqslant f(\mathbf{x}) \forall \mathbf{x} \in \mathcal{F}$. The difference between local and global minima is illustrated on Fig. 3.2.

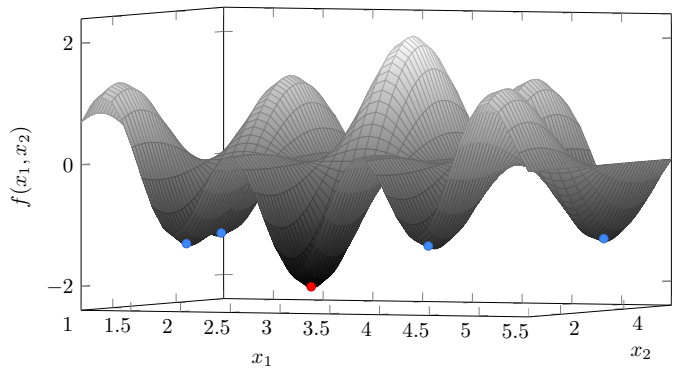

Fig. 3.2: Illustration of local (blue dots) and global (red dot) minima

3.2 Convexity in optimization

3.2.1 Convex sets and functions

A convex set $\mathcal{C}$ is such that the line segment joining any two points of $\mathcal{C}$ is entirely contained in $\mathcal{C}$ [16]. This is mathematically written as:

$$\mathcal{C} \text{ is convex } \Leftrightarrow x\theta + y(1-\theta) \in \mathcal{C} \quad \forall x, y \in \mathcal{C}, 0 \leqslant \theta \leqslant 1 \tag{13}$$

An important property of convex sets is that the intersection of convex sets is also a convex set. Examples of convex and non-convex sets are given on Fig. 3.3.

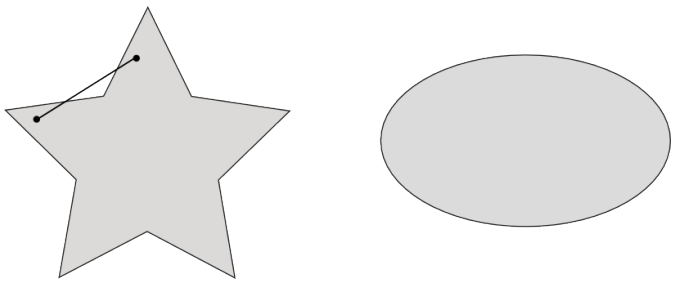

Fig. 3.3: Non-convex set (left) and convex set (right) in two-dimension

A function $f : \mathbb{R}^n \mapsto \mathbb{R}$ is convex if its domain is a convex set and the line segment joining any two points of its graph lies above the function [16]. For $x_1, x_2 \in \text{dom}(f)$, this is formally defined as

$$f \text{ is convex } \Leftrightarrow f(\theta x_1 + (1-\theta)x_2) \leqslant \theta f(x_1) + (1-\theta)f(x_2) \quad 0 \leqslant \theta \leqslant 1 \tag{14}$$

This is equivalently expressed by the condition that the *epigraph* of the function, i.e. the subspace of $\mathbb{R}^{n+1}$ containing all points located above the graph of the function, is a convex set [16]. These two equivalent properties are illustrated on Fig. 3.4

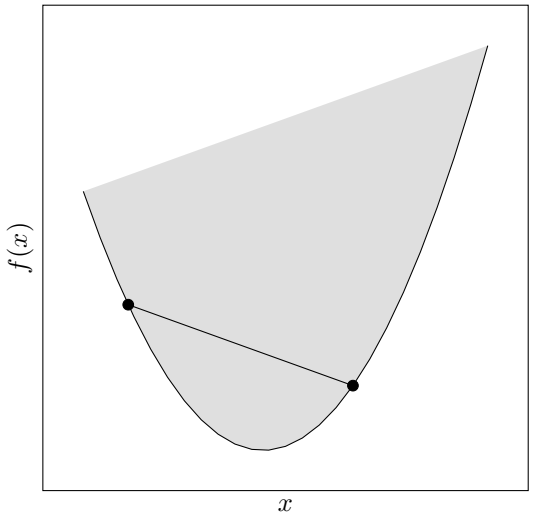

Fig. 3.4: The epigraph (shaded surface) of the convex function $f(x)$ is a convex set

3.2.2 Convex optimization problems

Characterization

A convex optimization problem is such that its objective function $f(\mathbf{x})$ and its feasible set are both convex [16]. A *convex constraint* defines a convex set. As mentioned above, the intersection of convex sets is also convex. Hence, if all constraints of the problem are convex, the feasible set $\mathcal{F}$ is also convex.
The only convex equality constraints $g_i(\mathbf{x}) = 0$ are linear ones. As a matter of fact, with $\mathbf{x} \in \mathbb{R}^n$, $g_i(\mathbf{x}) = 0$ defines an hypersurface in $\mathbb{R}^{n+1}$ (e.g. a curve in a plane, a surface in the three-dimensional space, etc). For this hypersurface to include all line segments connecting any two of its points, it necessarily needs to be an hyperplane defined by a linear equation of the form $a^T\mathbf{x} + b = 0$, $a \in \mathbb{R}^n$ and $b \in \mathbb{R}$ being constant. There is a wider range of convex inequality constraints as $h_i(\mathbf{x}) \leqslant 0$ is convex as soon as $h_i(\mathbf{x})$ is.
A convex optimization problem is thus of the following form with $f(\mathbf{x})$ and $h_i(\mathbf{x})$ convex functions:

$$\begin{aligned} &\min_{\mathbf{x}} f(\mathbf{x}) \\ &\text{s.t.} \\ &g_i(\mathbf{x}) = a_i^T\mathbf{x} + b_i = 0 \quad i = 1, ..., E \\ &h_i(\mathbf{x}) \leqslant 0 \quad i = 1, ..., I \end{aligned} \tag{15}$$

Global optimality

Convex problems have a highly valuable property in terms of optimization: any local minimum is also a global minimum [16]. Looking back at Fig. 3.2, it is easily seen that this function of two variables is not convex and presents several local minima with a function value strictly superior to that at the global minimum.

Classes of convex problems

We consider three classes of convex problems in this work:

(i) Linear Problems (LP)
(ii) Second-Order Cone Problems (SOCP)
(iii) SemiDefinite Problems (SDP)

These problems all have linear objective functions and equality constraints and differ in their inequality constraints.
A Linear Problem has linear inequality constraints of the form:

$$a_i^T \mathbf{x} + b_i \leqslant 0 \quad i = 1, ..., I \tag{16}$$

Second-order cone problems have inequality constraints of the following form, $A_i,\ C_i \in \mathbb{R}^{m \times n}$ and $b_i,\ d_i \in \mathbb{R}^m$[93]:

$$\| A_i^T \mathbf{x} + b_i \| \leqslant D_i^T \mathbf{x} + d_i \quad i = 1, ..., I \tag{17}$$

With $\mathbf{x} \in \mathbb{R}^n$, they rely on a second-order cone (also called Lorentz cone or ice-cream cone) in $\mathbb{R}^{m+1}$, for which a three-dimensional example is given on Fig. 3.5.

A semidefinite problem is expressed in its standard form as follows [93]. $\mathbf{X}$ is the matrix of variables, tr(.) is the trace operator and $\mathbf{X} \succeq 0$ means that the matrix $\mathbf{X}$ is positive-semidefinite.

$$\begin{aligned} &\min_{\mathbf{X}} \operatorname{tr}(C^* \mathbf{X}) \\ \text{s.t.} \quad &\\ &\operatorname{tr}(A_i^* \mathbf{X}) \leqslant b_i \\ &\mathbf{X} \succeq 0 \end{aligned} \tag{18}$$

It can be shown that LP is a particular case of SOCP which in turn is a particular case of SDP [93], i.e. $LP \subseteq SOCP \subseteq SDP$.

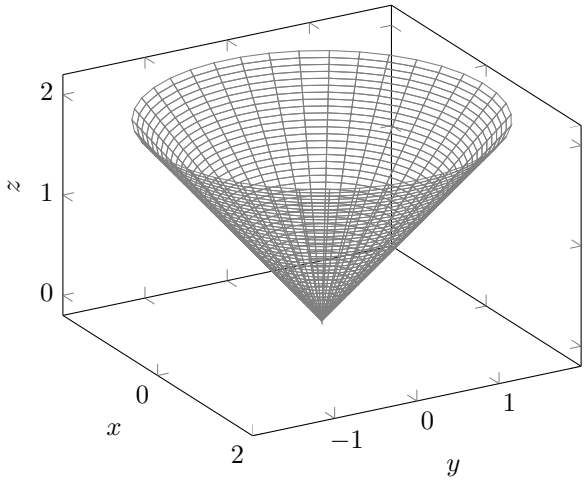

Fig. 3.5: Three-dimensional second-order cone defined by $\sqrt{x^2 + y^2} \leqslant z$,

3.3 From non-convex to convex problems

3.3.1 Relaxation and approximation

As it is shown in chapter 4, the autonomous microgrid planning problem is non-convex due to its constraints. We thus want to make it convex to benefit from efficient optimization algorithms. This can be done in two ways: *relaxing* or *approximating* the constraints. In the former case, non-convex constraints are replaced by convex constraints that are *weaker*, i.e. less stringent than the original ones. In the latter case, non-convex constraints are replaced by convex ones that are not necessarily weaker. This means that relaxing constraints does not remove any part of the feasible space while approximating them might, which is illustrated on Fig. 3.6.

Given that a relaxation does not remove any part of the feasible space of the original problem, its minimal objective value $f(\mathbf{x}_R^*)$ is a lower bound (as we are solving a minimization problem) on the actual minimal objective value $f(\mathbf{x}^*)$ of the original problem [16]:

$$f(\mathbf{x}_R^*) \leqslant f(\mathbf{x}^*) \tag{19}$$

This is easily understandable as the relaxed feasible space $\mathcal{F}^R$ includes the whole original feasible space $\mathcal{F}$. Hence, the minimal objective value $f(\mathbf{x}_R^*)$ is at most $f(\mathbf{x}^*)$ and might be inferior if $\mathbf{x}_R^* \in \mathcal{F}^R \backslash \mathcal{F}$.

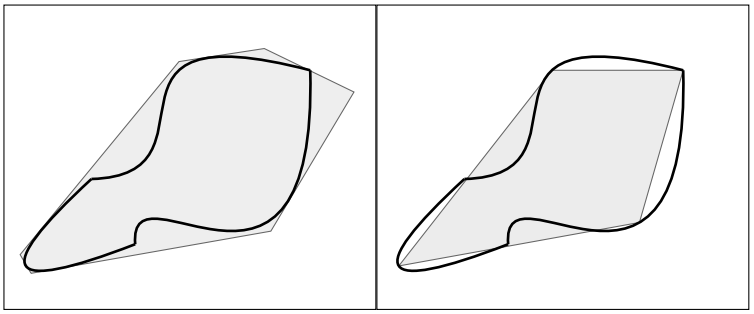

Fig. 3.6: The original non-convex feasible space is enclosed by the thick curve. The relaxed and approximated feasible spaces are in gray. (Left) A linearly relaxed feasible space that contains the whole original feasible space (Right) The approximated feasible space removes some parts of the original feasible space

3.3.2 Sources of non-convexity and convexification techniques

In this section, we address reformulation and convexification techniques that will be used in the various models presented in chapter 4.

Linear disjunctive reformulation for mixed-integer bilinear equality constraints

As it has been mentioned above, some investment decisions regarding the design of microgrid equipments are discrete to represent the finite set of available sizes, e.g. for electrical conductors. This introduces an additional complexity in the equations modelling the microgrid and its investment decisions. Let us for example consider equation (**4.4**), presented in chapter 4, that we reproduce here :

$$p_{ij} + p_{ji} = R_l l_{ij} \tag{20}$$

If we consider a given line with a resistance of $R_l[\Omega]$ between nodes i and j, equation (**20**) states that the losses on this line, expressed by the term $p_{ij} + p_{ji}$, are equal to the product of R_l and l_{ij}, respectively the line resistance and line current squared amplitude. Now, let us consider that the presence of a line between nodes i and j is no longer given as an input of the problem but depends on a decision variable μ_{ij}. This binary variable determines whether a line is placed between nodes i and j ($\mu_{ij} = 1$) or not ($\mu_{ij} = 0$). The resistance between nodes i and j is now variable and we denote it by the variable R_{ij} . There are two possible situations.

1. A line is built ($\mu ij = 1$) and the resistance is equal to R_l

2. No line is built ($\mu_{ij} = 0$) and the resistance is infinite. In this situation, the constraint does not apply as there should be no power flow, hence no losses, without any line.

This can be expressed by $R_{ij} = R_l/\mu_{ij}$. Then, (20) becomes

$$p_{ij} + p_{ji} = \frac{R_l}{\mu_{ij}} l_{ij} \Leftrightarrow \mu_{ij}(p_{ij} + p_{ji}) = R_l l_{ij} \tag{21}$$

While (20) was a linear equality constraint, we now have to deal with bilinear terms including continuous variables p_{ij} and p_{ji} and the binary variable μ_{ij} in (21). This constraint expresses a disjunction, i.e. it represents two different and disconnected parts of the feasible space, depending on the investment decision value μ_{ij}. We can reformulate (21) with two inequality constraints to get rid of bilinear terms. In the following, the operators $\bar{.}$ and $\underline{.}$ represent the upper and lower bound of a given expression respectively, which are constants that are computed offline.

$$(1-\mu_{ij})(\underline{R_l l_{ij}} - \overline{(p_{ij}+p_{ji})}) \leqslant R_l l_{ij} - (p_{ij}+p_{ji}) \leqslant (1-\mu_{ij})(\overline{R_l l_{ij}} - \underline{(p_{ij}+p_{ji})}) \tag{22}$$

The equivalence of (21) and (22) is easily checked. If $\mu_{ij} = 0$ then $(p_{ij}+p_{ji})$ and $R_l l_{ij}$ are not constrained, i.e. they may take any value in $(\underline{(p_{ij}+p_{ji})}, \overline{(p_{ij}+p_{ji})})$and $(\underline{R_l l_{ij}}, \overline{R_l l_{ij}})$ respectively. Hence $R_l l_{ij} - (p_{ij}+p_{ji})$ should be able to vary between $(\underline{R_l l_{ij}} - \overline{(p_{ij}+p_{ji})}, \overline{R_l l_{ij}} - \underline{(p_{ij}+p_{ji})})$ which is expressed by the inequalities. When $\mu_{ij} = 1$ then both left- and right-hand terms fall to 0 which implies $(p_{ij}+p_{ji}) = R_l l_{ij}$.

Lift-and-project relaxation

Products of continuous variables may be transformed with a *lift-and-project* relaxation. If we take x and y , both continuous variables and we want to remove a xy term of a constraint, we first *lift* it in a higher dimension space by introducing a new variable $z = xy$ and replacing all xy terms by z, which linearizes bilinear terms. The solution to the problem is then *projected* back onto the original (x, y) space to recover values of the true variables of the problem. While the linear disjunctive reformulation presented above is exact, the lift-and-project method is a relaxation, i.e. it is not necessarily exact as there might not be a one-to-one mapping between z and (x, y) [93]. The lift-and-project relaxation may also be used for any type of non-linear terms, such as quadratic terms (see for example squared amplitudes of currents and voltages in the (4) model presented in chapter 4).

Integrality constraints

Another source of non-convexity lies in the integrality constraints. These force a subset of the variables to be integer (binary variables are a particular case of integer variables). The resulting feasible space is non-connected, which makes it inherently non-convex. We illustrate this on Fig. 3.7.

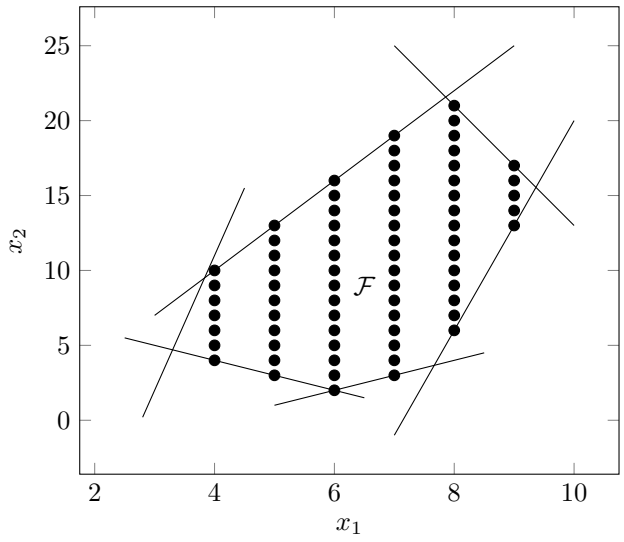

Fig. 3.7: Mixed-integer feasible set obtained by taking the feasible set described on Fig. 3.1 and adding integrality constraints on x_1 and x_2. The resulting feasible set, indicated by black dots, is clearly non-connected, hence non-convex

A mixed-integer problem is thus non-convex, even though all constraints but integrality constraints are convex.
In the following section, we describe the basic principles of the *branch-and-bound* (B&B) algorithm which allows to deal with mixed-integer problems.

3.3.3 Branch-and-bound algorithm

Mixed-integer problems are most of the time solved through the use of the B&B method [24]. We describe hereunder the basic operations of this algorithm based on [12] and we give an illustrating example inspired by the same reference. The interested reader is referred to [98] for a more detailed treatment of this topic.
The principle of the B&B algorithm is to solve a succession of continuous relaxations of the original mixed-integer problem until all integrality constraints are satisfied. It

relies on the fact that for a given problem P, the minimal value of a relaxation f_R^* acts as a lower bound on the minimal value of the actual problem: $f_R^* \leqslant f^*$ (c.f. above). The basic operations of this algorithm are the following:

- Determine a feasible solution to the original problem. It is called the incumbent and its objective value acts as an upper bound UB on the minimal objective value of the problem.
- Partition the feasible set, i.e. define a series of subproblems having the same objective but smaller, disconnected feasible spaces.
- For every subproblem SP, obtain a lower bound f_{SP}^*, R on the optimal objective value by solving a continuous relaxation of the subproblem. There are three possible outcomes
  1. A fractional solution is found (i.e. including non-integer values for variables that should be integer in the original problem). If $f_{SP,R}^* \geqslant UB$, then the feasible space of this subproblem is discarded because $UB \leqslant f_{SP}^*, R \leqslant f_{SP}^*$, which means that we cannot hope to find a better integer solution than we already have with the current incumbent on this subspace. Otherwise a new branching is performed
  2. If no feasible solution is found, then the subspace is discarded as well
  3. If an integer feasible solution with a strictly smaller objective value than UB is found, then it becomes the new UB. Otherwise it is discarded. In both cases, no further branching is required from this subproblem.

An illustration of a simple B&B algorithm execution is given on Fig. 3.8.
Implementations of B&B algorithms largely vary from one application to another [24]. Several parameters may be adapted, such as the search direction in the B&B tree (breadth first versus depth first) or branching criteria. Furthermore, additional cuts (i.e. constraints) may be added during the algorithm execution to efficiently remove some parts of the feasible space, hence speeding the tree exploration, by using the results already obtained during the tree exploration. Those include Gomory cuts [2], flow cuts or zero-half cuts.

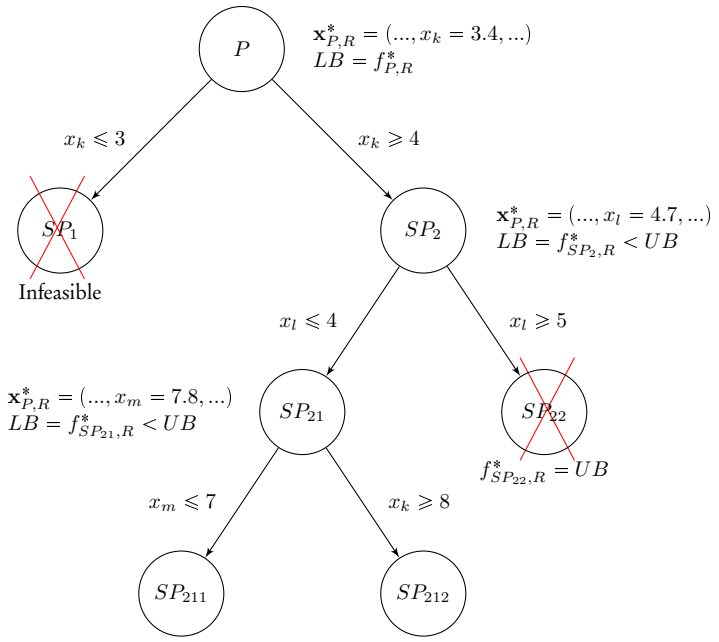

Fig. 3.8: Example of B&B algorithm execution. The tree represents the progressive partition of the initial feasible space
1) P is continuously relaxed and has a fractional solution: $x_k = 3.4$ while it should be integer. We *branch* on this variable and divide the feasible space in two parts: the first corresponds to $x_k \leqslant 3$ and the second one to $x_k \geqslant 4$
2) A continuous relaxation of SP_1 is solved and is infeasible, hence the corresponding subspace is discarded
3) The continuous relaxation of SP_2 also delivers an optimal solution that is fractional, hence a branching is performed on the x_l variable, creating two new subproblems
4) The continuous relaxation of SP_{22} has an optimal objective value equal to the current upper bound, hence it is discarded
5) The continuous relaxation of SP_{21} gives a fractional optimal solution, hence a branching is performed on the x_m variable, creating two new subproblems
6) The process continues until all parts of the feasible space have been discarded. The optimal solution to the original problem is the best integer solution found during the execution of the algorithm

Deterministic and convex formulations for the joint planning of autonomous microgrids

4

A preliminary and partial version of this chapter's content has been published as : B. Martin, E. D. Jaeger, and F. Glineur. Comparison of convex formulations for the joint planning of microgrids. In *CIRED - Open Access Proceedings Journal*, 2017(1):2174–2178, 2017. In particular, the real-world test-case and the use of Matpower to check the feasibility and accuracy of the planning solutions are new features of this thesis

Having introduced the necessary mathematical tools in chapter 3, we can now present the different planning models developed in this work.
First, we formulate a non-convex version of the joint planning problem. Then, we study various convex relaxations of power flow equations. This allows us to build a hierarchy of convex joint planning models. In a second phase, we test all these joint planning models on a real-world use case to assess the adequacy of their solution, the accuracy of power flow modelling and their runtime.

4.1 Definitions and modelling assumptions

This section defines the notations for the sets, parameters and variables that will be used throughout different formulations of the joint planning problem as well as the underlying modelling assumptions. All electric quantities are expressed in *per unit [pu]*. This is usual in power systems modelling because assets parameters values

(generators, lines,...) are similar to each other when expressed in pu, regardless of the rating of these assets. Furthermore, voltages remain close to the unity, hence reducing deviations in numeric values between different voltages and making the problem numerically better conditioned [52],[55].

4.1.1 Notations

A. Sets and related indices

$\mathcal{V}: \ i \in \mathcal{V}$	Set of vertices of the network
$\mathcal{E}: \ (i,j) \in \mathcal{E}$	Set of directed edges representing allowed lines location in the network
$\mathcal{G}: \ g \in \mathcal{G}$	Set of available generation technologies
$\mathcal{L}: \ l \in \mathcal{L}$	Set of available line types
$\mathcal{Y}: \ y \in \mathcal{Y}$	Set of years of the planning horizon
$\mathcal{T}: \ t \in \mathcal{T}$	Set of hourly timesteps of the planning horizon

B. Parameters

$n = \textbf{card}(\mathcal{V})$	Amount on nodes in the network
$\Lambda = \textbf{card}(\mathcal{L})$	Amount of different line types
D_{ij}	Distance between nodes i and j
H	Amount of simulated hours per year of the planning horizon
p_{it}^C, q_{it}^C	Active and reactive power consumption at node i at timestep t
g_l, b_l	Conductance and susceptance per unit length for line type l
r_l, x_l	Resistance and reactance per unit length for line type l
$\overline{S}_l$	Maximum apparent power for line type l
$\underline{v}$,$\overline{v}$	Min. and max. admissible voltage
Δ^θ	Max. admissible angle difference between two buses l
$\underline{p_g}^R, \overline{p_g}^R$	Min and max. rated power for units of generation technology g
$\overline{\overline{PF}}^g$	Min. power factor (inductive and reactive) for units of generation technology g
C_{gf}^{BG}	Fixed cost [MU] of building a technology g generator
C_{gv}^{BG}	Variable cost in MU per unit installed power of building a technology g generator
C_f^{BL}	Line structure cost in MU per unit length of building a line: excavation, pole installation
C_{lv}^{BL}	Conductor cost in MU per unit length of type l line
C_{gf}^P,C_{gv}^P	Fixed cost [MU] (resp. variable cost MU per unit produced power) of producing power for 1 hour with technology g generators
d	Discount rate

C. Variables

p^G_{igt}, q^G_{igt}	Active and reactive power production of a g technology generator located at node i at timestep t
p_{ijlt}, q_{ijlt}	Active and reactive power flowing from node i to node j on a type l line at timestep t
v_{it}	Voltage at node i at timestep t
θ_{ijt}	Voltage angle difference between nodes i and j at timestep t
$\lambda_{ijly} \in \{0,1\}$	Binary variable representing the presence or not of a type l line between nodes i and j at year y
$\omega_{ijly} \in \{0,1\}$	Binary variable indicating the presence of at least one line between nodes i and j at year y
γ_{igy}	Binary variable representing the decision to invest in a technology g generator located at node i during year y
ρ_{igy}	Rated power of technology g generator located at node i during year y
f_{ijy}	Fictitious flows used to ensure the connectivity of the network

The set of variables may be divided in two categories. The first one contains the investment decision variables, indexed over $\mathcal{Y}$: λ_{ijly} and ρ_{igy} (ω_{ijly} and f_{ijy} being auxiliary variables used to ensure connectivity of the network). The second category is composed of operational variables, indexed over $\mathcal{T}$: $p^G_{igt}, q^G_{igt}, p_{ijlt}, q_{ijlt}, v_{it}$ and θ_{ijt}.

4.1.2 Modelling assumptions

Time scales

We consider two time scales in the planning problem: the investment and the operational time scales. First, investments decisions are taken once a year throughout the planning horizon (Fig. 4.1, top). Then, we have to make a trade-off for the operational time scale resolution. It needs to be fine enough to capture the variation of loading conditions. However, we do not intend to model system dynamics nor transients but we rather want to assess the system 'steady-state' feasibility for the different forecast loading conditions. Furthermore, the finer the resolution, the heavier the computational burden. We thus choose to model a limited amount of representative days (e.g. weekday and weekend, winter and summer) on a hourly time scale (Fig.4.1, bottom).

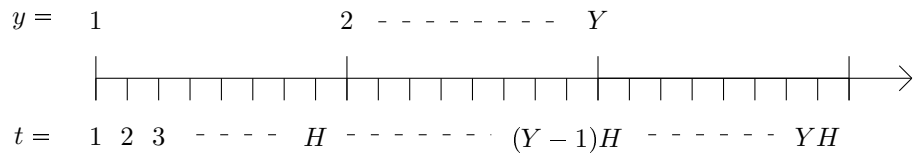

Fig. 4.1: Investment (top, yearly) and operational (bottom, hourly) time scales for the joint planning problem

Investment modelling

The decision to invest in some asset is intrinsically binary: either the investment is made or not. When the investment decision is taken (e.g. a line is built between nodes i and j), we consider that a choice is made between a finite set of options corresponding to a finite assets portfolio (e.g. a 100 mm^2 Aluminium Conductor Steel Reinforced cable is chosen among the following available sizes: 100,150 and 200 mm^2). Hence, the sizing variable is discrete for lines. However, regarding generation technologies that will be considered (Internal Combustion Engine (ICE), PV array,...), we consider that the available rated power range is wide enough to be considered as continuous.

Network modelling

As explained in the above paragraph, we consider a finite set of electric conductors for the wiring of the network. When planning investments in lines, there are two types of actions: *reinforcing* corresponds to adding an extra line in parallel of the existing ones in order to increase the available distribution capacity between two nodes, while *reconductoring* consists in removing existing conductors and replacing them by larger capacity conductors. In this context, we only consider reinforcement. Hence, a conductor may not be removed but new conductors may be added in parallel of existing ones. More precisely, there may be at most one line of each conductor type in parallel between two given nodes.
Hence, the power flow between two nodes is expressed as the sum of power flows on the parallel conductors between these nodes (eq. (**1.2**)) and each one of these flows has a non-zero value only if the investment in the corresponding conductor has been made ($\lambda_{ijly} = 1$ in eq. (**1.4**)).

The following hypotheses are made throughout the models presented in the rest of this work.

(i) The hourly timescale chosen at operational level implies that power system dynamics may be ignored. Hence the planning problem may be modelled as a

succession of steady states, which allows the use of the power flow equations framework.

(ii) Given the short line distances in a distribution network, shunt capacitances in the π model of lines are neglected. Nonetheless, the inclusion of line capacitance in the models is straightforward with the adopted modelling framework (see chapter 5 for models including line capacitances)

(iii) The network is considered to be perfectly balanced between the 3 phases, allowing the use of the equivalent single phase representation. This hypothesis may be questioned (see chapter 2), particularly at low voltage level where individual network connections are mostly single-phase, which introduces intrinsic unbalance between the three phases. However, in a green field context, it is possible to allocate the different users on the three phases in such a way as to obtain a globally balanced load at network scale. Furthermore, the three-phase modelling would constitute an additional computational burden whose cost does not justify the benefits.

(iv) loads are modelled as constant power (P) loads

Generator modelling

If the investment decision in technology g generator has been made for node i ($\gamma_{igy} = 1$), then we consider the rating of a generator ρ_{igy} as a continuous variable limited by lower and upper bounds $\underline{p_g}^R$ and $\overline{p_g}^R$. Inside these bounds, the rating of a generator may be continuously increased once a year but can't be decreased.
To avoid additional binary variables, the commitment decision of generators is not modelled. Furthermore, the active power output of a particular generator has no lower bound, it can operate from 0 to 100 $\%$ of its rated power.
The reactive capability curve of a generator is modelled with a maximum power factor which is symmetrical for injection and consumption of reactive power by the generator. This means that the capability curve is triangular.
Finally, we do not model voltage control and we do not impose voltage setpoints. In the models, the voltage at each node (with or without generator) is free to vary within the admitted range, while remaining determined by the power flow formulation specific to each model.

4.2 Non-convex joint planning model

We present here a first version for the joint planning model. This is an *intuitive* model, i.e. it is written without aiming at a particular mathematical form and expressed naturally in terms of the classical power system variables: voltages, power

flows and power productions. This model is non-convex, as it will be shown hereunder, hence it is referred to as Non-convex joint planning model (NC-JPM) .

4.2.1 Objective

As stated in chapter 1, different objectives might be considered depending on the planner. We choose a classic objective which consists in minimizing the total net present value of the system including investment and operation costs over the lifetime of the project. This may easily be adapted for other planning objectives such as the minimization of greenhouse gases emissions or the minimization of unserved energy.
The objective function of (NC-JPM) is composed of three terms. The first one, corresponding to the first line, is the investment cost in generators from different technologies throughout the planning horizon, hereafter referred to as generation CAPEX (capital expenditures). Generators have fixed investment costs, irrespective of their size, and variable investment costs, proportional to their rated power. As γ_{ijy} doesn't represent the investment *being* made at year y but the investment that has *already been made* at year y, the timing of investment is expressed through the difference of these variables between successive years. The second term corresponds to investments costs in lines, hereafter referred to as lines CAPEX. They are expressed similarly to generation CAPEX, with a fixed term representing structure costs and a variable term representing conductor costs. The last term represents operational expenditures (OPEX), which correspond here to fuel costs. In what follows, diesel generators are considered to have a linear generating cost function. Finally, as we want to minimize the net present value of the system, cash flows are discounted with a discount rate d after the first year.

4.2.2 Constraints

The constraints of the joint planning model may be divided in four categories.

The first one models the physics of the problem.(**1.2**) and (**1.3**) represent nodal active and reactive power balance arising from *Kirchhoff's current law (KCL)*. Active and reactive power flows are expressed through equations (**1.4**) and (**1.5**).

The second category of constraints is related to network equipments limits. The thermal limit of lines is modelled by (**1.6**), while (**1.7**) and (**1.8**) represent the limits on voltage magnitude and phase angle difference respectively. (**1.9**) determines whether or not two nodes are connected by at least a line. (**1.10**) ensures there are enough lines in the network to make it connected, i.e. to make it at least a tree. How-

ever, this doesn't guarantee connectivity. Hence, (**1.11**),(**1.12**) and (**1.13**) impose that the network is connected, i.e. contains no islands, through the use of fictitious flows f_{ijy}. Note that we don't force the network to be radial.

The third category of constraints is about generation equipment limits. Constraint (**1.14**) sets limits to the rated power of generators for the different available technologies and makes it conditional upon the investment decision for generators. Then, the active power output of a generator is limited by its rated power (**1.15**) and the reactive power production is limited by the maximal power factor of the generator (**1.16**).

The last category of constraints ensures that investments are not unmade, both for distribution and generation assets (**1.17**) -(**1.19**).

The model (NC-JPM) is non-convex because of the presence of binary variables and the load flow equations (**1.4**),(**1.5**) which are non-convex even in the absence of binary variables. The non-convexity introduced by binary/integer variables may be handled with branch-and-bound algorithms (c.f. chapter 3). In the following sections, we study the various power flow formulations and their convex relaxations.

4.3 Representations of power flows

We wrote (NC-JPM) with the classical polar representation of power flows. This is also called the *Bus Injection Model (BIM)* as it is written as a function of bus electrical quantities, i.e. voltage magnitude and angles [74]. This BIM is presented in (BIM) in its polar form. The non-convex character of the power flow equations is obvious in this formulation with the $\sin$ and $\cos$ terms, the bilinear and square terms.
However, there are other formulations of the power flow equations: the *Branch Flow Model (BFM)*, also known as *DistFlow*, which is the other well known formulation and two more recently proposed models, the *power divider* and the *elliptical power flow* formulations [74].

The *DistFlow* model, first proposed in [9] is based on branch quantities: currents and flows. It can be seen that this model is also non-convex, hence it is called Non-Convex DistFlow Model (NC-DFM) from this point. The current between nodes i and j is written I_{ij}, R and X refer to the line resistance and reactance. Note that for the sake of clarity, we present the formulation in its purest form without investment variables, i.e. the network is considered as already built.

Model 1 Non-convex joint planning model (NC-JPM)

Minimize:

$$\sum_{i\in\mathcal{V},g\in\mathcal{G}}\left(\gamma_{ig1}C^{BG}_{gf}+\rho_{ig1}C^{BG}_{gv}+\sum_{y\geqslant 2}\frac{1}{(1+d)^{y-1}}[(\gamma_{ig,y}-\gamma_{ig,y-1})C^{BG}_{gf}+(\rho_{ig,y}-\rho_{ig,y-1})C^{BG}_{gv}]\right)$$
$$+\sum_{(i,j)\in\mathcal{E}}D_{ij}\left(\omega_{ij1}C^{BL}_{f}+\sum_{l\in\mathcal{L}}\lambda_{ijl1}C^{BL}_{lv}+\sum_{y\geqslant 2}\frac{1}{(1+d)^{y-1}}[(\omega_{ig,y}-\omega_{ig,y-1})C^{BL}_{f}\right.$$
$$\left.+(\lambda_{ijl,y}-\lambda_{ijl,y-1})C^{BL}_{lv}]\right)+\sum_{i\in\mathcal{V},g\in\mathcal{G},t\in\mathcal{T}}\frac{1}{(1+d)^{t\ \mathrm{div}\ H}}\frac{8760}{H}\left(\gamma_{igy}C^{P}_{gf}+p_{git}C^{P}_{gv}\right) \tag{1.1}$$

Subject to:

Physical constraints

$$\sum_{g\in\mathcal{G}}p^{G}_{igt}-p^{C}_{it}=\sum_{(i,j)\in\mathcal{E}}p_{ijt} \qquad \forall i\in\mathcal{V},t\in\mathcal{T} \tag{1.2}$$

$$\sum_{g\in\mathcal{G}}q^{G}_{igt}-q^{C}_{it}=\sum_{(i,j)\in\mathcal{E}}q_{ijt} \qquad \forall i\in\mathcal{V},t\in\mathcal{T} \tag{1.3}$$

$$p_{ijt}=\sum_{l\in\mathcal{L}}(\lambda_{ijly}g_l/D_{ij})[v^2_{it}-v_{it}v_{jt}\cos(\theta_{ijt})]-\sum_{l\in\mathcal{L}}(\lambda_{ijly}b_l/D_{ij})[v_{it}v_{jt}\sin(\theta_{ijt})]$$
$$\forall(i,j)\in\mathcal{E},t\in\mathcal{T},y\in\mathcal{Y}:y=t\ \mathrm{div}\ H+1 \tag{1.4}$$

$$q_{ijt}=\sum_{l\in\mathcal{L}}(\lambda_{ijly}b_l/D_{ij})[v_{it}v_{jt}\cos(\theta_{ijt})-v^2_{it}]-\sum_{l\in\mathcal{L}}(\lambda_{ijly}g_l/D_{ij})[v_{it}v_{jt}\sin(\theta_{ijt})]$$
$$\forall(i,j)\in\mathcal{E},t\in\mathcal{T},y\in\mathcal{Y}:y=t\ \mathrm{div}\ H+1 \tag{1.5}$$

Network constraints

$$p^2_{ijt}+q^2_{ijt}\leqslant\sum_{l\in\mathcal{L}}(\lambda_{ijly}\overline{S}_l)^2 \qquad \forall(i,j)\in\mathcal{E},t\in\mathcal{T},y\in\mathcal{Y}:y=t\ \mathrm{div}\ H+1 \tag{1.6}$$

$$\underline{v}\leqslant v_{it}\leqslant\overline{v} \qquad \forall i\in\mathcal{V},t\in\mathcal{T} \tag{1.7}$$

$$-\Delta^{\theta}\leqslant\theta_{ijt}\leqslant\Delta^{\theta} \qquad \forall(i,j)\in\mathcal{E},t\in\mathcal{T} \tag{1.8}$$

$$\sum_{l\in\mathcal{L}}\frac{\lambda_{ijly}}{\Lambda}\leqslant\omega_{ijy}\leqslant\sum_{l\in\mathcal{L}}\lambda_{ijly} \qquad (i,j)\in\mathcal{E},l\in\mathcal{L},y\in\mathcal{Y} \tag{1.9}$$

$$\sum_{(i,j)\in\mathcal{E}}\omega_{ijy}\geqslant 2\times(n-1) \qquad \forall(i,j)\in\mathcal{E},y\in\mathcal{Y} \tag{1.10}$$

$$f_{ijy} \leqslant \omega_{ijy} \times n \qquad \forall y \in \mathcal{Y}, (i,j) \in \mathcal{E} \quad \textbf{(1.11)}$$

$$\sum_{(i,j)\in\mathcal{L}} f_{1jy} = n - 1 \qquad \forall i \in \mathcal{V}, y \in \mathcal{Y} \quad \textbf{(1.12)}$$

$$\sum_{(i,j)\in\mathcal{E}} f_{jiy} = 1 + \sum_{(i,j)\in\mathcal{L}} f_{ijy} \qquad \forall (i,j) \in \mathcal{E}, y \in \mathcal{Y} \quad \textbf{(1.13)}$$

Generation constraints

$$\gamma_{igy}\underline{p_g}^R \leqslant \rho_{igy} \leqslant \gamma_{igy}\overline{p_g}^R \qquad \forall i \in \mathcal{V}, g \in \mathcal{G}, y \in \mathcal{Y} \quad \textbf{(1.14)}$$

$$0 \leqslant p^G_{igt} \leqslant \rho_{igy} \qquad \forall i \in \mathcal{V}, g \in \mathcal{G}, t \in \mathcal{T}, y \in \mathcal{Y} : y = t \operatorname{div} H + 1 \quad \textbf{(1.15)}$$

$$|q^G_{igt}| \leqslant p^G_{igt} \tan(\cos^{-1}(\overline{PF}_g)) \qquad \forall i \in \mathcal{V}, g \in \mathcal{G}, t \in \mathcal{T} \quad \textbf{(1.16)}$$

Investment constraints

$$\gamma_{ig,y} \geqslant \gamma_{ig,y-1} \qquad \forall i \in \mathcal{V}, y \in \mathcal{Y} : y > 2 \quad \textbf{(1.17)}$$

$$\rho_{ig,y} \geqslant \rho_{ig,y-1} \qquad \forall i \in \mathcal{V}, y \in \mathcal{Y} : y > 2 \quad \textbf{(1.18)}$$

$$\lambda_{ijl,y} \geqslant \gamma_{ijl,y-1} \qquad \forall (i,j) \in \mathcal{E}, y \in \mathcal{Y} : y > 2 \quad \textbf{(1.19)}$$

(1.20)

Model 2 Bus Injection Model (polar)(BIM)

Solve:

$$\sum_{g\in\mathcal{G}} p^G_{ig} - p^C_i = \sum_{(i,j)\in\mathcal{E}} p_{ijt} \quad \textbf{(2.1)}$$

$$\sum_{g\in\mathcal{G}} q^G_{igt} - q^C_{it} = \sum_{(i,j)\in\mathcal{E}} q_{ijt} \quad \textbf{(2.2)}$$

$$p_{ij} = g_{ij}[v_i^2 - v_i v_j \cos(\theta_{ij})] - b_{ij}[v_i v_j \sin(\theta_{ij})] \quad \textbf{(2.3)}$$

$$q_{ij} = b_{ij}[v_i v_j \cos(\theta_{ij}) - v_i^2] - g_{ij}[v_i v_j \sin(\theta_{ij})] \quad \textbf{(2.4)}$$

Model 3 Non-Convex DistFlow Model (NC-DFM)

Solve:

$$\sum_{g\in\mathcal{G}} p_{ig}^G - p_i^C = \sum_{(i,j)\in\mathcal{E}} p_{ijt} \tag{3.1}$$

$$\sum_{g\in\mathcal{G}} q_{igt}^G - q_{it}^C = \sum_{(i,j)\in\mathcal{E}} q_{ijt} \tag{3.2}$$

$$p_{ij}^2 + q_{ij}^2 = |v_i|^2 |I_{ij}|^2 \tag{3.3}$$

$$p_{ij} + p_{ji} = R_{ij}|I_{ij}|^2 \tag{3.4}$$

$$q_{ij} + q_{ji} = X_{ij}|I_{ij}|^2 \tag{3.5}$$

$$|v_j|^2 = |v_i|^2 - 2(R_{ij}p_{ij} + X_{ij}q_{ij}) + (R_{ij}^2 + X_{ij}^2)|I_{ij}|^2 \tag{3.6}$$

The (NC-DFM) model is equivalent to (**1.2**)-(**1.5**) for radial networks only [74]. As a matter of fact, (**3.6**) is obtained by squaring the voltage drop equation $v_i - v_j = I_{ij}(R_{ij} + jX_{ij})$, i.e. by multiplying each term of the equation by its complex conjugate. The complex voltage drop equation consists of two real equations in polar coordinates: the first one equates the magnitude of left-hand and right-hand terms and the second one equates the phase of these two terms. The aformentioned relaxation thus consists in only enforcing the magnitude constraint, not the angle one, which means that angles are lost in this squaring process.

Hence, (NC-DFM) is a relaxation of (**1.2**)-(**1.5**) in the general context where networks can be meshed. However, in a radial setup, voltage angles may be recovered in a unique way after the computation, starting from any reference node and propagating the true complex voltage drop equation along the branches of the network. The reason for this is that there exists only one path between two nodes in a radial network. This is not the case in a meshed network where there exists some cycles. Yet, (NC-DFM) doesn't ensure that angle differences add up to $0 \pm 2k\pi$ along a cycle, hence there might be inconsistencies [74]. This means that, for example, when a bus belongs to a cycle and is considered as the reference bus ($\theta = 0$), then after propagating the voltage drop equation around the cycle back to the reference bus we might obtain $\theta \neq 0 \pm 2k\pi$.

As mentioned in [74], (NC-DFM) may be augmented with a set of cycle-related constraints to make it exact for meshed networks as well. Nonetheless, the networks obtained in the test-case presented below are always radial, hence these constraints are not necessary in this case.

4.4 Convex relaxations of power flow equations

The planning model (NC-JPM) presented above may be seen as a extension of the classical *Optimal Power Flow (OPF)* problem where not only operational costs linked to the operation of the system are minimized but also investment costs. Hence, in this section, we review the existing literature about convex formulations of the OPF problems that may be extended for our planning problem.
This section is, to a large extent, based on [74] regarding the formalism, the structure and content. The primary goal here is to give a basic understanding of the underlying mathematical concepts and to give a big picture of the convex relaxations used in power flow-related optimization problems. The interested reader may refer to [74] for more details. Note that, in accordance with the previous, we only focus on the formulation of power flows, hence investment variables are not considered here and the network is considered as fixed.

4.4.1 Semidefinite Programming relaxations

The *Bus Injection Model (BIM)* of the load flow equations is expressed in polar coordinates $v = |v|\angle\theta$ in (**2.1**)-(**2.4**). It may also be expressed in rectangular coordinates $v = v^R + jv^I$, with $v^R = \Re(v)$ and $v^I = \Im(v)$. In the latter coordinates, power flow equations are quadratic in v^R and v^I, i.e. they contain the degree 2 monomials $\{(v_1^R)^2, v_1^R v_2^R, ..., v_1^R v_n^R, v_1^R v_1^I, ...v_1^R v_n^I, ..., (v_n^I)^2\}$.

Shor relaxation Let's define the vector $\hat{x} \in \mathbb{R}^{2n}$ of degree 1 monomials of rectangular voltage components $\hat{x} = [v_1^R \ ... \ v_n^R \ v_1^I \ ... \ v_n^I]$ The Shor relaxation, proposed in [90] and applied to the OPF by [7] is composed of two steps: first the quadratic monomials are lifted in the W space by defining the $\mathbf{W} \in \mathbb{R}^{2n \times 2n}$ matrix as

$$\mathbf{W} = \hat{x}^T \hat{x}$$

This constraint may then be equivalently expressed as follows:

$$\begin{cases} \mathbf{W} \geq 0 \\ \text{rank}(\mathbf{W}) = 1 \end{cases}$$

The second step of the relaxation consists in dropping the rank constraint which is nonconvex. Expressing the power flow equations with the lifted variables stored in matrix $\mathbf{W}$, the feasible set of the relaxation thus takes the following form:

$$\begin{cases} \mathrm{tr}(\mathbf{A_1}\mathbf{W}) = a_1 \\ \dots \\ \mathrm{tr}(\mathbf{A_1}\mathbf{W}) = a_m \\ \mathbf{W} \succeq 0 \end{cases}$$

In this generic writing of the feasible set, the first block represents the set of power flow equations in the W space. They can all be expressed as a trace constraint on a product of $\mathbf{W}$ and another matrix of constant values depending on the parameters of the network. These constraints are thus linear. The last line represents the semidefinite constraint on $\mathbf{W}$, which gives its character to the relaxation and is convex.

This relaxation is shown to be exact on numerous IEEE test cases, however counterexamples exist. There exists sufficient conditions for it to be exact, however they do not apply to real-world networks [74].

Moment-based relaxation The moment-based relaxation proposed by [58] and first applied to the OPF by [73] can be seen as a generalization of the Shor relaxation. Its principle is to lift monomials in a higher dimension space Y. In this space, constraints that are redundant in the original space are added to the relaxation, tightening it.
We can formulate the principle as follows, $\hat{x}$ being defined as in the Shor relaxation. Let us first define x_k as the vector of degree k monomials based on the order 1 monomials of rectangular voltage components contained in $\hat{x}$ (hence $x_1 = \hat{x}$) . Let us assume a generic polynomial constraint $g(\hat{x}) \geqslant 0$. If we construct the matrix $x_k^T x_k$, it is semidefinite positive (SDP) by construction. Then, if we multiply it by the scalar $g(\hat{x})$, the resulting matrix remains SDP as $g(\hat{x})$ is constrained to be nonnegative. Hence, the constraint $g(\hat{x})x_k^T x_k \succeq 0$ is redundant with $g(\hat{x}) \geqslant 0$. It is then relaxed in the lifted Y space with a functional L_y and the order k-moment relaxation can be generically written as :

$$\begin{cases} L_y\{g(\hat{x}x_1^T x_1)\} \succeq 0 \\ \dots \\ L_y\{g(\hat{x}x_k^T x_k)\} \succeq 0 \end{cases}$$

The hierarchy of real-valued moment-based relaxations of the OPF is a Lasserre hierarchy. Each order of this hierarchy generalizes the previous order relaxations of the hierarchy. Under certain conditions, it can be shown that this hierarchy converges to global optimality for a finite order. In practical cases, it can be shown that low-order moment-based relaxations suffice to reach global optima for a broad variety of optimization problems including power flow equations. However, the computa-

tional burden of such relaxations rapidly grows with the order of the relaxations and systems over 10 nodes might become computationally intractable. Still, models with tens or hundreds of nodes might be treated by exploiting the sparsity (i.e. incidence matrices of power systems are sparse) of real networks and enforcing higher order relaxations only on a subset of nodes.

As a concluding remark for the Shor and moment-based relaxations, the authors in [74] point out that SDP relaxations and solvers cannot compete yet with nonlinear (NL) solvers when looking for a local optimum. Further developments are thus needed in this area.

4.4.2 Second Order Cone relaxations

The various SOCP relaxations presented hereunder are shown to be exact under certain conditions depending on the configuration of the network and the considered elements. Those are summarized in [62]. It should be noted that sufficient conditions for exactness are less stringent for radial networks than meshed networks as the angle relaxation is exact in the former case

Jabr relaxation This formulation proposed in [50] is based on the BIM model of power flow equations. It can be seen as a SOCP relaxation of the Shor relaxation presented above when written in complex variables. In this case, $\mathbf{W} \in \mathbb{C}^{n\times n}$ is hermitian. The SDP constraint imposes that all principal minors are positive [93]. The SOCP relaxation consists in keeping this condition only for 1×1 and 2×2 principal minors, which is written

$$\begin{cases} W_{ii} \geqslant 0 \\ W_{ii}W_{jj} \geqslant |W_{ij}|^2 \Leftrightarrow W_{ii}W_{jj} \geqslant (\Re(W_{ij}))^2 + (\Im(W_{ij}))^2 \end{cases}$$

The second constraint is a rotated Second Order Cone (SOC) constraint that may be rewritten as two canonical SOC constraints by introducing new variables $a = \frac{W_{ii}+W_{jj}}{2}$,$b = \frac{W_{ii}-W_{jj}}{2}$ and c as follows:

$$W_{ii}W_{jj} \geqslant (\Re(W_{ij}))^2 + (\Im(W_{ij}))^2 \Leftrightarrow a^2 - b^2 \geqslant (\Re(W_{ij}))^2 + (\Im(W_{ij}))^2$$

$$\Leftrightarrow \begin{cases} (\Re(W_{ij}))^2 + (\Im(W_{ij}))^2 \leqslant c^2 \\ c^2 + b^2 \leqslant a^2 \end{cases}$$

Quadratic Convex (QC) relaxation This relaxation developed in [27] starts from the polar formulation of the BIM model. The terms v_i^2, $v_i v_j \cos(\theta_{ij})$ and $v_i v_j \sin(\theta_{ij})$ are lifted, i.e. replaced by variables c_{ii}, c_{ij} and s_{ij} respectively. Then, these new variables are constrained to belong to convex envelopes of the terms they replace, i.e. v_i^2, $v_i v_j \cos(\theta_{ij})$ and $v_i v_j \sin(\theta_{ij})$ respectively. Convex envelopes of these terms are sets of constraints that delimit a convex portion of space comprising the nonconvex feasibility space for these terms based on the lower and upper bounds on the variables v and θ.The QC formulation is shown to be a tightening of Jabr's formulation.

Convex DistFlow relaxation This formulation [33] is a convex relaxation of (NC-DFM) . The first step is to introduce the variables $l_{ij} = |I_{ij}|^2$ and $w_i = |v_i|^2$. This removes the nonconvexity of (**3.4**),(**3.5**) and (**3.6**) that become (**4.4**),(**4.5**) and (**4.6**) respectively. However, (**3.3**) remains nonconvex due to the bilinear right-hand side $w_i l_{ij}$. This equality constraint defines the surface of a cone (see Fig. 4.2, left), which is clearly a non-convex space. The equality constraint is thus relaxed into an inequality constraint, which means that we consider the interior (volume) of the cone as well as its surface (see Fig. 4.2, right).
Eq. (**4.3**) appears as a rotated SOC constraint (**4.3**). This is transformed in two canonical SOC constraints in the same way as in Jabr's relaxation.

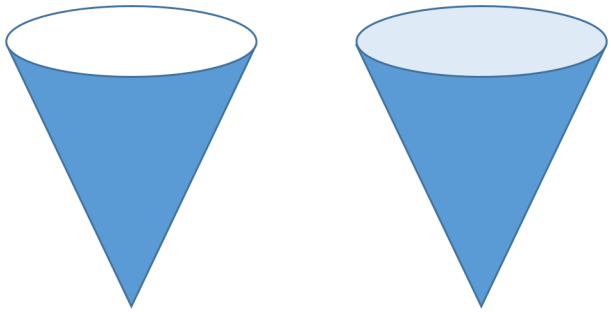

Fig. 4.2: Relaxation of (**3.3**) (left) into (**4.3**) (right) means that both the interior (volume) of the cone and its surface are considered

This relaxation implies that voltage and current variables, w_i and l_{ij}, could be larger than they should be with the power flow constitutive equation (**3.3**). If the objective is to minimize a convex function of the losses or the produced power, then the right-hand term of (**4.3**) should tend to be equal to the left-hand term. As a matter of fact, (**4.4**),(**4.5**) show the linear dependence between active and reactive losses and squared current amplitude. To reduce the value of the losses, hence to minimize the objective, the solver should take the lowest possible value for l_{ij}, i.e. $\frac{p_{ij}^2+q_{ij}^2}{w_i}$.
In radial networks, if both terms of (**4.3**) are equal, then the relaxation is exact. It is

important to mention that, as proven in [26], Jabr's formulation is equivalent to the CDF formulation. The latter has proven to be exact on radial setups in numerous practical cases. Chapter 5 takes a more detailed look at the accuracy of the CDF formulation in the context of an optimal reactive power dispatch for loss minimization in an onshore windfarm.

Model 4 Convex DistFlow Relaxation (C-DFM)

Solve:

$$\sum_{g\in\mathcal{G}} p_{ig}^{G} - p_{i}^{C} = \sum_{(i,j)\in\mathcal{E}} p_{ijt} \tag{4.1}$$

$$\sum_{g\in\mathcal{G}} q_{igt}^{G} - q_{it}^{C} = \sum_{(i,j)\in\mathcal{E}} q_{ijt} \tag{4.2}$$

$$p_{ij}^{2} + q_{ij}^{2} \leqslant w_i l_{ij} \tag{4.3}$$

$$p_{ij} + p_{ji} = R_{ij} l_{ij} \tag{4.4}$$

$$q_{ij} + q_{ji} = X_{ij} l_{ij} \tag{4.5}$$

$$w_j = w_i - 2(R_{ij}p_{ij} + X_{ij}q_{ij}) + (R_{ij}^{2} + X_{ij}^{2}) l_{ij} \tag{4.6}$$

Compared to SDP relaxations, SOCP relaxations offer computational advantages while being sometimes weaker (Fig. 4.3. In particular, the smaller number of variables of the SOCP compared to the matrix formulation of the SDP and the maturity of SOCP solvers compared to SDP solvers allows to apply the SOCP models on comparatively larger problems [93].

4.4.3 Linear relaxations

This section concludes the set of convex relaxations of power flow equations. Linear relaxations (LP) are weaker than SOCP and SDP relaxations (Fig. 4.3) but they offer the advantage to rely on very developed, state-of-the-art solvers able to handle very large problems. Furthermore, the inclusion of integer variables is highly facilitated by the maturity of Mixed Integer Linear Programming (MILP) solvers, that far surpasses that of MISOCP or MISDP.

The network flow relaxation This relaxation is the simplest one as it only retains network flow conservation constraints (**5.1**) and (**5.2**) . If there are no bus shunt admittances, then this formulation is independent of the voltages. Finally, constraints (**5.3**) and (**5.4**) prevent the lines to artificially "generate" power.

Model 5 Network flow relaxation (NFM)

Solve:

$$\sum_{g\in\mathcal{G}} p^G_{ig} - p^C_i = \sum_{(i,j)\in\mathcal{E}} p_{ijt} \tag{5.1}$$

$$\sum_{g\in\mathcal{G}} q^G_{igt} - q^C_{it} = \sum_{(i,j)\in\mathcal{E}} q_{ijt} \tag{5.2}$$

$$p_{ij} + p_{ji} \geqslant 0 \tag{5.3}$$

$$q_{ij} + q_{ji} \geqslant 0 \tag{5.4}$$

This relaxation only considers power flows and omits how these are related to currents and voltages. This has several implications:

(i) There are no losses as no constitutive equation models them
(ii) A power flow solution of this relaxed model, if observed in a real-case, could imply unacceptable voltage levels as these are not taken into account in the model

Taylor-Hoover relaxation This formulation developed in [94] uses lifted variables $w_i = |v_i|^2$ (the w symbol, though not being used in the original formulation is kept for sake of consistency) in linear combinations of power flow equations that lead to valid equalities linking lifted voltage variables and power flows (**6.3**) and (**6.4**) . It is presented here without bus shunt elements.

Model 6 Taylor-Hoover relaxation (THM)

Solve:

$$\sum_{g\in\mathcal{G}} p^G_{ig} - p^C_i = \sum_{(i,j)\in\mathcal{E}} p_{ijt} \tag{6.1}$$

$$\sum_{g\in\mathcal{G}} q^G_{igt} - q^C_{it} = \sum_{(i,j)\in\mathcal{E}} q_{ijt} \tag{6.2}$$

$$g_{ij}(p_{ij} - p_{ji}) - b_{ij}(q_{ij} - q_{ji}) = (g^2_{ij} + b^2_{ij})(w_i - w_j) \tag{6.3}$$

$$b_{ij}(p_{ij} + p_{ji}) + g_{ij}(q_{ij} + q_{ji}) = 0 \tag{6.4}$$

The linear combination of power flow equations that produces equations eqs. (**6.3**) and (**6.4**) causes a loss of information. Indeed, eqs. (**2.1**) and (**2.2**) both represent

two equations: one for the active/reactive power flow from node i to node j and one for the active/reactive power flow from node j to i.
Yet, equations (**6.1**) and (**6.2**) are the same in both directions (i, j) and (j, i). Half of the 'information' about power flows is thus lost in the relaxation process.

In this form, the Taylor-Hoover relaxation allows to have negative active/reactive losses with eq. (**6.4**) as long as they are compensated with positive positive reactive/active losses. It also allows a situation with no active nor reactive losses. To avoid non-physical negative losses, we will augment it with eqs. (**5.3**) and (**5.4**) in subsequent models.
The Taylor-Hoover relaxation does model voltages. Nonetheless, being a relaxation, these voltages can be under/overestimated in comparison with the true physical values corresponding to a given power flow situation, which might produce voltage bounds violations, hence infeasible solutions in real cases.

McCormick relaxations As mentioned before, power flow equations can be expressed as a degree 2 polynomial of bus voltages real and imaginary parts. McCormick relaxations [70] are convex envelopes of degree 2 monomials x^2 and xy based on valid inequalities derived from lower and upper bounds on x and y.

4.4.4 Hierarchy of convex power flow relaxations

We conclude this section with an analysis of the relationship between the different presented formulations (Fig. 4.3). A formulation is said to dominate another one if feasible space of the former is entirely contained in the feasible space of the latter. In other words, the former model is a more accurate relaxation of the AC power flow equations than the latter. This analysis originates from [74] and gives an up-to-date picture of the dominance relationships established by various authors regarding the presented models.

4.5 Linear approximations and relaxations of Second Order Cone constraints

We saw in the previous section a hierarchy of convex relaxations for power flow equations. In particular, SOCP relaxations are characterised by the presence of SOC constraints. In this context, an SOC constraint defines a conic feasible space of dimension 3 noted $\mathbb{L}^2$ and defined by $x^2 + y^2 <= z^2$. In this section, we introduce inner and outer linear approximation techniques for $\mathbb{L}^2$ that will be used in the following sections to develop linear models for the joint planning problem. They will

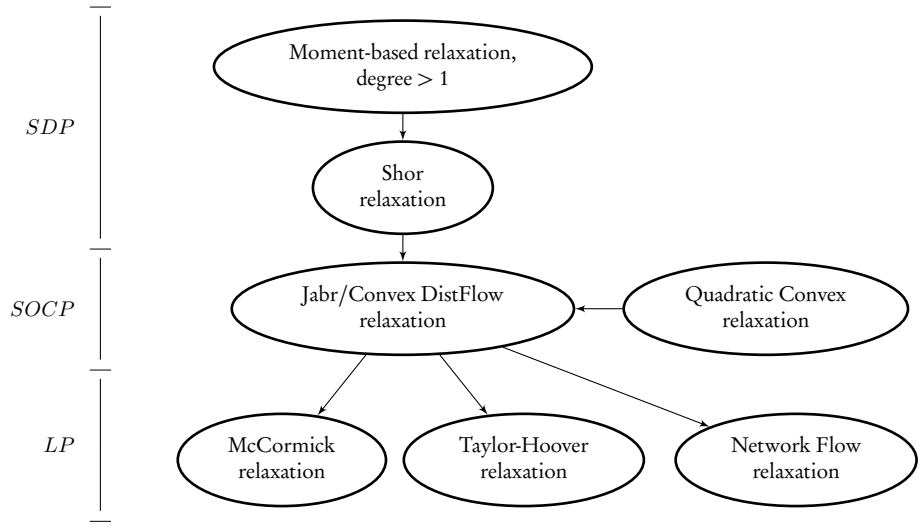

Fig. 4.3: Established dominance between the power flow relaxations presented above (the arrow head indicates the dominated formulation). Adapted from [74]

generically denoted by $\langle SOC\ \ constraint \rangle^{IA}$ and $\langle SOC\ \ constraint \rangle^{OA}$ respectively.

4.5.1 Inner approximation

A first way to linearly approximate $\mathbb{L}^2$ is to build an inner polyhedron with f faces that fits in it. In particular, we define the following approximation that corresponds to an inner square pyramid:

$$|x| + |y| \leqslant z \tag{23}$$

This is more restrictive than $\mathbb{L}^2$ as it defines a smaller feasible space enclosed in the the original one.

4.5.2 Outer approximation

This outer approximation is a relaxation of $\mathbb{L}^2$ as it defines a larger feasible space that encloses the original one by building an outer, circumscribed polyhedron with f faces, similarly to the inner approximation (Fig. 4.4). A naive way of doing it is to write one linear inequality for each of the f faces of this polyhedron. The accuracy ϵ of this relaxation is $\epsilon = \cos(\pi/f)^{-1} - 1 \approx \pi^2/2f^2$ [41].

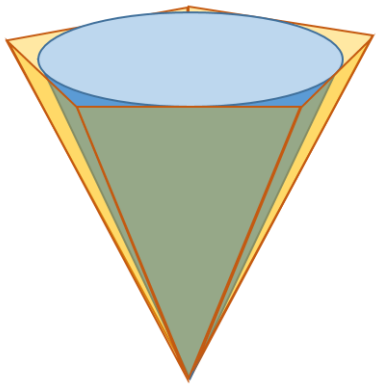

Fig. 4.4: Original feasible space defined by a conic constraint (blue) and relaxed feasible space defined by the outer approximation (yellow)

A more efficient method (i.e. with less additional constraints) to define an outer polyhedron has been first described by Ben-Tal and Nemirovski in [10]. We present here a slightly improved version presented in [41]. It approximates $\mathbb{L}^2$ with $\mathcal{L}^\kappa$ defined as follows.

$$\mathcal{L}^\kappa = \{(z, \alpha_0, \beta_0, ..., \alpha_\kappa, \beta_\kappa) \in \mathbb{R}^{2\kappa+3}\}$$

s.t.

$$\begin{cases} \alpha_0 = x \\ \beta_0 = y \end{cases}, \begin{cases} \alpha_{i+1} = \alpha_i \cos\frac{\pi}{2^i} + \beta_i \sin\frac{\pi}{2^i} \\ \beta_{i+1} \geqslant \beta_i \cos\frac{\pi}{2^i} - \alpha_i \sin\frac{\pi}{2^i} \\ \beta_{i+1} \leqslant \beta_i \cos\frac{\pi}{2^i} - \alpha_i \sin\frac{\pi}{2^i} \\ z = \alpha_\kappa \cos\frac{\pi}{2^\kappa} + \beta_\kappa \sin\frac{\pi}{2^\kappa} \end{cases} \forall 0 \leqslant i \leqslant \kappa$$

This is a lift-and-project relaxation as it introduces new variables. Nevertheless, it represents an outer polyhedron approximation when projected back in the original 3D space (x, y, z), i.e. when auxiliary variables α and β are not considered. The $\mathcal{L}^\kappa$ relaxation introduces $2\kappa + 2$ additional variables, $\kappa + 1$ additional equality constraints and 2κ additional inequality constraints. As shown in [41], its accuracy is expressed by $\epsilon = \cos(\pi/2^\kappa)^{-1} - 1 \approx \pi^2/2^{2\kappa}$.
This means that, for an accuracy $\epsilon \approx 10^{-4}$, κ needs to be equal to 8, which represents 18 new variables and 25 new constraints, while the naive approximation would require 223 additional constraints for the same level of accuracy.

4.6 Convex models for the joint planning problem

Thus far, we presented a non-convex joint planning model (NC-JPM) . We showed that the non-convexity had two principal causes: integer investment variables and power flow equations. We showed two different techniques to deal with the non-convexity of the former. We then presented a set of convex relaxations of power flow equations ranging from SDP to LP models. As mentioned, these formulations have a decreasing accuracy when going from SDP to LP.
When a power system investment planning problem integrates one of these formulations, it inherits its inaccuracy regarding continuous electrical variables, i.e. currents, voltages and power flows. However, as it has already been mentioned, the purpose of such a planning problem is to deliver an investment plan for the generation and distribution assets. Its useful output thus consists of discrete investment variables. Continuous electrical variables, linked to the operation of the system, only serve to check the feasibility of a particular investment solution regarding the operating conditions that might be encountered.
Hence, the idea is to compare a set of growing accuracy formulations for the joint planning problem regarding:

(i) The investment solution
(ii) The feasibility of this solution
(iii) The computation time

As a matter of fact, more accurate models might quickly become computationally intractable for a growing size of the problem, i.e. when there are more discrete investment options, nodes or timesteps. We thus intend to identify the trade-off between the computational burden and the quality of the solution.
In order to assess the quality of a solution, we need to compare it to a reference solution that is known to be feasible and accurate, whether in terms of the objective function value or the set of optimum variables values. We present a Convex DistFlow-based planning model in 4.6.3 that will be shown to be feasible in all tested cases and accurate. Hence, it will be used as the reference model. Three other models (NF-JPM) , (TH-JPM) , (TH-JPM-L) are introduced in 4.6.1 and 4.6.2. These are weaker but less computationally intensive relaxations of the problem, that will be compared to (CDF-JPM) . These three models all have IA and OA variants (Inner/Outer Approximation of thermal rating constraints).

4.6.1 Network flow joint planning model

This first model is the simplest one. It incorporates the network flow formulation (NF-JPM) . Capacity constraints are enforced for generators and lines. It may thus be cast as a multi-commodity capacitated facility location/network design problem

[71] where active and reactive power are two different commodities. The objective function is the same as in (NC-JPM) . Eqs. (**7.2**) - (**7.5**) are the network flow model equations. Connectivity of the network is enforced through constraints (**7.7**) - (**7.11**). Then, constraints (**7.13**)-(**7.15**) ensure no investments are unmade during the planning horizon. Finally, constraints (**7.16**) - (**7.18**) represent the rating and production limit of generators both for active and reactive power. These three constraints sets are identical in (NC-JPM) . Finally, as the thermal rating constraint of lines is a quadratic (SOC) constraint and we want to keep the model linear, we use one of the two linear approximations presented in section 4.5 in (**7.6**).

Model 7 Network Flow-based Joint Planning Model (NF-JPM)

Minimize:

$$\sum_{i\in\mathcal{V},g\in\mathcal{G}}\left(\gamma_{ig1}C^B_{gf}+\rho_{ig1}C^B_{gv}+\sum_{y\geqslant 2}\frac{1}{(1+d)^{y-1}}[(\gamma_{ig,y}-\gamma_{ig,y-1})C^B_{gf}+(\rho_{ig,y}-\rho_{ig,y-1})C^B_{gv}]\right)$$
$$+\sum_{(i,j)\in\mathcal{E}}D_{ij}\left(\omega_{ij1}C^{BL}_{f}+\sum_{l\in\mathcal{L}}\lambda_{ijl1}C^{BL}_{lv}+\sum_{y\geqslant 2}\frac{1}{(1+d)^{y-1}}[(\omega_{ig,y}-\omega_{ig,y-1})C^{BL}_{lf}\right.$$
$$\left.+(\lambda_{ijl,y}-\lambda_{ijl,y-1})C^{BL}_{lv}]\right)+\sum_{i\in\mathcal{V},g\in\mathcal{G},t\in\mathcal{T}}\frac{1}{(1+d)^{t\ \mathrm{div}\ H}}\frac{8760}{H}\left(\gamma_{igy}C^P_{gf}+p_{git}C^P_{gv}\right) \quad \textbf{(7.1)}$$

Subject to:

$$\sum_{g\in\mathcal{G}}p^G_{igt}-p^C_{it}=\sum_{(i,j)\in\mathcal{E}}p_{ijt} \qquad \forall i\in\mathcal{V},t\in\mathcal{T} \quad \textbf{(7.2)}$$

$$\sum_{g\in\mathcal{G}}q^G_{igt}-q^C_{it}=\sum_{(i,j)\in\mathcal{E}}q_{ijt} \qquad \forall i\in\mathcal{V},t\in\mathcal{T} \quad \textbf{(7.3)}$$

$$p_{ijt}+p_{jit}\geqslant 0 \qquad \forall(i,j)\in\mathcal{E},t\in\mathcal{T} \quad \textbf{(7.4)}$$

$$q_{ijt}+q_{jit}\geqslant 0 \qquad \forall(i,j)\in\mathcal{E},t\in\mathcal{T} \quad \textbf{(7.5)}$$

$$\left\langle p_{ijt}^2 + q_{ijt}^2 \leqslant \left(\sum_{l \in \mathcal{L}} \lambda_{ijly} \overline{S}_l \right)^2 \right\rangle^{IA \text{ or } OA} \quad \forall (i,j) \in \mathcal{E}, t \in \mathcal{T}, y \in \mathcal{Y} : y = t \text{ div } H + 1 \tag{7.6}$$

$$\sum_{l \in \mathcal{L}} \frac{\lambda_{ijly}}{\Lambda} \leqslant \omega_{ijy} \leqslant \sum_{l \in \mathcal{L}} \lambda_{ijly} \quad \forall (i,j) \in \mathcal{E}, l \in \mathcal{L}, y \in \mathcal{Y} \tag{7.7}$$

$$\sum_{(i,j) \in \mathcal{E}} \omega_{ijy} \geqslant 2 \times (n-1) \quad \forall (i,j) \in \mathcal{E}, y \in \mathcal{Y} \tag{7.8}$$

$$f_{ijy} \leqslant \omega_{ijy} \times n \quad \forall y \in \mathcal{Y}, (i,j) \in \mathcal{E} \tag{7.9}$$

$$\sum_{(i,j) \in \mathcal{E}} f_{1jy} = n - 1 \quad \forall i \in \mathcal{V}, y \in \mathcal{Y} \tag{7.10}$$

$$\sum_{(i,j) \in \mathcal{E}} f_{jiy} = 1 + \sum_{(i,j) \in \mathcal{E}} f_{ijy} \quad \forall (i,j) \in \mathcal{E}, y \in \mathcal{Y} \tag{7.11}$$

(7.12)

$$\gamma_{ig,y} \geqslant \gamma_{ig,y-1} \quad \forall i \in \mathcal{V}, y \in \mathcal{Y} : y > 2 \tag{7.13}$$

$$\rho_{ig,y} \geqslant \rho_{ig,y-1} \quad \forall i \in \mathcal{V}, y \in \mathcal{Y} : y > 2 \tag{7.14}$$

$$\lambda_{ijl,y} \geqslant \gamma_{ijl,y-1} \quad \forall (i,j) \in \mathcal{E}, y \in \mathcal{Y} : y > 2 \tag{7.15}$$

$$0 \leqslant p_{igt}^G \leqslant \rho_{igy} \quad \forall i \in \mathcal{V}, g \in \mathcal{G}, t \in \mathcal{T}, y \in \mathcal{Y} : y = t \text{ div } H + 1 \tag{7.16}$$

$$\gamma_{igy} \underline{p_g}^R \leqslant \rho_{igy} \leqslant \gamma_{igy} \overline{p_g}^R \quad \forall i \in \mathcal{V}, g \in \mathcal{G}, y \in \mathcal{Y} \tag{7.17}$$

$$|q_{igt}^G| \leqslant p_{igt}^G \tan(\cos^{-1}(\overline{PF}_g)) \quad \forall i \in \mathcal{V}, g \in \mathcal{G}, t \in \mathcal{T} \tag{7.18}$$

4.6.2 Taylor-Hoover models

The following model is based on the Taylor-Hoover model for power flows (THM) . It is constructed by adding constraints from this formulation to the feasible set of (NF-JPM) . As it already contains (**7.2**) and (**7.3**), we only have to add the valid equalities (**8.3**) and (**8.4**) and to bind voltages at every node to be within the admissible range (**8.5**). Note that (**8.3**) corresponds to (**6.3**) rewritten in a disjunctive way. Indeed, as mentioned in section 4.1, the power flow on a conductor l between nodes i and j should be non-zero only if $\lambda_{ijly} = 1$. If it is equal to zero, the equality constraint describing this power flow (here, (**6.3**)) should be inactive as it would induce non physical constraints. For example, if there is no conductor between nodes i and j, i.e. $\lambda_{ijly} = 0 \ \forall l \in \mathcal{L}$, then p_{ijlt} and q_{ijlt} would be null (**7.6**) and letting (**6.3**) active

would result in imposing $w_{it} = w_{jt}$ which is unwanted.

The disjunctive formulation allows to activate this constraint when it is necessary to do so. Lower and upper bounds are thus selected as the smallest values such that the constraint is inactive for $\lambda_{ijly} = 0$. As a matter of fact, we want to tighten the feasible space as much as possible.
Note that (**8.4**) doesn't include voltage variables and is valid even when there is no conductor between i and j, hence it is written in its initial form.
Lastly, (**7.4**) and (**7.5**) have been included in this formulation while they do not belong to Taylor-Hoover model (THM) . As a matter of fact, we observed that without these constraints, (THM) allowed power losses on line to take non-physical negative values, which was also highlighted in [25].

It is important here to put the emphasis on the fact that this formulation uses the admittance of the line rather than the impedance. $Z_l = r_l + jx_l \ [\Omega/km]$ is the impedance of a 1 km-long type l line. It is multiplied by $D_{ij}[km]$ to get the total impedance in Ω of the line between i and j with the type l conductor. $Y_l = (g_l + jb_l)[\Omega^{-1}]$ is the admittance of the same 1 km-long type l line but we avoid writing $[\Omega^{-1}/km]$ as it suggests to multiply Y_l by D_{ij} to get the total admittance of the whole line between i and j with the type l conductor. Yet, the opposite should be done: if a 1-km long line has an admittance of Y_l, then a 2-km long line with the same conductor will have a twice as small admittance! This is what is written in (**8.3**) and (**8.4**).

Model 8 Taylor-Hoover-based Joint Planning Model(TH-JPM)

Minimize:

(**7.1**)

Subject to:

(**7.2**)-(**7.18**)

$$p_{ijt} = \sum_{l \in \mathcal{L}} p_{ijlt} \qquad \forall (i,j) \in \mathcal{E}, t \in \mathcal{T} \quad \textbf{(8.1)}$$

$$q_{ijt} = \sum_{l \in \mathcal{L}} q_{ijlt} \qquad \forall (i,j) \in \mathcal{E}, t \in \mathcal{T} \quad \textbf{(8.2)}$$

$$(1 - \lambda_{ijly}) \frac{g_l^2 + b_l^2}{D_{ij}^2} (\underline{v}^2 - \overline{v}^2) \leqslant \frac{g_l}{D_{ij}} (p_{ijlt} - p_{jilt}) - \frac{b_l}{D_{ij}} (q_{ijlt} - q_{jilt}) - \frac{g_l^2 + b_l^2}{D_{ij}^2} (w_{it} - w_{jt})$$

$$\leqslant (1 - \lambda_{ijly}) \frac{g_l^2 + b_l^2}{D_{ij}^2} (\overline{v}^2 - \underline{v}^2) \qquad \forall (i,j) \in \mathcal{E}, l \in \mathcal{L}, t \in \mathcal{T}, y \in \mathcal{Y} : y = t \text{ div } H + 1 \quad \textbf{(8.3)}$$

$$\frac{b_l}{D_{ij}} (p_{ijlt} + p_{jilt}) + \frac{g_l}{D_{ij}} (q_{ijlt} + q_{jilt}) = 0 \quad \forall (i,j) \in \mathcal{E}, l \in \mathcal{L}, t \in \mathcal{T}, y \in \mathcal{Y} : y = t \text{ div } H + 1 \quad \textbf{(8.4)}$$

$$\underline{v}^2 \leqslant w_{it} \leqslant \overline{v}^2 \qquad \forall i \in \mathcal{V}, t \in \mathcal{T}, \quad \textbf{(8.5)}$$

The (TH-JPM) model is a lossless model. Indeed, none of its equations imposes non-zero losses. In the absence of (**7.4**) and (**7.5**), the (THM) formulation of power flows even allows non-physical negative losses as discussed previously.
We thus introduce an alternative model (TH-JPM-L) in which the objective is slightly adapted to penalize losses. Losses are typically quadratic functions of currents or voltages and we want to keep the model linear. We penalize in the objective function the distribution of power over long and resistive lines, i.e. $p_{ijt} \times r_{ij} \times D_{ij}$. Nevertheless, as $p_{ijt} = p_{jit}$ in this formulation, the terms corresponding to both directions (i,j) and (j,i) would cancel each other and sum of this term over all lines in both directions would be zero. Hence, we only consider select the direction for which the active power flow is positive.

A new variable p^+_{ijlt} is introduced which is equal to p_{ijlt} when it is positive and zero otherwise. This is expressed by constraint (**9.1**). Note that this constraint alone doesn't ensure that $p^+_{ijlt} = 0$ if $p_{ijlt} \leqslant 0$ nor $p^+_{ijlt} = p_{ijlt}$ if $p_{ijlt} \geqslant 0$. However, as

it is the only constraint including p^+_{ijlt}, the minimization objective will always tend to make p^+_{ijlt} as small as allowed by (**9.1**).
It should also be mentioned that for the sake of convenience, the penalty coefficient for this term has been arbitrarily chosen to be equal to the variable cost of production for the first considered generation technology ($g = 1$), another choice could be made.

Model 9 Taylor-Hoover-based Joint Planning Model with losses approximation(TH-JPM-L)

Minimize:

(**7.1**) $+C^P_{1v} \sum_{(i,j)\in\mathcal{E},l\in\mathcal{L},t\in\mathcal{T}} D_{ij} p^+_{ijlt}/g_l$

Subject to:

(**7.2**)-(**7.18**),(**8.1**)-(**8.5**)

$$-\overline{S}_l(1-\lambda_{ijly}) \leqslant p^+_{ijlt} - p_{ijlt} \leqslant \overline{S}_l \quad \forall (i,j)\in\mathcal{E}, l\in\mathcal{L}, t\in\mathcal{T}, y\in\mathcal{Y} : y = t \text{ div } H + 1 \tag{9.1}$$

4.6.3 Convex DistFlow model

As mentioned above, the (C-DFM) formulation is exact for numerous practical cases of radial networks. We thus formulate a planning problem based on it that will be considered as our reference planning model.

For this planning model, we have to model line investments in a slightly different way. As a matter of fact, the impedance of a line depends linearly on the different λ_{ijly}. Hence, equation (**4.6**) will depend quadratically on λ_{ijly} values, which brings another source of non-convexity. We thus model all the different combinations of conductors offline and each $l \in \mathcal{L}$ now represents one of these combinations instead of representing the presence of this conductor in parallel of the other ones on a particular section. Hence, all λ_{ijly} are mutually exclusive as imposed by (**10.1**).

Eq. (**10.2**) is taken from (C-DFM) . Eqs. (**10.3**)-(**10.7**) are reformulated from (C-DFM) in a disjunctive way. As before, lower and upper bounds are determined as the smallest value such that the constraint is not active if $\lambda_{ijly} = 0$, in order to tighten the feasible space as much as possible. Note that $\max_l(r_l\overline{S}_l^2)$ and $\max_l(x_l\overline{S}_l^2)$ in right-hand terms of (**10.3**) and (**10.4**) respectively, are computed offline, they do not represent another optimization objective within the problem.

We also add constraints (**10.5**) and (**10.6**) to the model. These are redundant with (**10.3**) and (**10.4**). However, it is observed that they significantly reduce the solver runtime.
Then, we introduce the auxiliary variable τ_{ijy} in (**10.8**) to formulate the thermal rating constraint with the canonical three dimensional form (**10.9**).
The last constraint (**10.10**) ensures that the squared line current amplitude is the same in both directions (from i to j and j to i)

Model 10 Convex DistFlow-based Joint Planning Model (CDF-JPM)

Minimize:

(**7.1**)

Subject to:

(**7.2**)-(**7.5**),(**7.8**)-(**7.18**)

$$\sum_{l\in\mathcal{L}} \lambda_{ijly} = \omega_{ijy} \qquad \forall (i,j)\in\mathcal{E}, l\in\mathcal{L}, y\in\mathcal{Y} \quad \textbf{(10.1)}$$

$$p_{ijt}^2 + q_{ijt}^2 \leqslant w_{it} l_{ijt} \qquad \forall (i,j)\in\mathcal{E}, t\in\mathcal{T} \quad \textbf{(10.2)}$$

$$-(1-\lambda_{ijly}) r_l D_{ij} \frac{\overline{S}_\Lambda^2}{\underline{v}^2} \leqslant p_{ijt} + p_{jit} - r_l D_{ij} l_{ijt} \leqslant D_{ij} \max_l (r_l \overline{S}_l^2) \frac{1}{\underline{v}^2} (1-\lambda_{ijly}) \qquad \forall (i,j)\in\mathcal{E}, l\in\mathcal{L}, y\in\mathcal{Y} \quad \textbf{(10.3)}$$

$$-(1-\lambda_{ijly}) x_l D_{ij} \frac{\overline{S}_\Lambda^2}{\underline{v}^2} \leqslant q_{ijt} + q_{jit} - x_l D_{ij} l_{ijt} \leqslant D_{ij} \max_l (x_l \overline{S}_l^2) \frac{1}{\underline{v}^2} (1-\lambda_{ijly}) \qquad \forall (i,j)\in\mathcal{E}, l\in\mathcal{L}, y\in\mathcal{Y} \quad \textbf{(10.4)}$$

$$p_{ijt} + p_{jit} \geqslant 0 \qquad \forall (i,j)\in\mathcal{E}, t\in\mathcal{T} \quad \textbf{(10.5)}$$

$$q_{ijt} + q_{jit} \geqslant 0 \qquad \forall (i,j)\in\mathcal{E}, t\in\mathcal{T} \quad \textbf{(10.6)}$$

$$\begin{aligned}(1-\lambda_{ijly})[\underline{v}^2 - \overline{v}^2 - 2D_{ij}\overline{S}_\Lambda (r_l + x_l) - D_{ij}^2 (r_l^2 + x_l^2) \frac{\overline{S}_\Lambda^2}{\underline{v}^2}] \\ \leqslant w_{jt} - w_{it} + 2D_{ij}(r_l p_{ijt} + x_l q_{ijt}) - D_{ij}^2 (r_l^2 + x_l^2) l_{ijt} \\ \leqslant (1-\lambda_{ijly})[\overline{v}^2 - \underline{v}^2 + 2D_{ij}\overline{S}_\Lambda (r_l + x_l)] \\ \forall (i,j)\in\mathcal{E}, t\in\mathcal{T}, y\in\mathcal{Y} : y = t \text{ div } H + 1 \quad \textbf{(10.7)}\end{aligned}$$

$$\tau_{ijy} = \sum_{l\in\mathcal{L}} \lambda_{ijly} \overline{S}_l \qquad \forall (i,j)\in\mathcal{E}, y\in\mathcal{Y} \quad \textbf{(10.8)}$$

$$p_{ijt}^2 + q_{ijt}^2 \leqslant \tau_{ijy}^2 \qquad \forall (i,j)\in\mathcal{E}, t\in\mathcal{T}, y\in\mathcal{Y} : y = t \text{ div } H + 1 \quad \textbf{(10.9)}$$

$$l_{ijt} = l_{jit} \qquad \forall (i,j)\in\mathcal{E}, t\in\mathcal{T} \quad \textbf{(10.10)}$$

The last model we introduce in this section is an outer approximation relaxation of (CDF-JPM) in order to make it linear.

Model 11 Outer Approximation of Convex DistFlow-based Joint Planning Model(CDF-JPM-OA)

Minimize:

(**7.1**)

Subject to:

(**7.2**)-(**7.5**),(**7.8**)-(**7.18**),(**10.1**),(**10.3**)-(**10.7**)

$$\left\langle p_{ijt}^2 + q_{ijt}^2 \leqslant w_{it} l_{ijt} \right\rangle^{OA} \qquad \forall (i,j) \in \mathcal{E}, t \in \mathcal{T} \tag{11.1}$$

$$\left\langle p_{ijt}^2 + q_{ijt}^2 \leqslant (\sum_{l \in \mathcal{L}} \lambda_{ijly} \overline{S}_l)^2 \right\rangle^{OA} \qquad \forall (i,j) \in \mathcal{E}, t \in \mathcal{T}, y \in \mathcal{Y} : y = t \text{ div } H + 1 \tag{11.2}$$

4.6.4 Hierarchy of convex models for the joint planning problem

From here, the 'JPM' is omitted in the models acronyms for the sake of clarity. Thus far, eight models have been presented for the joint planning problem. Three of them, i.e. NF-IA, TH-IA and TH-L-IA, are *approximations* of NC (NC-JPM) as they do not contain its whole non-convex feasible set. As a matter of fact, in these models, constraint (**1.6**) that defines a cone is approximated with the more restrictive constraint (**23**) that defines a square pyramid inscribed in the cone, which removes some parts of NC original feasibility space.
The TH-L-OA model is also considered as an *approximation* of NC. Indeed, TH-L-IA and TH-L-OA models define the same feasible set as TH-IA and TH-OA respectively but they minimize a slightly different objective than the original problem.
Other models NF-OA, TH-OA, CDF-OA and CDF form a growing accuracy hierarchy of *relaxations* of NC , i.e.

$$\text{NC} \subseteq \text{CDF} \subseteq \text{CDF-OA} \subseteq \text{TH-OA} \subseteq \text{NF-OA} \tag{24}$$

This is illustrated on Fig. 4.5.

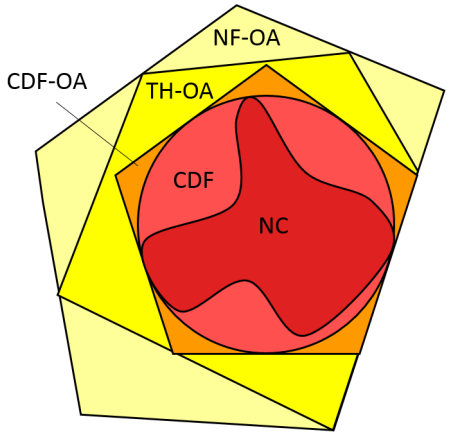

Fig. 4.5: Illustration of the hierarchy of convex relaxations

First, as mentioned in section 4.3 ,(NC-DFM) is a relaxation of NC. This implies that CDF, being a relaxation of (NC-DFM) (section 4.4.2), is also a relaxation of NC. Furthermore, CDF-OA is by construction a relaxation of CDF as it relaxes SOC constraints with outer tangent cutting planes (cf. section 4.6.3).
It is then straightforward to see that NF-OA is a relaxation of TH-OA as the latter is constructed by adding a set of constraints to those defining NF-OA feasible set (cf. section 4.6.2) which necessarily implies that TH-OA feasible set is contained in NF-OA feasible set.
Finally, it remains to be demonstrated that CDF-OA $\subseteq$ TH-OA. For that, it is necessary and sufficient to show that the power flow representation included in TH-OA is a relaxation of that of CDF-OA, which is stated in the following lemma:

Lemma 1. *A solution* $\{p^*_{ij}, p^*_{ji}, q^*_{ij}, q^*_{ji}, w^*_i, w^*_j, l^*_{ij}\}$ *of (C-DFM) automatically satisfies (THM) constraints.*

Proof. Eqs. (**4.1**) and (**6.1**) are identical as well as (**4.2**) and (**6.2**).
Considering that $Z_{ij} = R_{ij} + jX_{ij} = 1/Y_{ij} = 1/(g_{ij} + jb_{ij})$, we have $R_{ij} = g_{ij}/(g^2_{ij}+b^2_{ij})$ and $X_{ij} = -b_{ij}/(g^2_{ij}+b^2_{ij})$ respectively. Substituting these expressions of R_{ij} and X_{ij} in (**4.4**) and (**4.5**), we get:

$$\begin{aligned} p^*_{ij} + p^*_{ji} &= \frac{g_{ij}}{g^2_{ij} + b^2_{ij}} l^*_{ij} \\ q^*_{ij} + q^*_{ji} &= \frac{-b_{ij}}{g^2_{ij} + b^2_{ij}} l^*_{ij} \end{aligned} \tag{25}$$

Introducing these expressions in the left hand term(**6.4**) makes it identically zero, hence (**6.4**) is automatically satisfied by any (C-DFM) solution.

We may now rewrite l_{ij} with (**25**) :

$$l_{ij}^* = \frac{g_{ij}^2 + b_{ij}^2}{g_{ij}}(p_{ij}^* + p_{ji}^*) = -\frac{g_{ij}^2 + b_{ij}^2}{b_{ij}}(q_{ij}^* + q_{ji}^*) \tag{26}$$

Finally, by replacing R_{ij} and X_{ij} by their expression in function of g_{ij} and b_{ij} and l_{ij}^* by (**26**) in (**4.6**), we get

$$(w_i^* - w_j^*)(g_{ij}^2 + b_{ij}^2) = g_{ij}(p_{ij}^* - p_{ji}^*) - b_{ij}(q_{ij}^* - q_{ji}^*) \tag{27}$$

which is exactly constraint (**6.3**) from model (THM) . ■

We summarize and compare the different models features in table 4.1 that lists constraints and their mathematical form for all models presented in chapter 4.

Acronym	NF-IA	NF-OA	TH-IA	TH-OA	TH-L-IA	TH-L-OA	CDF-OA	CDF
Model	Network Flow		Taylor- Hoover		Taylor-Hoover w/ losses approx.		Convex DistFlow	
Connectivity	The network is connected, i.e. no islands							
Investments	No disinvestment							
Generators	Maximum generator rating (sizing) and capability curve (operation)							
Flow conservation	Flow conservation at every node							
Power flow constitutive equation	None		Linear lift-and-project relaxation				Linear OA of SOC relaxation	SOC relaxation
Voltage bounds	No		Yes					
Line thermal rating	Linear IA	Linear OA	Linear IA	Linear OA	Linear IA	Linear OA	Linear OA	SOC
Losses	None				Penalization in objective		Exact formulation	

Table 4.1: Summarizing comparison of the different planning models presented in chapter 4 in terms of constraints and mathematical forms. The accuracy of the models is increasing from left to right.

4.7 Efficient MILP solving with Benders decomposition

As mentioned in chapter 3, the classical way to deal with Mixed-Integer problems is to use branch-and-bound algorithms. We began testing the different convex relaxations presented in this chapter on a problem of a similar size to the test case introduced in the following section: 20 nodes, two conductor sizes and a single generator size.
For the CDF-OA model, the B&B algorithm had not yet converged after four days. Hence, we used an alternative approach to handle the complexity introduced by integer variable: the Benders decomposition. The complete description of this method being beyond the scope of this text, we shortly introduce it based on the detailed explanation in [79].
The main idea of this method is to transform the problem into easier master/slave problems that are solved iteratively until convergence to a solution. More precisely, the basic premise is that the problem contains *complicating variables* that appear in numerous constraints. Hence, they do not allow to separate the problem into independent subproblems with independent variables and sets of constraints, that would be easier to solve independently. To mitigate this issue, all variables but complicating ones are treated in a separate subproblem called the slave problem. We reproduce hereunder an example drawn from [79], using the exact same notation. Let us consider the problem (**28**) in which $\mathbf{x_1}$ is the vector of complicating variables (they appear in all constraints) and $\mathbf{x}_2$ represents the rest of variables.

$$
\begin{aligned}
&\min_{\mathbf{x}_1,\mathbf{x}_2} f(\mathbf{x}_1,\mathbf{x}_2) = c_1^T\mathbf{x}_1 + c_2^T\mathbf{x}_2 \\
&s.t. \\
&A\mathbf{x}_1 \geqslant b \\
&E\mathbf{x}_1 + F\mathbf{x_2} \geqslant h \\
&\mathbf{x}_1 \geqslant 0, \mathbf{x_2} \geqslant 0
\end{aligned}
\tag{28}
$$

Problem (**28**) may be exactly reformulated as (**29**). We observe that the master problem (left) only contains complicating variables while the slave problem (right) is dealing with non-complicating variables, complicating variables only appearing in the constraints and not in the objective. The contribution of non-complicating variables to the objective is approximated by $\alpha(\mathbf{x}_1)$ in the master problem. More precisely, $\alpha(\mathbf{x}_1)$ is a lower bound on this contribution. The principle of Benders decomposition is to progressively increase the value of this lower bound by solving the slave

problem.

$$\begin{aligned} &\min_{\mathbf{x}_1} f(\mathbf{x}_1) = c_1^T \mathbf{x}_1 + \alpha(\mathbf{x}_1) && \alpha(\mathbf{x}_1) = \min_{\mathbf{x}_2} c_2^T \mathbf{x}_2 \\ &s.t. && s.t. \\ &A\mathbf{x}_1 \geqslant b && F\mathbf{x}_2 \geqslant h - E\mathbf{x}_1 \\ &\alpha(x_1) \geqslant \alpha_{min} && \mathbf{x}_2 \geqslant 0 \\ &\mathbf{x}_1 \geqslant 0 \end{aligned} \tag{29}$$

In order to do this, the dual of the slave problem is formulated (30). Indeed, dual variables define a series of supporting hyperplanes (tangent lines for one-dimensional problems) of $\alpha(\mathbf{x}_1)$. These hyperplanes thus constitute a lower approximation of $\alpha(\mathbf{x}_1)$. The approximation accuracy increases with the number of hyperplanes, hence with the different values of dual variables.

$$\begin{aligned} &\alpha(\mathbf{x}_1) = \max_{\lambda} (h - F\mathbf{x}_1)^T \lambda \\ &s.t. \\ &E^T \lambda \leqslant c_2 \\ &\lambda \geqslant 0 \end{aligned} \tag{30}$$

The Benders decomposition is an iterative approach that can be summarized as follows:

1. Solve master problem with a lower bound for $\alpha(\mathbf{x}_1)$ (default, 0)
2. Inject the value found for $\mathbf{x}_1$ in the slave problem and get the dual variables λ
3. Add a Benders cut $\alpha(x_1) \geqslant \lambda^i(h - F\mathbf{x}_1)$ to the master problem and solve it again
4. Repeat steps 2) and 3) until convergence.

We illustrate the k^{th} iteration of the method in (31).

$$\begin{aligned} &\min c_1^T \mathbf{x}_1 + \alpha(\mathbf{x}_1) && \xrightarrow{\text{Trial value } \mathbf{x}_1^k} && \max (h - F\mathbf{x}_1^k)^T \lambda \\ &s.t. && && s.t. \\ &A\mathbf{x}_1 \geqslant b && && E^T \lambda \leqslant c_2 \\ &\alpha(x_1) \geqslant \lambda^i(h - F\mathbf{x}_1) \; i = 1, ..., k-1 && && \lambda \geqslant 0 \\ &\mathbf{x}_1 \geqslant 0 && \xleftarrow[\text{Dual variable } \lambda^k]{} \end{aligned}$$

(31)

Benders decomposition is applied for all test cases presented in the rest of this document. We use an automatic implementation of this algorithm included in CPLEX 12.7.0. We select the default settings of this implementation: the master problem deals with integer variables while all continuous variables are handled in the slave problem.

4.8 Numerical results

4.8.1 The Michiquillay test case

As stated in section 4.6, we want to compare the different convex models for the Joint Planning Problem on the feasibility of the solution, the investment solution and the computation time in order to identify a trade-off between accuracy and computational burden. Furthermore, we also want to assess the accuracy of the different models regarding the physics of power flows.
As mentioned in the previous section, we apply the Benders decomposition algorithm to all models in order to speed up the mixed-integer optimization process.
The models are tested on a real dataset corresponding to the district of Michiquillay, located in the Cajamarca department, North-West of Peru (Fig. 4.6). This hilly district is located in the part of the country with the lowest electrification rate. There are almost 6700 households in this district, most of them not being electrified [42]. The district has been identified as a Rural Electrification System by the government in the National Plan for Rural Electrification, by which a 11-kV supply network has been projected for the district on the period 2008-2017[42].
The Michiquillay district has been studied in the framework of the *Low-cost energy technologies for Universal Access*, a research project jointly led by the Massachusetts Institute of Technology (MIT, USA) and the IIT Comillas University (Spain) that resulted in the REM/RNM planning tool presented in section 1.2.2. In the particular Michiquillay test case, the result of the REM/RNM planning tool consists of 81 isolated microgrids and 8 grid extensions.

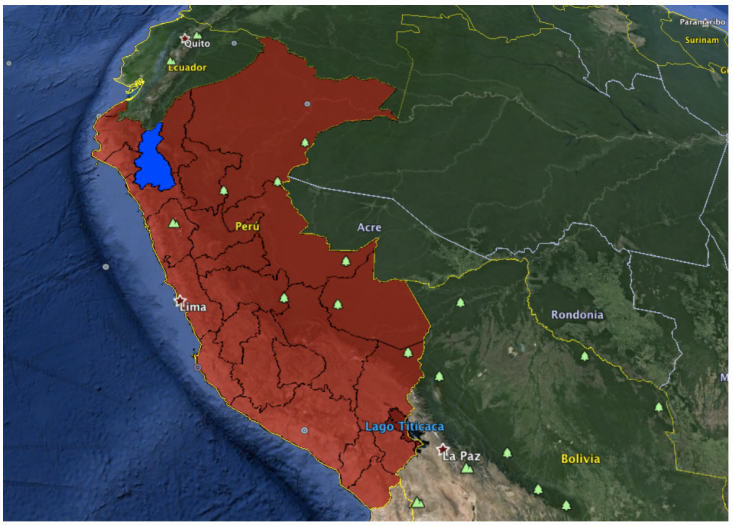

Fig. 4.6: Peru, Cajamarca department (blue) in which the Michiquillay district is located. Adapted from [42]

4.8.2 Modelling hypotheses

For the purpose of testing the different relaxed models presented earlier in this chapter in various configurations, 4 small-size microgrids are selected among the 81 covering the region in the solution from the REM/RNM planning tool. They respectively supply 18, 16, 20 and 21 households. These are single-phase microgrids including two conductor types, described in table 4.2: *Mole* and *Gopher*. The goal of this section is to compare the different models performances on the same cases. However, as shown further (Figs. 4.16a-4.16d) the CDF-OA model runtime is three to four order of magnitudes larger than other models runtimes and it proves to be computationally challenging even for small instances of the problem. For the purpose of comparing like with like, we need to choose a limited system size when running tests, hence only 12 nodes are selected in the aforementioned microgrids and the planning horizon is limited to one year. In order to further alleviate the computational burden for determining the optimal network graph, the set of allowed lines locations is heuristically reduced. First, the complete graph of the network is formed, connecting all nodes. Then, for each node, the three shortest edges connecting this node to another one are selected, forming a subset of the complete graph edges on which lines can be built. For a 10-node network, this may reduce the possible number of lines from 90 to 15.

We solve the different relaxed models on the groups of nodes corresponding to these 4 microgrids, i.e. we only consider the node locations and consumptions, the lines and generator data and solve the different relaxations of the Joint Planning Model

(JPM). The REM/RNM planning tool can choose among a large catalogue of generation technologies, including photovoltaïc (PV) generators and diesel generators. For this comparison, we only consider diesel generators options, while the REM/RNM planning solution only includes PV generators. The data for diesel generators can be found in table 4.3. It has to be noted that the cost function of diesel generator is based on a 2 $[\$/l]$ fuel cost, a high value which reflects the remoteness and the lack of road infrastructure in the Michiquillay district[42] .
The consumption profile of a household is built using the reference profile shown in Fig. 4.7 to which a random noise is added to create load diversity among the different consumption points. Finally, for all outer approximations (OA) models, i.e. NF-OA, TH-OA, TH-L-OA and CDF-OA, the κ parameter is set to 3. This value is chosen such that problems remain computationally tractable. Indeed, we want to compare all models on a common basis. Yet, as shown below, the CDF-OA model is already very long to solve for this small κ value, hence we could not make it higher if we wanted to keep the problem tractable. For this reason, we do not analyse the CDF formulation (in)exactness in this chapter. This topic is discussed in more detail in chapter 5 in the context of a purely operational problem, i.e. without considering investments.

Conductor		Mole	Gopher
Resistance	$[\Omega/km]$	20.37	8.41
Reactance	$[\Omega/km]$	1.58	1.41
Rating	$[kVA]$	15.24	26.56
Structure cost	$[\$/km]$	0	0
Conductor cost	$[\$/km]$	1174	2019
Yearly O&M cost	$[\$/(km.yr)]$	56.8	56.8

Table 4.2: Technical and cost parameters of different types of lines

Rated power	$[kVA]$	3
Max. power factor (capacitive/inductive)	$[/]$	0.8
Fixed investment cost	$[\$]$	2200
Variable investment cost	$[\$/kW]$	200
Fixed hourly generation cost	$[\$/h]$	0.85
Variable hourly generation cost	$[\$/kW]$	0.7
Fixed annual O&M cost	$[\$]$	109.8
Variable annual O&M cost	$[\$/kW]$	11.6

Table 4.3: Technical and cost parameters of diesel generators

Planning horizon	$[Year]$	1
Min. voltage	$[pu]$	0.9
Max. voltage	$[pu]$	1.1
Base voltage	$[V]$	230
Base power	$[kVA]$	1
Optimality gap	$[\%]$	1
Outer approximation (OA) parameter κ	$[/]$	3

Table 4.4: General problem data

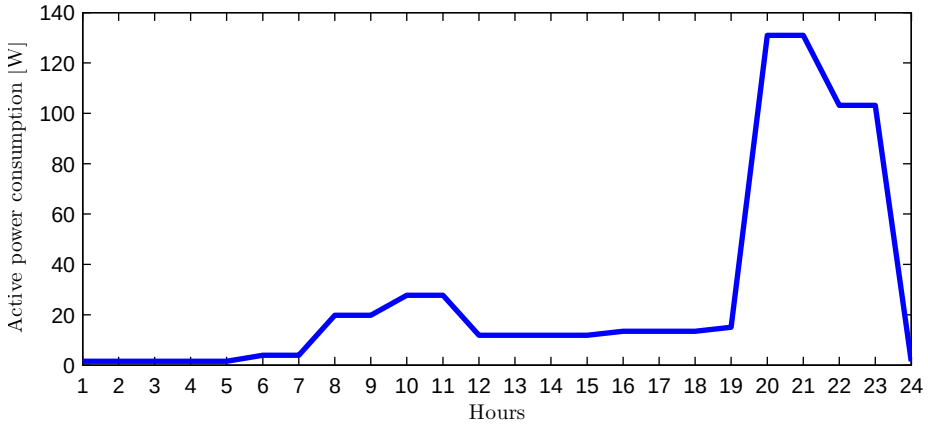

Fig. 4.7: Residential consumption profile for the Michiquillay region

4.8.3 Computational setup

The relaxed models presented in the previous sections are written in the specialized algebraic modelling language AMPL [36] and solved with CPLEX 12.7.1 using the embedded Benders decomposition tool for handling integer variables. The models are run on a 3.4Ghz Intel Core i7 processor with 8Go memory. The nonlinear AC-OPF problems are solved with *Matpower* 6.0 [104], a *Matlab*-based tool for solving the original non-linear AC Power Plow (PF) and Optimal Power Flow (OPF) problems. The solver being used is MIPS (Matlab Interior-Point Solver).

4.8.4 Feasibility of relaxed models solutions

To assess the quality of a relaxed model, the first step is to determine whether it produces feasible solutions to the original problem. As a matter of fact, relaxing some

of the original problem's constraints allows the solver to find an optimal solution to the relaxed problem that does not belong to the original feasible space.
It is necessary here to re-emphasize the difference between investment and operational decision variables. Investments are to be made accordingly to optimisation results, while operational decisions are likely to be recomputed closer to real-time with an operational dispatch tool.
In this section, we will define the feasibility of a solution in a slightly different manner from the usual mathematical definition. As a matter of fact, this would require all variables from the relaxed model solution to belong to the original feasible space. Yet, we mentioned above that this would likely not be the case for operational variables. Hence, a relaxed solution will considered to be feasible for the original problem if:

(i) Investment variables from the relaxed model solution belong to the original feasible space.
(ii) A feasible operational dispatch can be found by solving an exact, non-linear load-flow problem for every timestep of the problem

To find a feasible operational dispatch using an exact, non-convex representation of power flows, we use *Matpower* with the following procedure:

(i) Distribution and generation assets location and size originating from the relaxed models solutions are given to *Matpower* as an input, along with relevant technical parameters (impedance, rating,...) and generator cost functions
(ii) The exact, non-convex AC power flow representation (BIM) is chosen
(iii) An AC-OPF is solved for every timestep
(iv) The constraints of the AC-OPF are the following: generator capability curves, line thermal rating and voltage bounds. These are the same equipment limits that are used in the different relaxations presented above
(v) The objective is to minimize the generation cost over the different generators
(vi) The MIPS (Matlab Interior Point Solver) is used to handle the non-convex power flow equations

If a feasible solution exists for the non-linear problem, then conditions (i) and (ii) are both satisfied and the investment solution is considered feasible.
The feasibility of the different models is illustrated in Fig. 4.8 for the 4 considered microgrids in the form of the percentage of the 24 timesteps when *Matpower* is able to find a feasible operational dispatch. The first result is that the CDF-OA model delivers fully feasible solutions for all considered microgrids, despite the relatively low $\kappa = 3$ parameter. Then, it can be seen that NF-IA/OA and TH-IA/OA models have the same feasibility rate of 83% and 88% for microgrids 1-3 and 4 respectively. Finally, TH-L-IA/OA models perform similarly to these models except for microgrid 2 where they slightly outperform them, with a 88% feasibility rate. These feasibility rates are considered unacceptable. Indeed, an infeasible situation would translate into load shedding. Furthermore, in all test cases, it is observed that the problematic

timesteps are found between 20h and 23h. This is due to the fact that this timeframe corresponds to the evening peak consumption (Fig. 4.7). At this moment, the network loading is at its highest level as well as the constraints severity. The unserved energy in these cases would thus be very high.
When a feasible solution can be found, we notice that the binding constraints are always related to the voltage level, as it usually the case in rural distribution networks. This result can be expected as the lines are long and have a high impedance per unit length (see Tab. 4.2).

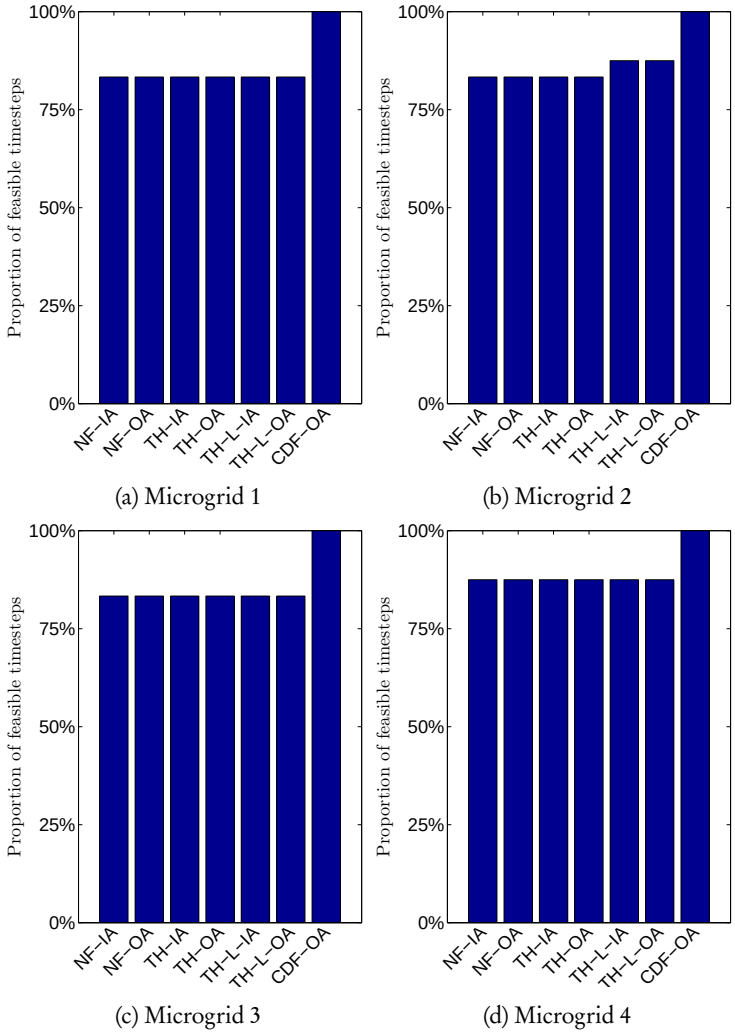

(a) Microgrid 1 (b) Microgrid 2

(c) Microgrid 3 (d) Microgrid 4

Fig. 4.8: Proportion of timesteps with a feasible solution for the 4 studied microgrids

4.8.5 Comparison of relaxed models investment solutions

In this section, the different models investment solutions are compared for each microgrid,. These are illustrated on Fig. 4.9 - 4.12. On this figure, generators locations are marked with red dots, black dots represent load points and thin and thick blue lines represent *Mole* and *Gopher* line sections respectively. It has to be noted that generators are located at load points, hence a generator node also has a load.
It can be observed that the lines are undersized in models NF-IA/OA,TH-IA/OA and TH-L-IA/OA with respect to the CDF-OA solution. As a matter of fact, for every considered microgrid, the CDF-OA solution is the only one including *Gopher* line sections (Figs. 4.9c, 4.10c, 4.11b and 4.12b). Regarding lines location, all models deliver the same network graphs for microgrids 2 and 3 while they only differ in the position of one line for microgrids 1 and 4. It is mentioned above that models other than CDF-OA exhibit a 12 % to 17 % infeasibility rate and that binding constraints are systematically related to the voltage level. Yet, for microgrids 2 and 3, the principal difference between CDF-OA solutions and other models solutions lies in the lines sizes as generator and lines locations change only slightly. It can therefore be deduced that line undersizing is the major factor for the operational infeasibility of solutions from models NF-IA/OA,TH-IA/OA and TH-L-IA/OA during heavy loading conditions. On the contrary, CDF-OA solutions including lower impedance *Gopher* line sections allow for lower voltage drops and thus satisfying voltage levels at every node.
As regards with power production, we see on Figs. 4.9, 4.10, 4.11 and 4.12 that a single generator is sufficient for all microgrids, irrespective of the considered model. As a matter of fact, the evening peak consumption for the whole network is a bit under 2 kW and the rated power of a generator is 3 kW. The location however differs between the different models. CDF-OA model tends to place the generator at the center of the network (Figs. 4.9c, 4.10c, 4.11b and 4.12b), which logically reduces network losses by diminishing the average distance between loads and the generator. Models NF-IA/OA neither account for losses nor voltage which is reflected in the generator location. Indeed, in these conditions, the location doesn't impact the objective (via additional losses) nor constraints (voltage not considered). A similar reasoning holds for TH-IA/OA as they are also lossless models, but approximated voltage variables are considered in these models, hence the generator location could affect the satisfaction of voltage level constraints. In practice, it is observed that all these 4 models place the generator at the same node for a given microgrid, which is close to the center (Figs. 4.9a and 4.11a) or not (Figs. 4.10a and 4.12a) . Finally, models TH-L-IA/OA should perform better regarding generator location as they penalize a proxy of the losses in the objective function. This is observed for micro-

grid 2 (4.11b) where the generator location is the same as in the CDF-OA solution. However, they place the generator at the same location as less accurate models for microgrids 3 and 4 and TH-L-OA even places it at a more outlying node for microgrid 1 (Fig. 4.9b).

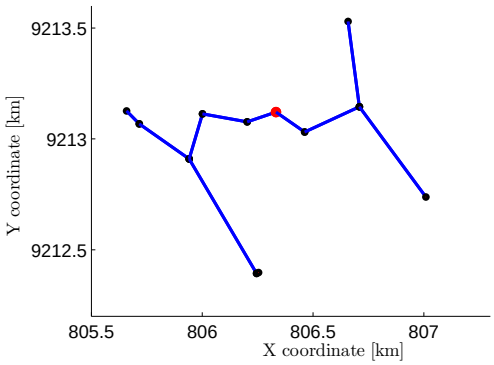

(a) Investment solution for models NF-IA/OA, TH-IA/OA and TH-L-IA

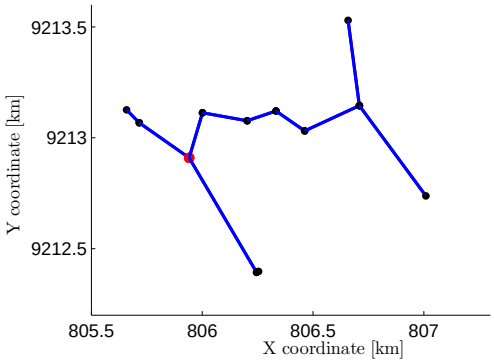

(b) Investment solution for model TH-L-OA

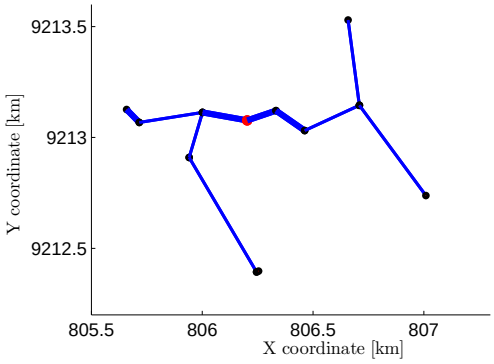

(c) Investment solution for model CDF-OA

Fig. 4.9: Investment solutions for Microgrid 1

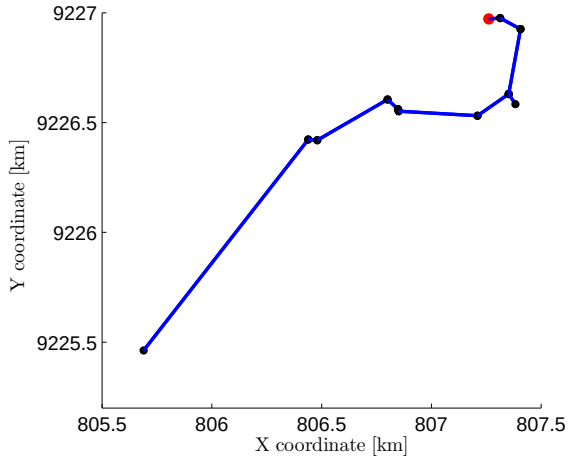

(a) Investment solution for models NF-IA/OA and TH-IA/OA

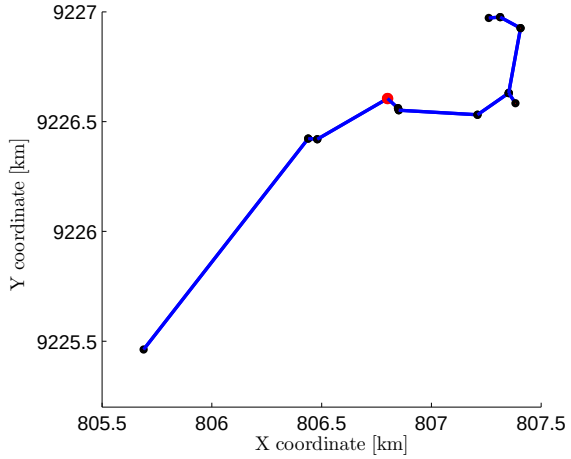

(b) Investment solution for model TH-L-IA/OA

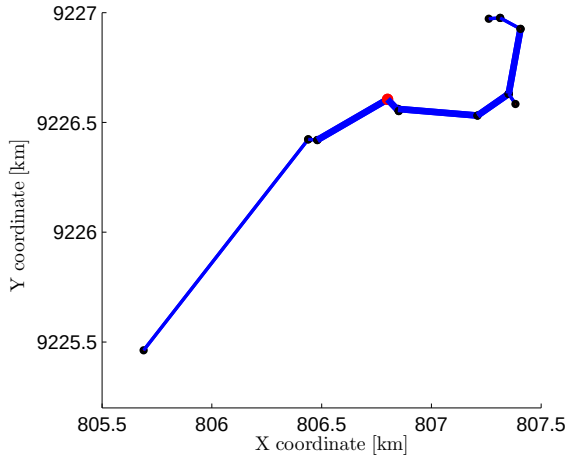

(c) Investment solution for model CDF-OA

Fig. 4.10: Investment solutions for Microgrid 2

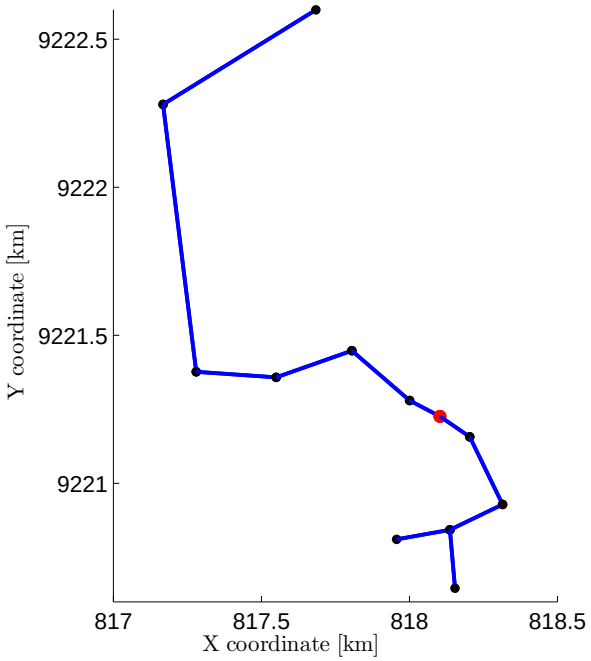

(a) Investment solution for models NF-IA/OA, TH-IA/OA and TH-L-IA/OA

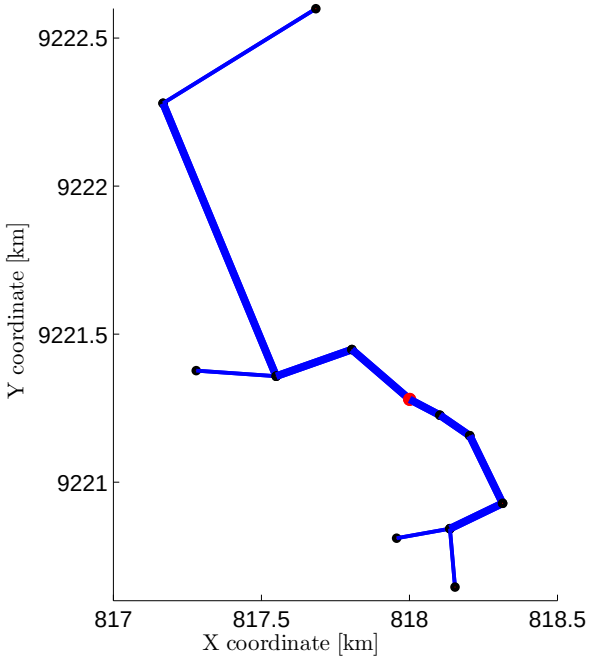

(b) Investment solution for model CDF-OA

Fig. 4.11: Investment solutions for Microgrid 3

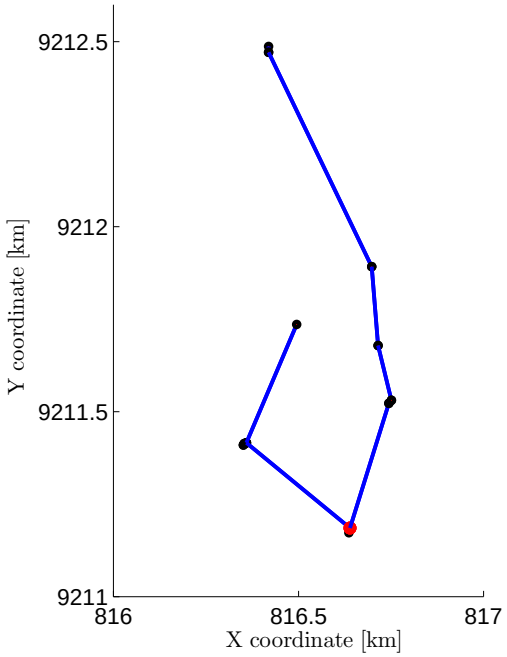

(a) Investment solution for models NF-IA/OA, TH-IA/OA and TH-L-IA/OA

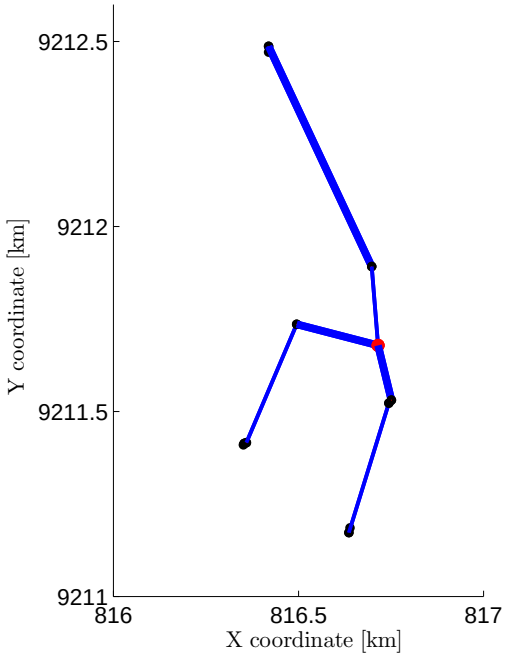

(b) Investment solution for model CDF-OA

Fig. 4.12: Investment solutions for Microgrid 4

4.8.6 Comparison of relaxed models solution costs

Total cost

The total solution cost is plotted on Fig. 4.13 for each model and microgrid. It includes lines CAPEX, generators CAPEX, fuel cost and operation and maintenance (O&M) cost for a period of 20 years. The first three cost components are detailed in section 4.2 and correspond to the generic model objective (**1.1**). For the present Michiquillay test case, the O&M component is added to comply with the REM/RNM results. It is expressed as a yearly cost per line length unit for distribution assets. For generation assets, it is composed of a yearly cost per generator rated power unit and a fixed yearly cost per installed generator. When computing fuel costs, we only considered timesteps when a feasible operational dispatch could be found for every model in order to compare like with like. This means that the period between 20h and 23h was not taken into account for fuel costs. We could also consider to put a price on the unserved energy in order to extend the operational cost comparison to all timesteps.
We can first observe on Fig. 4.13 that the different models solutions costs are very similar, the lines investments costs being the main observable difference between CDF-OA solutions and other models solutions. These graphs also show that the system cost is largely composed of fuel costs, which represent roughly 90% of the total. These fuel costs are very similar for all models, which will be further developed hereunder. O&M costs are the second most important cost component (5 to 6% of the total). Investment costs in generation and distribution assets each represent around 2% of the total cost, which is marginal compared with fuel costs. This is due to the fact that the power levels at stake are relatively low (the maximal power consumption at the scale of the microgrid is around 2 kW). Low capacity and relatively inexpensive components (lines and generators) are thus sufficient for these microgrids. In addition to that, as mentioned above, the fuel cost is high (2 $[\$/l]$) in this geographical remoteness context. Investment costs in generators are the same for every model in the 4 considered microgrids. Indeed, as shown above, there is a single 3 kW generator in all models solutions.

Lines cost

It is shown above that network graphs are very similar if not the same in the different solutions while the main difference between solutions is lines sizing. For all microgrids, CDF-OA solutions are the only ones to include higher capacity, more expensive, *Gopher* line sections. This is reflected on Figs. 4.14a - 4.14d where all model solutions share the same line investment cost except for CDF-OA solutions. This implies an extra line investment cost of 15 to 50 %.

Fuel cost

We finally compare the fuel costs for the different model solutions on Fig. 4.15, where the relative difference in these costs between any model solution and the corresponding CDF-OA solution is plotted. This difference is maximal for microgrid 2 where it reaches 0.4% for models NF-IA/OA and TH-IA/OA (Fig. 4.15b), as compared to a value around 0.1% for other microgrids.
We can observe for microgrid 1 and 2 that fuel costs from TH-L-IA/OA are slightly closer to those obtained with CDF-OA than other models, due to the approximation of losses in the objective that allows to find a better location for the generator, hence diminishing losses. Depending on the timestep, it is found that losses in less accurate models solutions may be almost twice as large as losses in the CDF-OA solution. Nonetheless, this does not impact the total fuel cost significantly (less than 1%) due to the fixed cost component in the generator cost function.

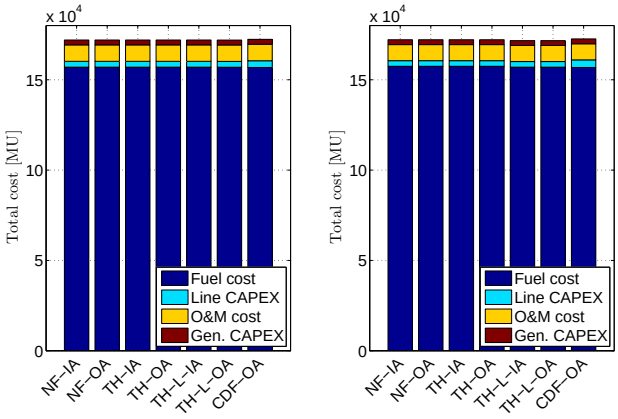

(a) Microgrid 1 (b) Microgrid 2

(c) Microgrid 3 (d) Microgrid 4

Fig. 4.13: Comparison of total costs for the 4 studied microgrids

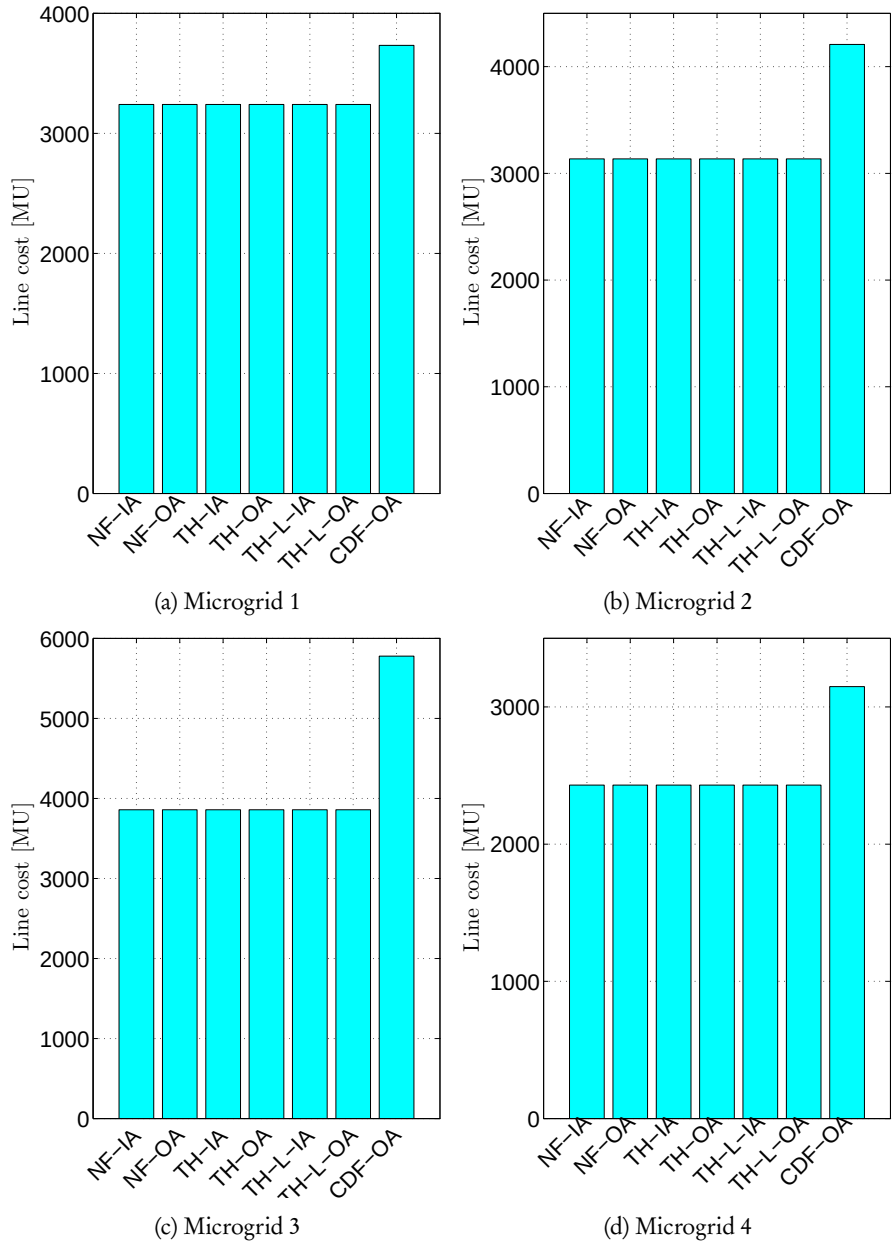

(a) Microgrid 1

(b) Microgrid 2

(c) Microgrid 3

(d) Microgrid 4

Fig. 4.14: Comparison of line costs for the 4 studied microgrids

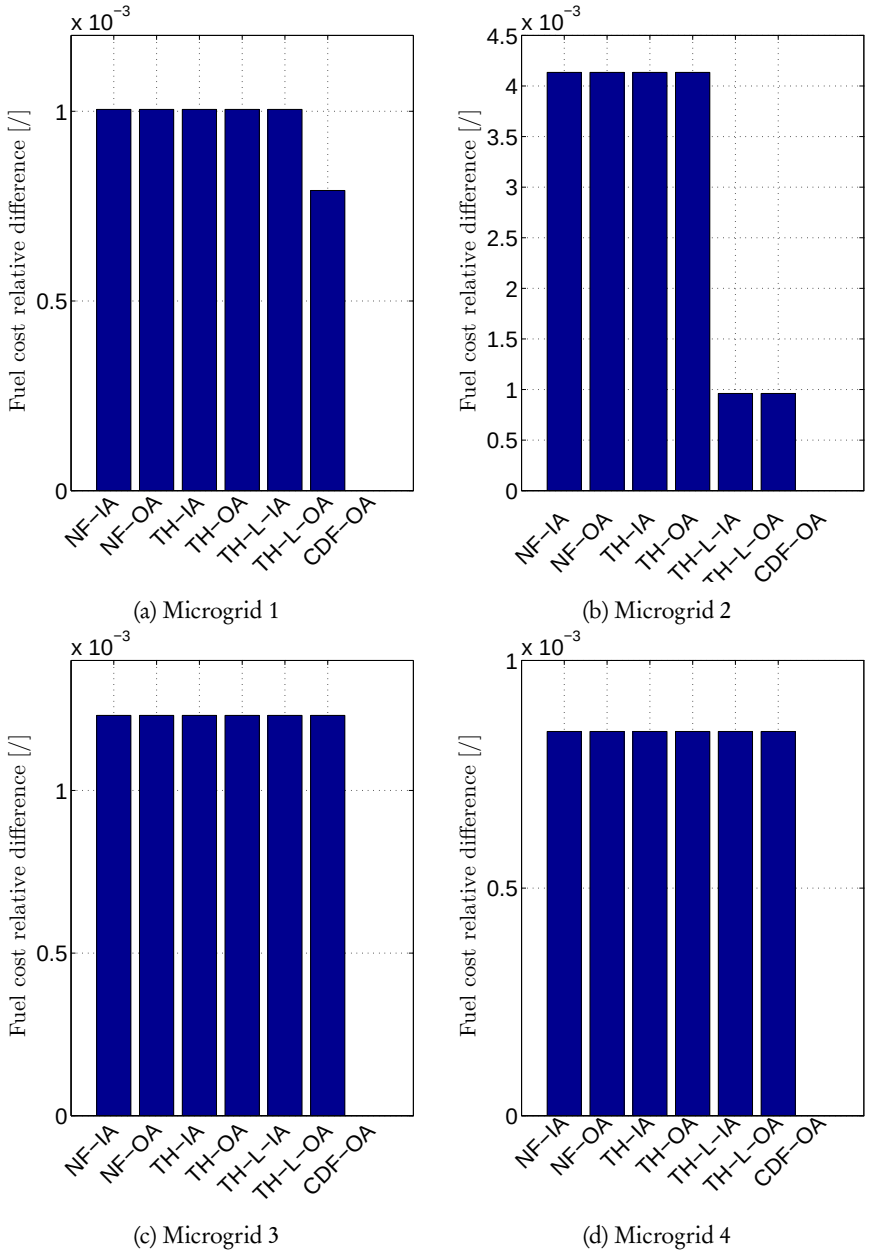

(a) Microgrid 1 (b) Microgrid 2

(c) Microgrid 3 (d) Microgrid 4

Fig. 4.15: Relative fuel cost difference with CDF-OA model for the 4 studied microgrids

4.8.7 Comparison of relaxed models runtimes and scalability

The NF-IA solution is used as an initial value for others models in order to accelerate the computation (warm start). Hence, the total runtime for a particular model is composed of its own runtime after initialization to which the NF-IA model runtime is added. It is important to notice that only runtimes after initialization are displayed in the subsequent results. The stopping criterion for the solver is to have an optimality gap inferior to 1%.
First, it can be observed that models NF-IA/OA and TH-IA/OA have similar runtimes in the second range for all microgrids (Fig. 4.16). Then, models TH-L-IA/OA have one to two orders of magnitudes larger runtimes that range from about 10 up to 50 s. This is explained by the additional disjunctive constraints (**9.1**) including binary variables λ_{ijly}. Finally, CDF-OA runtimes are much larger to other models ones as they range between 10^4 (Fig. 4.16a) and 10^5 s (Fig. 4.16b). This can be explained by various factors. First, there are more disjunctive constraints including binary variables ((**10.3**), (**10.4**) and (**10.7**)) than in other models (none for NF-IA/OA, (**8.3**) for TH-IA/OA and (**8.3**) and (**9.1**) for TH-L-IA/OA). Then, as opposed to other Outer Approximation (OA) models NF-OA, TH-OA and TH-L-OA there is another linearly approximated SOC constraint (**10.2**) besides the thermal rating constraint (**7.6**) that increases the computational burden. Finally, as explained above, the CDF-OA model is based on an exhaustive enumeration of all line investment configurations in order to remain convex. Practically, in the present testcases, two different conductors may be in parallel on each line section (*Gopher* and *Mole*). This means that there may be (i) a *Mole* conductor, (ii) a *Gopher* conductor, (iii) a *Mole* and a *Gopher* conductor in parallel or (iv) no conductor at all (hence no line). In other models, two binary variables are sufficient for that: λ_{ij1y} and λ_{ij2y} that model the presence of a *Mole* and a *Gopher* conductor respectively between nodes i and j at year y. Here, three mutually exclusive binary variables are needed: λ_{ij1y} equals 1 in case (i), λ_{ij2y} equals 1 in case (ii), λ_{ij3y} equals 1 in case (iii) and $\lambda_{ij1y} = \lambda_{ij2y} = \lambda_{ij3y} = 0$ in case (iv). Hence, more binary variables are needed in the CDF-OA model than in other ones, making it computationally more challenging.

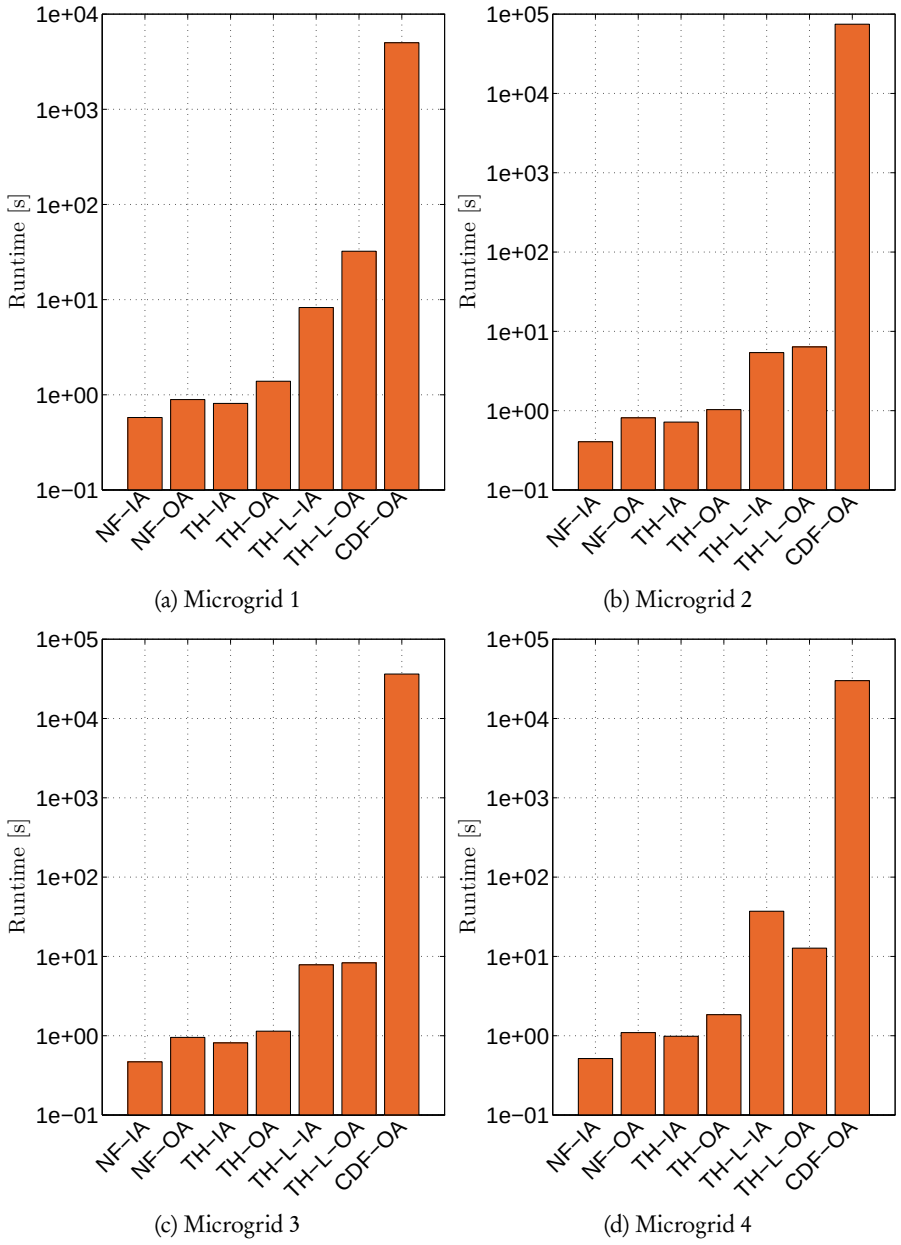

(a) Microgrid 1

(b) Microgrid 2

(c) Microgrid 3

(d) Microgrid 4

Fig. 4.16: Runtimes of the different models for the 4 studied microgrids

We now want to see how the different models scale. Hence, the models are run on the 'full' set of 18 nodes for microgrid 1. Furthermore, the planning horizon is now five years long instead of one. The other parameters (lines, generators, etc) remain unchanged. The results are displayed on Fig. 4.17 and are to be compared

to those of Fig. 4.16a which are obtained with a 12-nodes subset of the full dataset and a one year-long planning horizon. It can be observed that runtimes for models NF-IA/OA, TH-IA/OA and TH-L-OA are around an order of magnitude larger for the full dataset. Then, the runtime for the TH-L-IA model is around three orders of magnitude larger in the full dataset. Finally, the CDF-OA model was stopped after 70300 s ($\sim$ 19.5 hours) with a 84.61 % optimality gap.
While runtimes of less accurate models remain reasonable for the larger testcase, the CDF-OA is unable to converge in a reasonable time in this context.

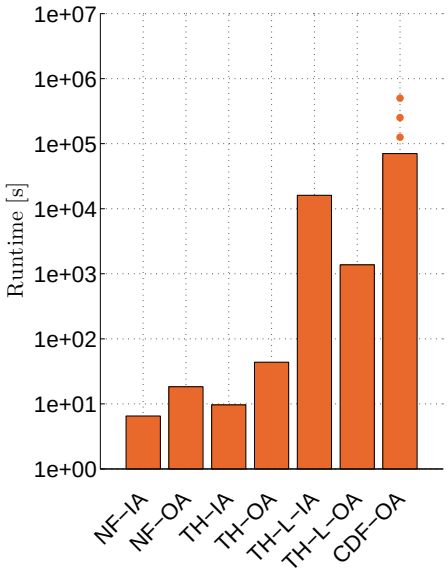

Fig. 4.17: Runtimes of the different models for the full microgrid 1 test case. The dots illustrate that the indicated runtime did not allow to converge with an optimality gap inferior to 1 %

4.8.8 Accuracy of the relaxed model regarding operational variables

In this section we compare the accuracy of the models regarding operational variables: voltages, active and reactive power flows, active and reactive power generation and currents. This is based on the results obtained when an OPF is solved with *Matpower* on the microgrid corresponding to the optimal investment solution of a given model. We compare the optimal values of operational variables we obtain from the relaxed models with those obtained with *Matpower* .
This comparison is meaningful as all solutions presented for the Michiquillay test case include a single generator. Indeed, we aim at assessing the accuracy of each model regarding power flows modelling It is therefore about determining the dif-

ferences between (re)active power flows and voltages as computed by relaxed models and Matpower at equal nodal power injections/withdrawals. Yet, the optimal generation dispatch could be different in relaxed models and *Matpower* with more than one generator. Nodal power injections/withdrawals would thus be potentially different between both, which would make the comparison irrelevant.
In all the following figures, the error E on a quantity Q is computed as follows, RM standing for 'Relaxed model' and MAT for *Matpower* :

$$E = \frac{|Q_{RM} - Q_{MAT}|}{Q_{MAT}}$$

Active and reactive power flows

It can be observed on Fig. 4.18 and 4.19 that CDF-OA performs better than other models, with relative errors not larger than 10^{-1} and 10^{-2} for active and reactive power flows respectively. Other models include much larger relative errors, up to 10^2 and 10^4 for active and reactive power flows respectively on microgrid 4 (cf. Figs 4.18d and 4.19d).

Active and reactive power production

The different models achieve a better accuracy for power injections than for power flows, with maximal relative errors in the order of 10^{-1} . This can be explained by the fact that the only difference between relaxed models and the exact one is the modelling of losses. Hence, the relative error for power production must correspond to the ratio of losses to total production. This is confirmed in the results with a maximal relative error of 20% observed for microgrid 2 (Fig.4.18b) that corresponds to a 20 % ratio of losses to total production observed during the evening peak demand for models NF-IA/OA and TH-IA/OA.
The relative error on the generated reactive power is lower than its active counterpart. This can be explained with a reasoning similar to that developed above, knowing that reactive losses are lower than active ones in the present case given the resistive character of low-voltage networks.
We can finally note that CDF-OA performs better again than other models, with maximal relative errors in the order of 10^{-2} and 10^{-3} for active and reactive power production respectively.

Voltages

Models NF-IA/OA do not represent voltages, hence they are not included in the

comparison with *Matpower* . It can be seen that TH-IA/OA and TH-L-IA/OA models have very similar relative error distribution which is normal as they include the same power flow relaxation. For these models, the largest observed relative error is around 15% (Fig. 4.22). The maximal observed relative error on CDF-OA voltages is also around 15%, but the error distribution much more expands towards smaller values.

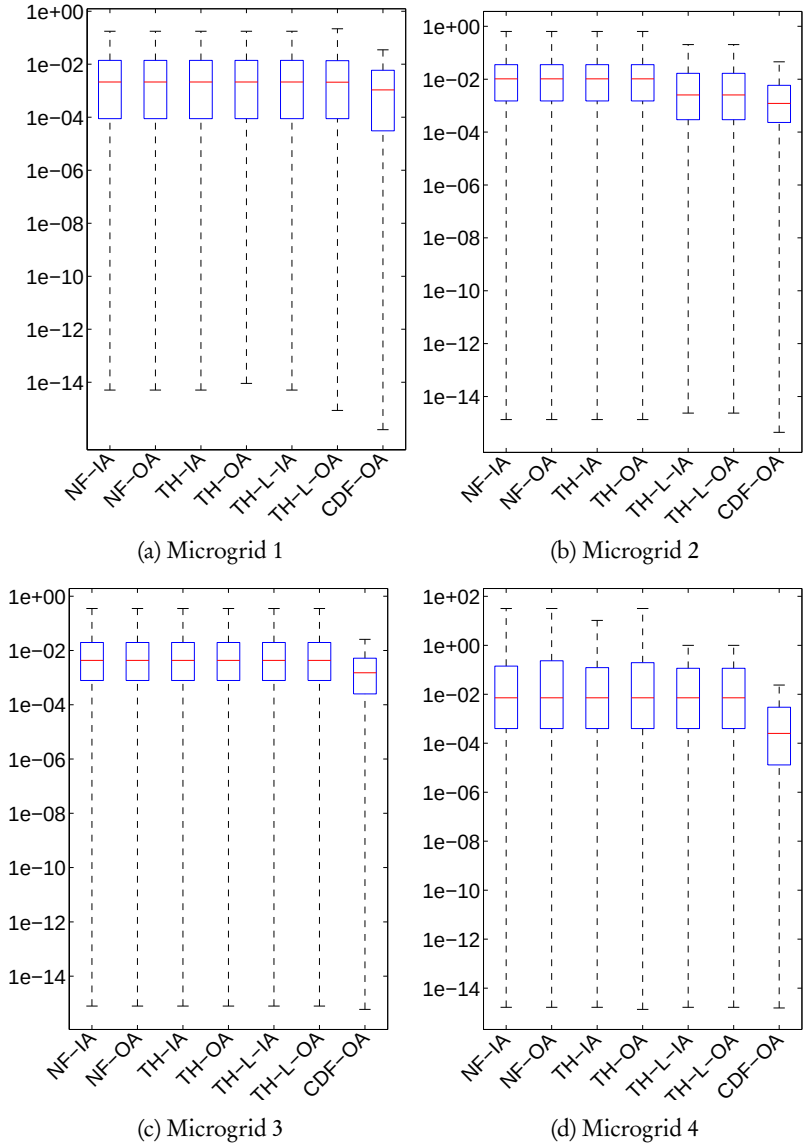

(a) Microgrid 1 (b) Microgrid 2

(c) Microgrid 3 (d) Microgrid 4

Fig. 4.18: Relative error on active power flows for the 4 studied microgrids

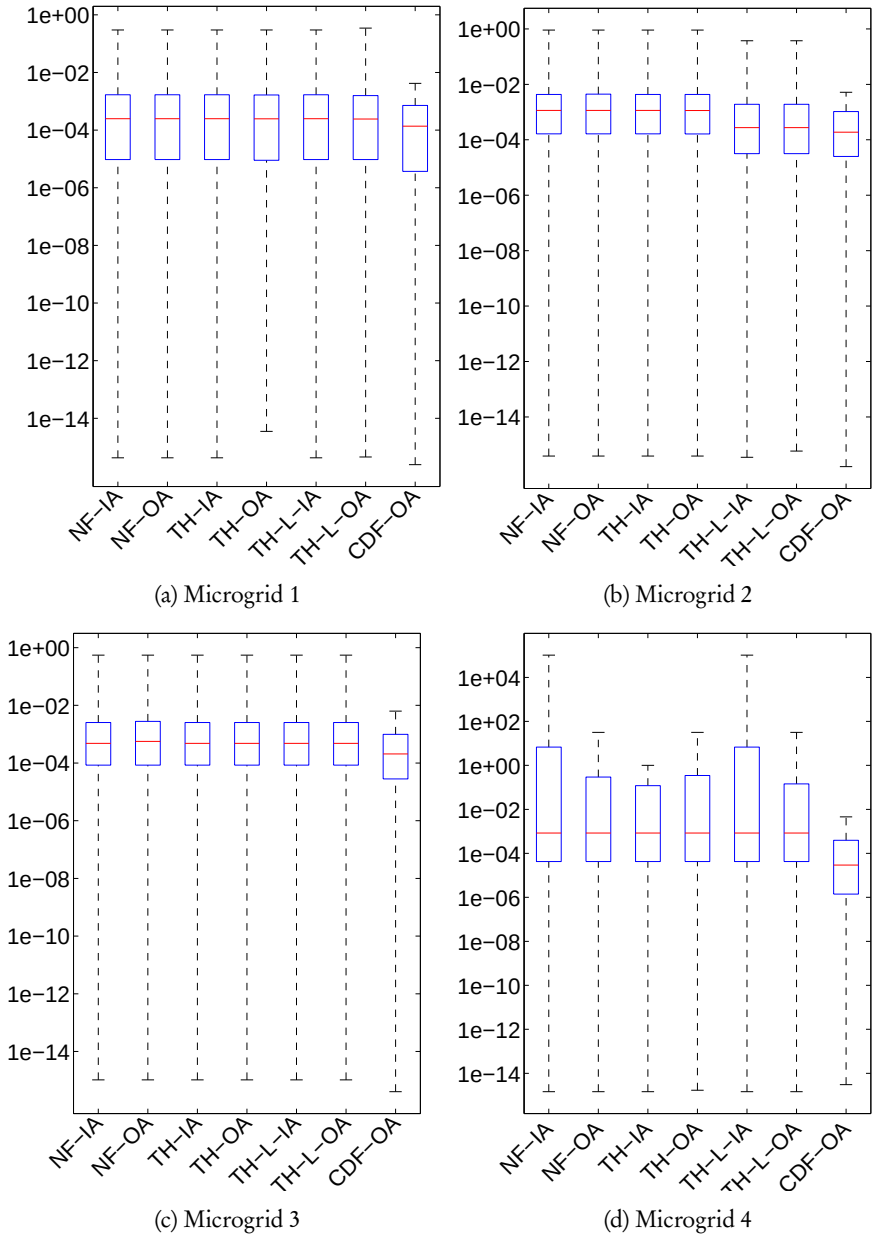

(a) Microgrid 1

(b) Microgrid 2

(c) Microgrid 3

(d) Microgrid 4

Fig. 4.19: Relative error on reactive power flows for the 4 studied microgrids

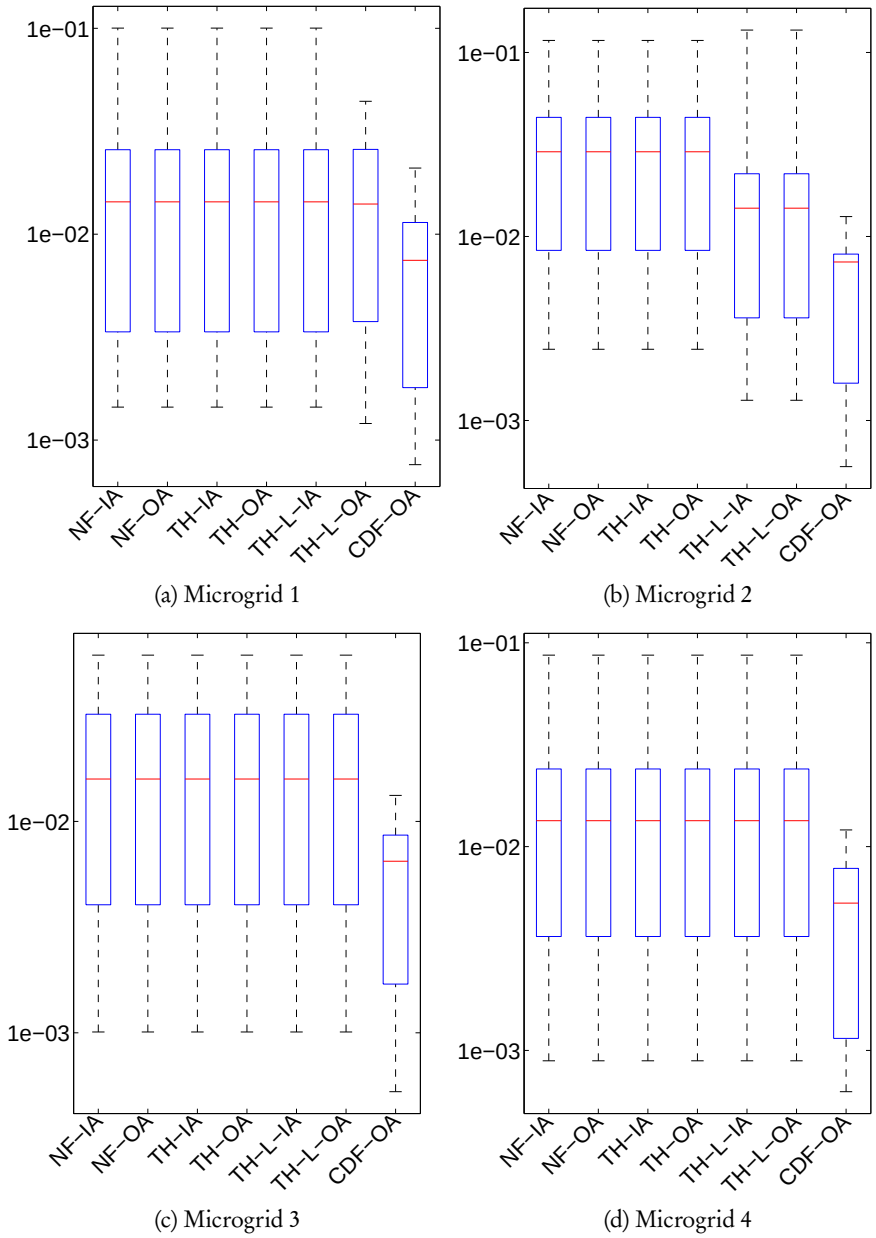

(a) Microgrid 1

(b) Microgrid 2

(c) Microgrid 3

(d) Microgrid 4

Fig. 4.20: Relative error on generated active power for the 4 studied microgrids

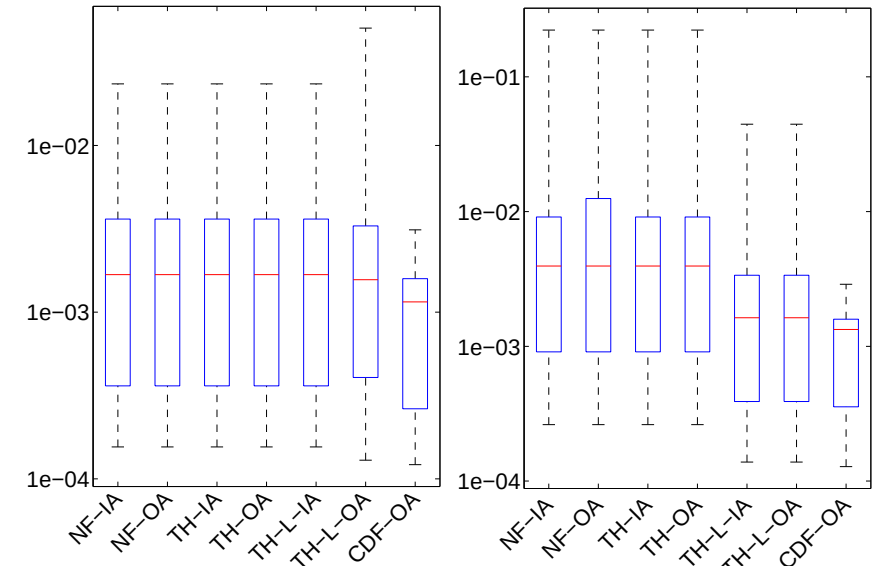

(a) Microgrid 1 (b) Microgrid 2

(c) Microgrid 3 (d) Microgrid 4

Fig. 4.21: Relative error on generated reactive power for the 4 studied microgrids

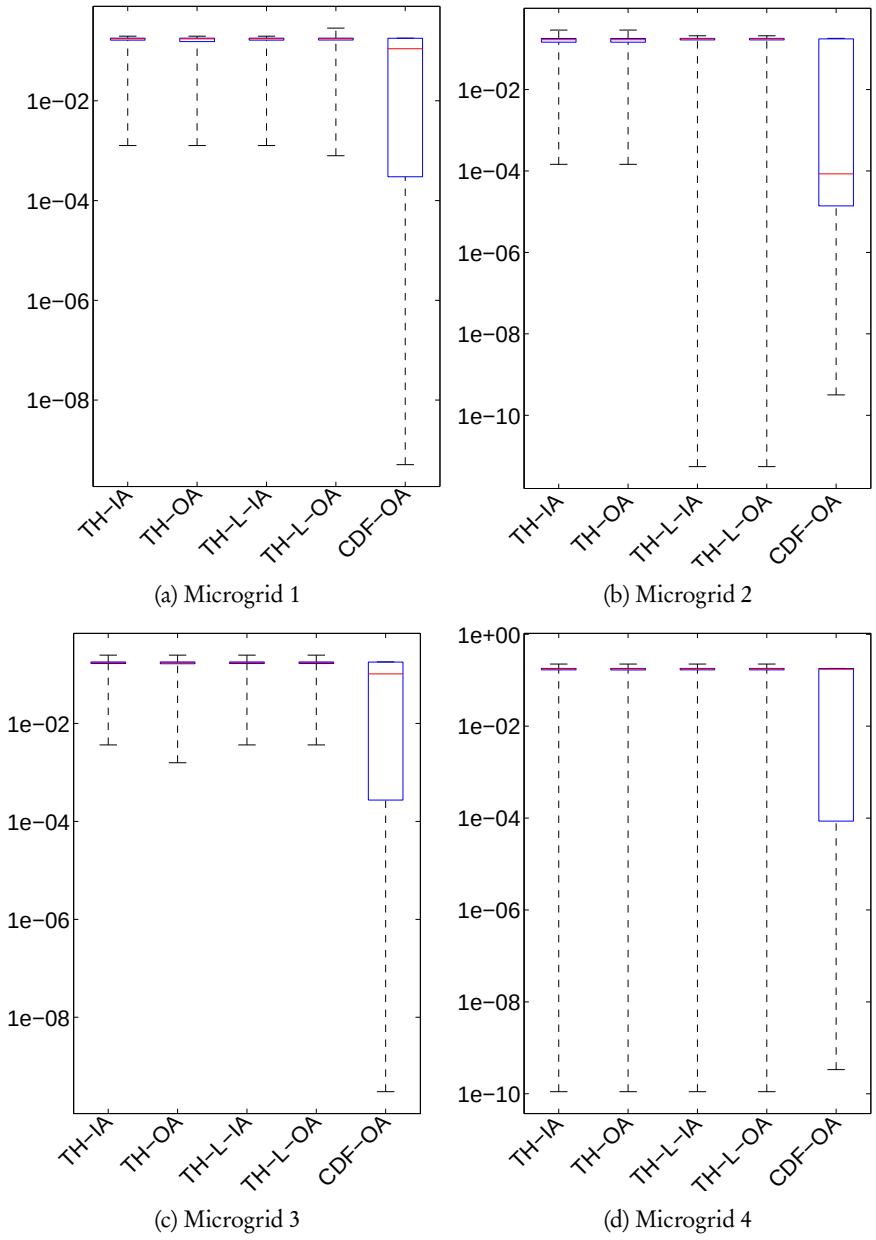

(a) Microgrid 1

(b) Microgrid 2

(c) Microgrid 3

(d) Microgrid 4

Fig. 4.22: Relative error on voltages for the 4 studied microgrids

4.9 Discussion and perspectives

In the previous sections, we compared the various models developed for the joint planning problem based on their solutions feasibility, cost and accuracy regarding power flow modelling. The observations can be summarized as follows:

(i) NF-IA/OA, TH-IA/OA and TH-L-IA/OA models do not deliver solutions feasible for all considered operational conditions and the infeasibility rate of the solutions delivered by these models is considered as unacceptable. Furthermore, they can suffer from non-negligible inaccuracy regarding operational variables, notably active and reactive power flows. However, they have been proven to be computationally tractable for small problems (one year planning, twelve nodes) and scale well for moderate size problems (five years planning, 18 nodes).

(ii) Among the above-mentioned models, voltages (TH-IA/OA) and losses (TH-L-IA/OA) approximations do not bring significant improvements in comparison with simple network flow (NF-IA/OA) models whether in terms of accuracy, feasibility or costs. Furthermore, TH-L-IA/OA models have significantly higher runtimes than NF-IA/OA and TH-IA/OA. Hence, the simplest Network Flow Models (NF-IA/OA) should be preferred over the TH-IA/OA and TH-L-IA/OA models as they offer very similar performances with a reduced computing budget. This is particularly true when we compare them to TH-L-IA/OA models for which the runtimes are up to two orders of magnitude larger.

(iii) The CDF-OA model delivers solutions that are always feasible for the considered operational conditions. It outperforms other models regarding the accuracy of power flows modelling, even though it could produce more accurate solutions with larger κ values for the outer approximation. Nevertheless, the model is shown to be already challenging from a computational point of view even for small size problems and $\kappa = 3$. In addition to that, it does not scale well as it did not converge in a reasonable time for a moderate size problem.

Thus far, there is a trade-off between a computationally tractable model offering limited quality results (NF-IA/OA) and another model delivering good and accurate solutions while being computationally intractable for real-world problems (CDF-OA). Hence, we conclude this chapter by investigating improvement perspectives for the purpose of targeting both satisfactory solutions and scalability to real-world problems.

To begin with, we implemented a lazy cuts approach to try and reduce the computational burden. It consists in an iterative procedure where a reduced problem is

first solved only considering a subset of the constraints. We then check whether the remaining constraints are satisfied or not. Those that are not are added to the model and the problem is solved again. At each iteration, constraints are added in a lazy fashion, i.e. as soon as they are violated. The procedure is stopped when all remaining constraints (i.e. not yet included in the model) are satisfied. This allows to solve the problem with fewer constraints, hence reducing the computational burden and from there the runtime. In the present case, the CDF-OA model was initially solved without constraints corresponding to outer approximations of SOC constraints, i.e. relaxed power flows constitutive equations (**11.1**) and line thermal rating constraints (**11.2**). A similar approach has been implemented in [77] for SOC constraints included in a resilient transmission expansion planning problem.
In the current work, the lazy cuts approach did not improve CDF-OA computational tractability. Indeed, after a few iterations, the amount of added constraints already made the reduced problem computationally intractable.

A second approach could be to solve less accurate models with more restrictive operational margins than the actual ones in order to get solutions feasible for more challenging conditions. However, as shown in the results section, problematic constraints observed in the rural setup of the Michiquillay test case were always related to the voltage level. Hence, Network Flow (NF-IA/OA) models would not be suited for the proposed approach as voltages are not represented in these models. This approach should thus be tested using TH-IA/OA or TH-L-IA/OA models.

Finally, decomposition approaches could offer interesting perspectives in this context. In [40], such approaches are studied in the context of the operational co-optimization of transmission and distribution grids in presence of renewables, which is also a computationally challenging problem. Among these algorithms, a Lagrangian relaxation scheme is proposed. It consists of removing complicating constraints that link transmission and distribution-related variables from the problem and penalize them in the objective function. This is done by formulating the Lagrangian of the problem, which is composed of the initial objective function to which a weighted sum of complicating constraints is added. This allows to separate the initially large problem into several smaller independent subproblems (i.e. with independent sets of variables) where the link between the subproblems is entirely located in their respective objective functions. A suitable iterative approach has then to be devised in order to update each subproblem objective in function of other subproblems.
As an illustration, the fastest decomposition algorithm used in [40] manages to solve a 24-timesteps unit commitment problem on a 24-node network within 400[s], while CPLEX takes about 8000[s] for the same problem.

Accuracy of the Convex DistFlow relaxation

5

This chapter is an adaptation of: B.Martin, P.De Rua, E.De Jaeger, and F.Glineur. Loss reduction in a windfarm participating in primary voltage control using an extension of the Convex DistFlow OPF (Forthcoming). In *20th Power Systems Computation Conference, Dublin, 2018*.

In this chapter, the goal is to study the accuracy of the outer approximation of the (C-DFM) model that has been presented in chapter 4. We examine it in the context of an OPF problem, i.e. the optimal operation of an existing power system. This means that we do not make any investment decisions.
We consider one of the largest French onshore wind farms that is requested by the transmission system operator (TSO) to participate in primary voltage control. This implies exchanging reactive power with the grid, by using both the wind turbines and static switchable capacitor and inductor banks installed in the windfarm. The reactive power setpoint dispatch between the wind turbines and the static units is currently suboptimal, leading to additional energy losses inside the collector grid of the wind farm. The goal is thus to formulate the problem as an Optimal Power Flow (OPF) to optimally determine the tap at the on-load tap changer (OLTC) and the reactive power dispatch among the WTs and the static units. The objective is to reduce the active power losses in the transformers and cables of the wind farm while performing the primary voltage control.
We base our approach upon the extended Convex DistFlow (CDF) model developed in [26]. This model is an extension of the (C-DFM) model presented in chapter 4 in which both the π model of lines and variable ratio transformers are considered. We further extend it by including discrete models of OLTC and static unit banks switching. The resulting model can be cast as MISOCP and we relax it with the linear Outer Approximation (OA) detailed in section 4.5, in the same way as we did for the (CDF-JPM) joint planning model. We then assess the accuracy of this model

in function of the degree of the OA, and we compare its performances to a non linear implementation of the problem using *Matpower* [104].
The chapter is organised as follows: section 5.1 describes the problem at hand and the windfarm under study, section 5.2 describes the augmented model we propose for solving the problem, numerical results and comparison with *Matpower* are presented in section 5.3 and discussed in section 5.4.

5.1 Problem description

The 78 MW-wind farm considered in this chapter participates in primary voltage control by injecting or absorbing reactive power at the point of common coupling (PCC), proportionally to the difference between the voltage at PCC and a voltage setpoint. For such a voltage static law, the reactive setpoint is limited by maximum capacitive and inductive values (Fig. 5.1).

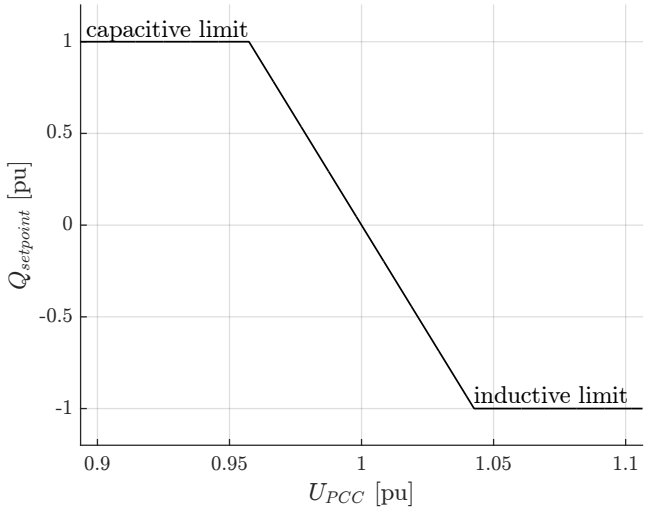

Fig. 5.1: Example of voltage static law

The reactive power is produced or consumed by the WTs and by switchable static units installed at the MV busbar of the substation. Currently, the WTs are used first and the static units are only used in case of large reactive setpoints. In addition, the WTs receive equal reactive power setpoints, which might be suboptimal.
The wind farm comprises 39 DFIG-based WTs grouped in 7 subparks. Transformers of 2.5 MVA connect the WTs to a 31 kV radial collector grid composed of buried cables. At the substation, a 120 MVA transformer equipped with an OLTC connects

the 31 kV collector grid to the 235 kV transmission network.

Currently, the purpose of the OLTC is to maintain the voltage on the medium voltage (MV) side of the substation as close as possible to its rated value. The static units comprise three capacitor banks of $+5$ MVAR and three inductor banks of -5 MVAR. The reactive power capability of the WTs is defined by a capability curve in the PQ plane. Although the WTs can behave as loads in stand-by mode (i.e. consuming active power), they cannot produce nor consume reactive power for negative active power outputs, as displayed in Fig. 5.2. This is imposed beforehand by setting the maximum capacitive and inductive capabilities to zero for all the WTs with a negative active power output.

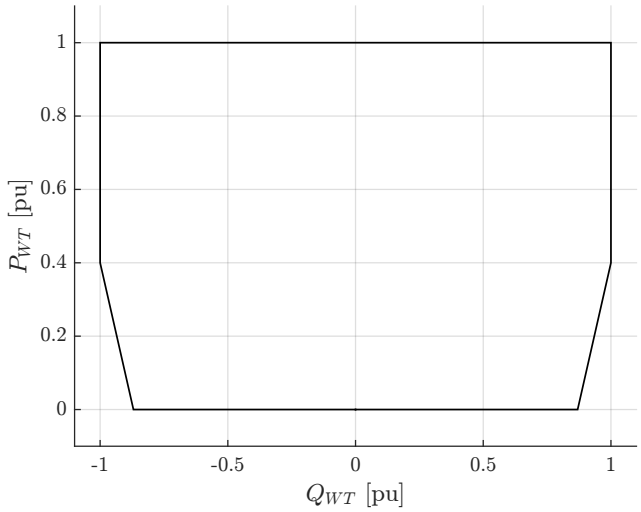

Fig. 5.2: Example of capability curve in the PQ space

5.2 Extended formulation of the Convex DistFlow Optimal Power Flow

5.2.1 Symbol Definitions

We define the sets, parameters and variables used in the proposed model as follows.

A. Sets

N	The set of nodes in the network
E	The set of directed arcs representing the lines in the network

E^R	The set of lines in E taken in the opposite direction

B. Parameters

n_{taps}	Amount of taps for the OLTC
n_{banks}	Amount of poss. states for the static unit banks
$r^k_{s,OLTC}, x^k_{s,OLTC}$	Series elements of the OLTC at k^{th} tap
t^k_{OLTC}	Turns ratio of the OLTC for the k^{th} tap
p^i_g	Measured active power produced by the wind turbine at node i
v_{PCC}	Voltage at the point of common coupling
$q^{set}_{PCC} = f(v_{PCC})$	Reactive power exchange at PCC, fixed by the droop characteristic of the plant
$y^s_i = g^s_i + \boldsymbol{j} b^s_i$	Shunt admittance at node i
b^k_{bank}	Equivalent shunt susceptance of the static unit banks for the k^{th} state
b^c_{ij}	Line charging susceptance of the π model of the line between nodes i and j
$z_{ij} = r_{ij} + \boldsymbol{j} x_{ij}$	Impedance of the line between i and j
$t_{ij} = t^R_{ij} + \boldsymbol{j} t^I_{ij}$	Turns ratio of the transformer located between i and j, in rectangular form
$tz^{*R}_{ij} = r_{ij} t^R_{ij} + x_{ij} t^I_{ij}$	
$tz^{*I}_{ij} = r_{ij} t^I_{ij} - x_{ij} t^R_{ij}$	
θ^{Δ}	Max. phase angle diff. between 2 nodes
$\overline{s}_{ij}$	Line thermal limit
$\underline{v}_i, \overline{v}_i$	Lower and upper voltage bounds at i
$\underline{q}, \overline{q}, q^-_{sl}, q^+_{sl}, q^0$	Constants for the WTS capability curve
ν	Weight for the reactive mismatch in the objective

C. Variables

p_{PCC}	Active power exchange at PCC, $\leqslant 0$ (resp. $\geqslant 0$) if injected on (resp. drawn from) the grid
q_{PCC}	Idem for reactive power
$q^+_{mis}, q^-_{mis} \geqslant 0$	Mismatch with the reactive setpoint if $q_{PCC} \geqslant 0$ (q^+_{mis}) or $q_{PCC} \leqslant 0$ (q^-_{mis})
μ	Binary representing whether the reactive mismatch is positive or negative
$\underset{\sim}{.}$	Vector quantity notation.
$\tilde{i}_{ij}$	Current $\forall (i,j) \in E$
v_i	Voltage $\forall i \in N$
$l_{ij} = \lvert i_{ij} \rvert^2$	$\forall (i,j) \in E$
$w_i = \lvert v_i \rvert^2$	$\forall i \in N$
p_{ij}	Active power flow $\forall (i,j) \in E \cup E^R$
q_{ij}	Reactive power flow $\forall (i,j) \in E \cup E^R$
q^g_i	Reactive power generation/consumption $\forall i \in N$
τ^k	Binary, $= 1$ if tap k is chosen $k \in \{1, ..., n_{taps}\}$
σ^k	Binary, $= 1$ if static unit bank state k is chosen $k \in \{1, ..., n_{banks}\}$

5.2.2 Original formulation

The model we present hereunder is an extension of the one developed in [26]. The block of constraints A corresponds to the original formulation while blocks B and C are original contributions of the present work. The original formulation has been developed in order to tackle transmission network-related problems including transformers and for which line charging capacitances may not be neglected. In this model, branches are modelled in the same way as in *Matpower* (Fig. 5.3). More precisely, each branch is composed of an ideal transformer followed by a π-section line. This branch model, in combination with bus shunt admittances, allows to model non-ideal transformers ($b^c_{ij} = 0$) as well as simple line sections ($t_{ij} = 1$). The complete derivation of this model being beyond the scope of this chapter, the interested reader is referred to [26] for more details.

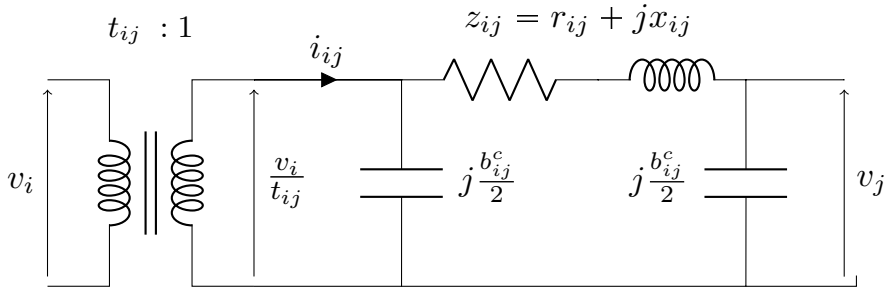

Fig. 5.3: *Matpower*-like line model

The objective to be minimized in this problem is composed of three terms. The first corresponds to the losses on the collector grid. Minimizing this term is equivalent to minimizing p_{PCC} (as p_{PCC} is negative if it is injected on the transmission network). The two other terms in the objective are penalty terms to be explained in subsection 5.2.3.

The first set of constraints in the model (Block A) originates from [26]. As mentioned above, this block of constraints is an extension of the (C-DFM) model that we analysed in section 4.4.2. Eqs. (**12.1**) and (**12.2**) represent the active and reactive power balance at every node of the network. Eqs. (**12.3**) and (**12.4**) model the active and reactive losses in the branches (lines and transformers) of the system and Eq. (**12.5**) represents the voltage drop on these branches. Eq. (**12.6**) represents the thermal rating limit for each branch. It is a second order cone (SOC) constraint, i.e. it defines a convex cone in $\mathbb{R}^3$ whose vertex is at the origin. Constraints (**12.7**) and (**12.8**) are linear inequalities describing the capability curve of WTs displayed in Fig. 5.2. Note that no limit is imposed on active power output of WTs as it is

considered as a parameter of the present problem. Eq. (**12.9**) is a relaxation of the constitutive equation $p_{ij}^2 + q_{ij}^2 = \frac{w_i}{t_{ij}^2} l_{ij}$ linking power flows to voltage and current variables. It is a rotated SOC constraint that can be equivalently represented by two three-dimensional SOC constraints (see chapter 4). Eq. (**12.10**) represents the voltage bounds at every node. Finally, constraints (**12.11**) and (**12.13**) model the limit on the voltage angle difference between two nodes.
It should be noted that two relaxations steps are made in this model: the SOC relaxation (**12.9**) and the convexification of the voltage drop equation that leads to (**12.5**). This convexification implies that voltage angles are not considered in the model anymore. However, in a radial setup (which is the case for the wind farm), angles can be recovered in a unique way from the solution as there are no cycles in the network, which would not be the case anymore in meshed networks. Hence, in this radial context, the relaxation is exact if and only if the right-hand term of (**12.9**) is equal to its left-hand term.

5.2.3 Point of common coupling

As mentioned above, the main transformer of the wind farm connects the collector grid to the PCC. Eqs. (**12.14**) and (**12.15**) model the power balance at the PCC while Eq. (**12.16**) models the transmission network voltage at the PCC. Eq. (**12.17**) models the fact that there might be a positive or negative mismatch between the reactive setpoint imposed to the wind farm and what the wind farm can actually produce/consume. Eqs. (**12.18**) and (**12.19**) impose that this mismatch is either positive or negative in a disjunctive way (big-M constraint, M being a suitable positive constant). The wind farm should follow the reactive setpoint if it is able to do so. Hence, we penalize $\nu\ (q_{mis}^+ + q_{mis}^-)$ in the minimization objective to avoid any reactive mismatch if there is no need for it. Finally, Eqs. (**12.20**) and (**12.21**) represent the activation of the static unit banks. Eq. (**12.20**) states that only a single state can be chosen for these units. Eq. (**12.21**) is a big-M constraint that represents the reactive power exchange with the static units in function of their state in a disjunctive way.

5.2.4 On-load tap changer

The main transformer of the wind farm, connecting the collector grid to the transmission network, is equipped with an OLTC that allows to modify the turns ratio of this transformer by discrete increments/decrements in a certain range around its nominal value. Eq. (**12.22**) models the fact that only one tap may be chosen at a given time. Eqs. (**12.23**) and (**12.24**) are the equivalent of eqs. (**12.3**) and (**12.4**) for the OLTC, written as a big-M constraint to account for the discrete nature of the tap changer while keeping convexity. Similarly, Eqs. (**12.25**) and (**12.26**) are the big-M

equivalents of (**12.5**) and (**12.9**) respectively for the OLTC. For sake of brevity, the computation of M values in big-M constraints is not detailed . However, the underlying rationale is to choose the lowest possible value of M such that the corresponding constraint is not binding when the considered binary variable (σ, τ) is equal to 0, in order to keep the model as tight as possible.

Model 12 Extended CDF-OPF for wind farm loss reduction

Minimize: $p_{PCC} + \nu\ (q^{+}_{mis} + q^{-}_{mis})$
Subject to:

A. Lines, transformers and nodes of the collector grid

$$p_i^g - g_i^s w_i = \sum_{(i,j)\in E\cup E^R} p_{ij} \tag{12.1}$$

$$q_i^g + b_i^s w_i = \sum_{(i,j)\in E\cup E^R} q_{ij} \tag{12.2}$$

$$p_{ij} + p_{ji} = r_{ij}\left(l_{ij} + b^c_{ij} q_{ij} + \left(\frac{b^c{}_{ij}}{2}\right)^2 \frac{w_i}{t_{ij}^2}\right) \tag{12.3}$$

$$q_{ij} + q_{ji} = x_{ij}\left(l_{ij} + b^c_{ij} q_{ij} + \left(\frac{b^c_{ij}}{2}\right)^2 \frac{w_i}{t_{ij}^2}\right) - \frac{b^c_{ij}}{2}\left(\frac{w_i}{t_{ij}^2} + w_j\right) \tag{12.4}$$

$$\left(1 - x_{ij} b^c_{ij}\right)\frac{w_i}{t_{ij}^2} - w_j = 2(r_{ij}p_{ij} + x_{ij}q_{ij}) - (r_{ij}^2 + x_{ij}^2)\left(l_{ij} + b^c_{ij} q_{ij} + \left(\frac{b^c_{ij}}{2}\right)^2 \frac{w_i}{t_{ij}^2}\right) \tag{12.5}$$

$$p_{ij}^2 + q_{ij}^2 \leqslant (\overline{s}_{ij})^2 \tag{12.6}$$

$$\underline{q} \leqslant q_i^g \leqslant \overline{q} \tag{12.7}$$

$$-q^0 - q^-_{sl} p_g^i \leqslant q_i^g \leqslant q^0 + q^+_{sl} p_g^i \tag{12.8}$$

$$p_{ij}^2 + q_{ij}^2 \leqslant \frac{w_i}{t_{ij}^2} l_{ij} \tag{12.9}$$

$$(\underline{v}_i)^2 \leqslant w_i \leqslant (\overline{v}_i)^2 \tag{12.10}$$

$$\tan(-\theta^{\Delta})\left(\left(t_{ij}^R + tz_{ij}^{*I}\left(\frac{b^c_{ij}}{2}\right)\right)\frac{w_i}{t_{ij}^2} - tz_{ij}^{*R} p_{ij} + tz_{ij}^{*I} q_{ij}\right) \tag{12.11}$$

$$\leqslant \left(t^I{}_{ij} - tz^{*R}{}_{ij}\left(\frac{b^c_{ij}}{2}\right)\right)\frac{w_i}{t_{ij}^2} - tz_{ij}^{*R} q_{ij} - tz_{ij}^{*I} p_{ij} \tag{12.12}$$

$$\tan(\theta^{\Delta})\left(\left(t_{ij}^{*R} + tz_{ij}^{*I}\left(\frac{b^c_{ij}}{2}\right)\right)\frac{w_i}{t_{ij}^2} - tz_{ij}^{*R} p_{ij} + tz_{ij}^{*I} q_{ij}\right)$$

$$\geqslant \left(t_{ij}^{*I} - tz_{ij}^{*R}\left(\frac{b^c_{ij}}{2}\right)\right)\frac{w_i}{t_{ij}^2} - tz_{ij}^{*R} q_{ij} - tz_{ij}^{*I} p_{ij} \tag{12.13}$$

B. Point of Common Coupling

$$p_{PCC} - g_1^s w_1 = \sum_{(1,j)\in E\cup E^R} p_{1j} \tag{12.14}$$

$$q_{PCC} + b_1^s w_1 = \sum_{(1,j)\in E\cup E^R} q_{1j} \tag{12.15}$$

$$w_1 = v_{PCC}^2 \tag{12.16}$$

$$q_{PCC} + q_{mis}^+ - q_{mis}^- = q_{PCC}^{set} \tag{12.17}$$

$$q_{mis}^+ \leqslant \mu M \tag{12.18}$$

$$q_{mis}^- \leqslant (1-\mu) M \tag{12.19}$$

$$\sum_{k\in\{1,\ldots,n_{banks}\}} \sigma^k = 1 \tag{12.20}$$

$$-(1-\sigma^k)M \leqslant q_2^g + b_{bank}^k w_i - \sum_{(2,j)\in E\cup E^R} q_{2j} \leqslant (1-\sigma^k)M \tag{12.21}$$

C. On Load Tap Changer

$$\sum_{k\in\{1,\ldots,n_{taps}\}} \tau^k = 1 \tag{12.22}$$

$$-(1-\tau^k)M \leqslant p_{ij} + p_{ji} - r_{s,OLTC}^k \left(l_{ij} + b_{ij}^c q_{ij} + \left(\frac{b_{ij}^c}{2}\right)^2 \frac{w_i}{t_{ij}^2} \right) \leqslant (1-\tau^k)M \tag{12.23}$$

$$-(1-\tau^k)M \leqslant q_{ij} + q_{ji} - x_{s,OLTC}^k \left(l_{ij} + b_{ij}^c q_{ij} + \left(\frac{b_{ij}^c}{2}\right)^2 \frac{w_i}{t_{ij}^2} \right) + \frac{b_{ij}^c}{2} \left(\frac{w_i}{t_{ij}^2} + w_j \right) \leqslant (1-\tau^k)M \tag{12.24}$$

$$-(1-\tau^k)M \leqslant \left(1 - x_{ij} b_{ij}^c\right) \frac{w_i}{t_{ij}^2} - w_j - 2(p_{ij} r_{s,OLTC}^k + q_{ij} x_{s,OLTC}^k) + ({r_{s,OLTC}^k}_{ij}^2 + {x_{s,OLTC}^k}_{ij}^2) \left(l_{ij} + b_{ij}^c q_{ij} + \left(\frac{b_{ij}^c}{2}\right)^2 \frac{w_i}{t_{ij}^2} \right) \leqslant (1-\tau^k)M \tag{12.25}$$

$$p_{12}^2 + q_{12}^2 \leqslant \frac{w_1}{{t_{OLTC}^k}^2} l_{12} + (1-\tau^k)M \tag{12.26}$$

5.2.5 Accuracy of the SOC relaxation under multi-objective optimization

The relaxation of $p_{ij}^2 + q_{ij}^2 = \frac{w_i}{t_{ij}^2} l_{ij}$ to an inequality means that l_{ij} could be higher than it should be in reality. However, as the losses increase with l_{ij}, the solver should not find it advantageous to have artificially larger currents and the right-hand term of Eq. (**12.9**) should reach its lower bound, i.e. the value of the left-hand term. Nonetheless, as the objective also includes the minimization of the reactive power mismatch, it could be conflicting with the loss minimization objective and currents might take artificially larger values than they should, hence making the relaxation inexact. In practice, this is observed in some cases that will be illustrated in the following section. Artificially large currents impacts the reactive production/consumption of the wind farm. On one side, they artificially increase reactive losses on the series reactance of the lines, hence helping the wind farm to absorb reactive power. On the other side, when WTs are consuming active power (no wind, auxiliary consumption), the voltage profile decreases towards the WTs and higher currents will cause larger voltage drops towards the WTs, hence lower voltages on line charging capacitances and reduced reactive power production from these elements. This analysis is valid when the voltage at the secondary of the collector transformer is constant. However, the OLTC can adapt this voltage hence the observed behaviour might differ from what has been described here.

5.2.6 Linear outer approximation of second order cone constraints

The model presented above is a mixed-integer second order cone program. We further relax it with the linear outer approximation of conic constraints presented in chapter 4. As a matter of fact, a large amount of instances of the problem have to be solved in order to cover the range of different operating conditions encountered throughout a year in the windfarm. Yet, the state-of-the-art Mixed-Integer Quadratically Constrained (MIQCP) solvers are not as mature as the mixed-integer linear programming solvers (MILP) [72], which is reflected on the computation time.

The OA is an ϵ^{OA}-approximation of SOC constraints in the sense that $||(x, y)|| \leqslant (1 + \epsilon^M)z$ with $\epsilon^M = \cos(\pi/2^{\kappa+1})^{-1}$ the largest possible error of the relaxation as shown in [10]. As ϵ^{OA} decreases exponentially with the relaxation degree κ, a reasonably small degree should be sufficient in order to reach a satisfying level of accuracy. In the particular case of the OA of (**12.9**), the observed ϵ will imply that the product of squared voltage and current amplitudes could be underestimated, in turn causing an underestimation of losses.

5.3 Numerical results

5.3.1 Accuracy of the relaxation

The solution s to the relaxed problem presented in the previous section is considered to be the combination of setpoints for the OLTC, bus voltages and reactive power production/consumption of WTs and static units, i.e. $s = (\underset{\sim}{q^g}, \sqrt{\underset{\sim}{w}}, \underset{\sim}{\sigma}, \underset{\sim}{\tau})$. As explained in the previous section, the SOC relaxation is exact in this radial case if and only if (**12.9**) is satisfied with equality. Let us define the relative relaxation error $\epsilon_{ij} \in \mathbb{R} \; \forall \; (i,j) \in E \cup E^R$ as follows:

$$||(p_{ij}, q_{ij})|| = \sqrt{p_{ij}^2 + q_{ij}^2} = (1 + \epsilon_{ij}) \sqrt{\frac{w_i}{t_{ij}^2} l_{ij}}$$

It has been shown that the additional OA allowed the right-hand term of (**12.9**) to be underestimated, i.e. $\epsilon_{i,j} > 0$. Furthermore, as explained in the previous section, with potentially conflicting objectives, the right-hand term of (**12.9**) might be overestimated as well, i.e. $\epsilon_{ij} < 0$. This is illustrated on Fig. 5.4.

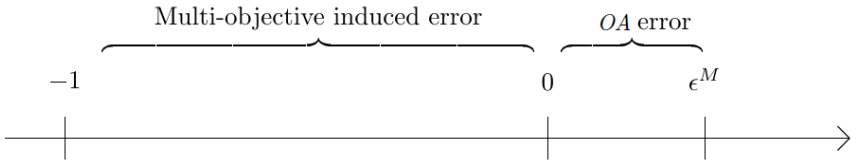

Fig. 5.4: Error introduced by the linear outer approximation and the multi-objective character

Let us further define the maximal error $\overline{\epsilon}$ as

$$\overline{\epsilon} = \{\epsilon_{ij} \text{ with } (i,j) \text{ s.t. } |\epsilon_{ij}| = \max_{(i,j)} |\epsilon_{ij}|\}$$

A solution obtained with the presented model will be considered accurate under the following conditions:

(i) The observed $\overline{\epsilon}$ is sufficiently small

(ii) The solution is feasible. This is determined by running a Power Flow problem (PF) with *Matpower* using s as an input.

Note that this is not the mathematical definition of feasibility. For the relaxation solution to be mathematically feasible, $\underset{\sim}{q^g}, \underset{\sim}{\sigma}, \underset{\sim}{\tau}, \underset{\sim}{p_{ij}}, \underset{\sim}{q_{ij}}$ should satisfy power flow equations exactly which will obviously not be the case because power flows are affected by the relaxation inaccuracies. This is compensated by the fact that the PCC is the slack bus in the PF problem. Active and reactive power injections at this bus thus serve as adjustment variables that compensate for those inaccuracies. Hence, the PF gives the exact value of p_{PCC} that would be obtained if the solution $s = (\underset{\sim}{q^g}, \underset{\sim}{\sqrt{w}}, \underset{\sim}{\sigma}, \underset{\sim}{\tau})$ of the relaxed problem was implemented in the wind farm.
For the purpose of testing the accuracy of the relaxations, 6 test-cases are defined according to the active power production (P) of the wind farm, whether it should absorb or inject reactive power (Q) from/to the transmission network and whether or not a mismatch is foreseen between the wind farm reactive setpoint and its effective reactive power output. The latter element determines whether there are two conflicting objectives or not, which has to be investigated regarding the accuracy of the SOC relaxation, as mentioned in the previous section. Those are considered to be limit cases representing the various extreme configurations that could be encountered in the operation of this wind farm:

Case 1	P: high	Q: consumption	no expected mismatch
Case 2	P: high	Q: consumption	expected mismatch
Case 3	P: low	Q: consumption	expected mismatch
Case 4	P: high	Q: injection	no expected mismatch
Case 5	P: high	Q: injection	expected mismatch
Case 6	P: low	Q: injection	expected mismatch

Table 5.1: 6 extreme test-cases

The results for theses 6 cases are shown in table 5.2. First, it can be observed that for cases 1 and 4, when no reactive mismatch is foreseen, the relaxed problem gets more and more accurate as κ grows. A value of 10 for this relaxation parameter allows to reach a satisfying precision of 3.3×10^{-3} and 2×10^{-4} for cases 1 and 4 respectively. Hence, in these cases, the relaxation can be made to arbitrary accuracy by increasing κ at the cost of a higher computational burden. For cases 2 and 3, the accuracy of the relaxation does not improve with κ and ϵ is even negative. This is due to the fact that the wind farm is supposed to absorb a higher amount of reactive power than it is capable of and there is a reactive mismatch which is penalized in the objective function. To reduce this mismatch and the objective value, the solver finds it advantageous to give larger values to currents in order to cause artificial reactive losses on the collector grid of the wind farm as explained in the previous section,

even though active losses are also increased.
A mismatch is also expected in case 6. However, since the wind farm is absorbing active power, artificially large currents cannot help to reach the reactive injection setpoint, hence the relaxation is observed to be increasingly accurate with κ. Finally, the relaxed problem may not be considered accurate in case 5 as the relaxation error is not decreasing at it should. Indeed, currents were expected to be as small as possible to decrease line reactive losses, hence better following the reactive injection setpoint. This is not what is observed as the relaxation error does not decrease with κ. We may thus conclude that the relaxed problem delivers accurate solutions when there is no foreseen reactive mismatch and might give poorer results when there is a reactive mismatch.

Table 5.2: Accuracy and feasibility of the relaxation for 6 test cases

Case	Total production [MW]	Reactive setpoint [MVar]	κ	$\bar{\epsilon}$	Feasible
1	-80	12	6	8.7×10^{-2}	yes
			8	1.8×10^{-2}	yes
			10	3.5×10^{-3}	yes
			12	3.3×10^{-5}	yes
2	-80	100	6	-8.2×10^{-1}	yes
			8	-7.3×10^{-1}	yes
			10	-9.7×10^{-1}	yes
			12	-9.8×10^{-1}	yes
3	0.2	100	6	∞	yes
			8	-6.1×10^{-1}	yes
			10	-6.1×10^{-1}	yes
			12	-6.1×10^{-1}	yes
4	-80	-12	6	1.1×10^{-1}	yes
			8	3.4×10^{-2}	yes
			10	2×10^{-4}	yes
			12	2.8×10^{-4}	yes
5	-80	-100	6	1.9×10^{-1}	yes
			8	8.1×10^{-2}	yes
			10	-9.9×10^{1}	yes
			12	-9.9×10^{1}	yes
6	0.2	-100	6	∞	yes
			8	1.5×10^{-1}	yes
			10	5.5×10^{-3}	yes
			12	1×10^{-4}	yes

5.3.2 Comparison with a *Matpower*-based approach

In this section, the goal is to compare the results obtained with the relaxed model to those obtained on the exact, nonlinear model with *Matpower* using MIPS (*Matpower* Interior Point Solver). *Matpower* does not provide tools to include elements such as the static units and the OLTC that are characterized by binary variables. For this reason, external loops are used to solve the OPF in each of the 147 configurations corresponding to the 21 taps of the OLTC and the 7 states of the static units. Real data originating from the wind farm covers the whole year 2014 on a 10 min basis. This represents 52560 timesteps. In order to alleviate the computational burden, these data have been clustered into 100 fictitious timesteps with the k-means algorithm. The goal of the comparison is to see if the solution of the relaxed problem might be better than that of the exact one, i.e. if p_{PCC} is smaller in the former case (recall that $p_{PCC} < 0$ if injected on the grid).
As mentioned in the previous section, a solution s of the relaxed model is injected in a *Matpower* PF to check its feasibility and the exact power output of the wind farm. To assess the accuracy of the relaxed model in terms of results, we also compute the difference between active and reactive power injections at the PCC in the solution of the exact problem and in the solution of the relaxed one. A smaller difference means a lesser slack compensation, hence lesser inaccuracies on power flows in the relaxed model. The performance of the relaxed model compared to the exact one is presented in Fig. 5.5 where the objective value improvement of the non-convex OPF in comparison with the relaxed OPF is plotted against the accuracy of the relaxed model for several degrees κ of the OA. Negative ordinates represent situations where the solution of the relaxed problem gives a better objective than the one from the exact non-convex problem. In these cases, the non-linear solver thus falls in local minima and the convex optimization is able to find a better solution. Positive ordinates, on the other side, represent situations where the non-linear solver is able to find a better solution than the relaxed convex model.
Several observations can be made about this graph. First, it can be seen that a higher accuracy is obtained by increasing κ, which was already shown on extreme cases from the previous section. Indeed, the cloud of points progressively shifts towards the left as κ is increased, which means that the slack compensation gets smaller, hence the relaxed model is more accurate. Then, it can be observed that the relaxed model outperforms the *Matpower*-based approach on a significant fraction of cases, roughly ranging from 10% to 25% when κ goes from 8 to 12. Finally, we can see that the points where the relaxed model performs significantly worse or better than the exact one are the ones with the lowest accuracy $\forall\kappa$. This result seems counterintuitive and needs further investigation to be explained.
It can be concluded from these results that *Matpower* sometimes falls in local minima, as it is expected from nonconvex problems, since the relaxed model is able to

find better solutions in some cases. We also compare the results based on the computation time for the different models. As it can be seen on Fig. 5.6, the relaxed model is faster to solve than the exact one for most cases for $\kappa = 8$. However, this is not the case anymore for $\kappa = 10$ and 12 as the computation time increases by up to one and two orders of magnitude respectively.

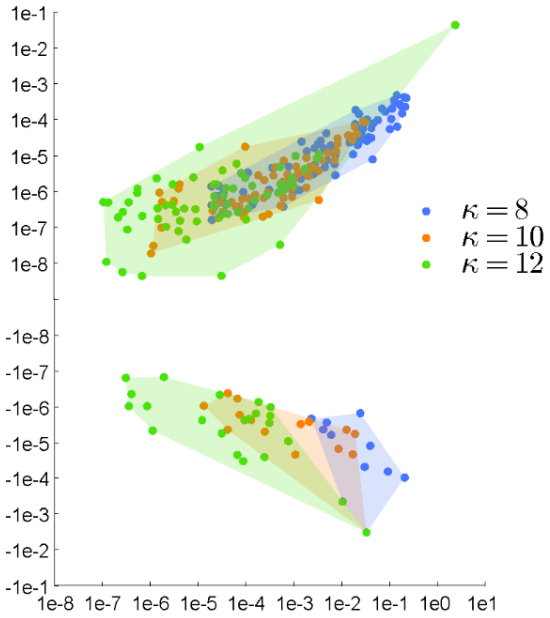

Fig. 5.5: Comparison of performances of the exact model and the relaxed models. X-axis: $|\Delta P_{slackBus,PF}| + |\Delta Q_{slackBus,PF}|[MVA]$ Y-axis: $|P_{PCC,exact}| - |P_{PCC,rel}|[MW]$

5.4 Discussion

In this chapter, we presented an extended convex DistFlow relaxation of the OPF problem able to cope with real-world network elements such as OLTC and capacitive cables. This relaxation is first formulated as a MISOCP and then further relaxed into a more tractable MILP, using an efficient outer approximation that can be made arbitrarily accurate (at the price of an increase in size of the model). This relaxed model is exact or close to exact in many situations. However, when the two components in its objective function are conflicting with each other, i.e. active loss minimization and compliance with a reactive setpoint, the relaxed model's performance is degraded. Nonetheless, this model already outperforms the *Matpower*-based approach on a sig-

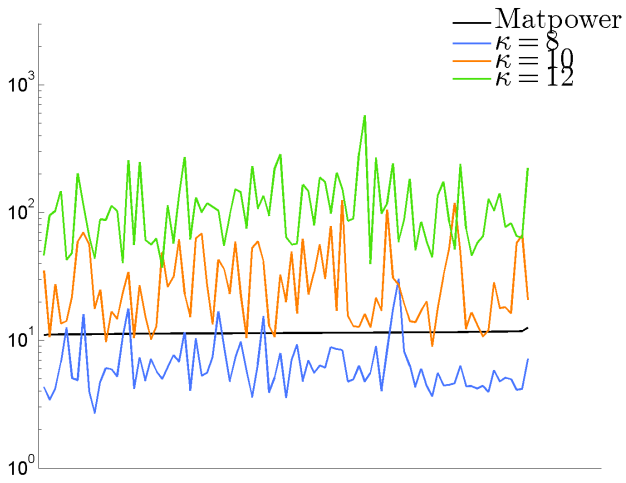

Fig. 5.6: Computation time $[s]$ for the different fictitious points and models

nificant fraction of test cases, in terms of objective value and computation time, and it is expected that the relaxed model becomes more advantageous for instances including more discrete variables. Finally, it has been observed that the performance of our model is either significantly worse or better than *Matpower* when the accuracy of the relaxed problem is lower. This counterintuitive result has not been explained yet and requires further testing for a better understanding of such a behavior.

Accounting for uncertainty in autonomous microgrid planning

6

The models presented in chapter 4 are all based on the implicit hypothesis that variables and parameters of the autonomous planning problem are deterministic, which is obviously not the case in reality. In particular, three sources of uncertainty can be identified in this problem:

(i) Load consumption forecast errors
(ii) Generation forecast errors when intermittent renewable energy based generation is considered
(iii) Outages of generation and distribution assets

This chapter deals with the uncertainty in the autonomous microgrid planning problem. First, it will review how uncertainty can be incorporated in general power systems modelling and optimization. Then, a non-convex chance constrained formulation of the autonomous microgrid planning problem is described. Finally, a computationally tractable robust optimization model of the problem is formulated and implemented to include load consumption-related forecast errors. It is shown that it can be seen as a conservative approximation of the non-convex chance constrained problem.

6.1 Uncertainty in power systems modelling and optimization: state-of-the-art

6.1.1 Probabilistic and possibilistic frameworks

There are two main ways of modelling uncertainty:*probabilistic* and *possibilistic* approaches. As stated in [29], uncertainty may either arise from the variability, e.g. the wind speed forecast is uncertain, or from the incompleteness of the available information, e.g. A says to B there is a dozen wind turbines in a particular wind farm. While the former case is uncertain because there exists no perfect forecast method, in the latter case, the true information might be available, e.g. by going to the windfarm and counting the number of wind turbines. However, with the sole information given by A to B, the number of wind turbines in the wind farm remains an uncertain quantity for B. More generally, the possibilistic framework models the possibility of an event rather than its probability, the latter representing the likelihood of occurrence of the event based on empirical measures [37]. For example, an adult might be able to eat 5 apples a day, hence the proposition 'an adult eats 5 apples a day' might be considered to have a high possibility. However, statistics on a certain group of adults might show it is very unlikely for an adult to eat 5 apples a day (example inspired by [99]).
The possibilistic framework can be based on fuzzy sets [29]. In [37] and [91], the authors use a fuzzy representation to account for load-related uncertainty. The reliability of network components is also modelled using fuzzy numbers in[82]. In [53], the authors not only model load uncertainty but also network parameters uncertainty (i.e. impedance of the lines) with fuzzy numbers. In [39], it is stated that the fuzzy representation can represent the risk of constraint violation, making it well suited for risk-based optimization.
It should be noted that the majority of this literature is either from the late 1990s or from the early 2000s, which shows a decreasing interest in possibilistic modelling for power systems. This is the reason why the rest of this section is focused on the probabilistic framework.

6.1.2 Probabilistic modelling: analytical and scenario approaches

Random variables corresponding to uncertain phenomena, e.g. household power consumption in this context, affect other variables such as power flows or voltages, which in turn makes these variables random. The former variables, as the cause of uncertainty, are independent variables while the latter are considered as dependent variables [97].

In the probabilistic framework, the goal is to determine the probability distribution of dependent variables based on the probability distribution of independent variables. Here, a distinction can be made between approaches where the distribution of dependent variables is analytically computed from the model equations (e.g. power flow equations) and independent variables distributions, and approaches where the the distribution of dependent variables is estimated on a finite set of scenarios .
In the former case, a single problem has to be solved while in the latter case, a finite set of scenarios are determined by sampling independent variable distributions and the problem has to be solved once for each such scenario.

Analytical approaches

In the analytical approaches category, references [92] and [95] both deal with the probabilistic load flow problem. In [92], load uncertainty is modelled with stochastic processes and the power flow computation is performed a first time around the expected operating point. Then, the load flow equations are linearized around the solution obtained for the expected operating point so that dependent variables (line flows, voltages) are expressed as linear combinations of random variables. In [95], typical distribution system features (short lines, limited voltage drop) are exploited to get linearised power flow equations using a constant current load model. Furthermore, random processes are assumed to be normally distributed in order to be able to determine dependent variables distributions analytically. Then, references [11] and [85] deal with uncertainty in the context of the OPF problem by using chance constraints (CC). The principle of a chance constraint is to allow this constraint to be violated with a certain probability (usually small) to avoid having to cope with some extreme and rare cases that would otherwise incur additional costs if they were considered. This concept is refined in the following section.
In [11], the classical OPF problem is formulated as a chance-constrained OPF to account for renewable generation uncertain fluctuations. More precisely, generation capacity constraints and line thermal rating constraints are formulated as chance constraints. Conventional generators follow an affine control policy to counter the RES fluctuations that are considered to be independent and normally distributed. These assumptions allow to reformulate the problem as a convex conic problem. However, due to the heavy computational burden of second order cone constraints, this problem quickly becomes intractable on realistic test-cases. Hence, the authors propose an iterative cutting plane algorithm where the conic constraints corresponding to reformulated chance constraints are initially relaxed. A linear relaxation of the problem is solved and after each iteration, the satisfaction of conic constraints is checked. A linear outer inequality cut corresponding to the most violated conic constraint is added to the problem, which is solved again. This process is repeated until all conic constraints are satisfied up to a predefined tolerance. In [85], wind

turbines are asked to participate in the provision of reserve as their uncertain active power output creates a growing need for additional reserves. Weighted chance constraints are used that allow to account for both the frequency and the amplitude of constraint violation to implement a true risk-based approach. Even though the resulting reformulated constraints are still convex, they give rise to impractically hard problems. Hence, an algorithm similar to the one proposed in [11] is used.

Scenario approaches

Numerous authors resort to scenario sampling to deal with uncertainty in power system related optimization problems as it does not affect the model form. The problem of losses reduction through network reconfiguration is studied in [86] under load growth uncertainty uncertain, using a Monte-Carlo approach to generate scenarios. In [20], a network expansion planning is performed considering load and electricity tariff uncertainty. First, a pool of near-optimal solutions are computed with an Immune System Inspired algorithm. Then, a Monte-Carlo (MC) approach is implemented where different scenarios are extracted from known probability distributions. The expected cost of failures as well as the expected cost of capital and operational expenditures are then computed on this scenario set for every solution from the pool. An expert judgement is then applied based on the following criteria: feasibility rate of a solution, expected operation cost and expected failure cost. In [88], uncertainty affects load demand and gas prices in an integrated generation and transmission planning problem. A scenario set is built from known probability distributions and a stochastic mixed integer linear program is formulated where the objective function aggregates the investment costs for generation and transmission assets, the expected cost of generation and the expected cost of CO_2 emissions on the whole set of scenarios. A similar approach is implemented in [102] where a distribution system expansion planning is formulated that integrates distributed generation (DG) investment and aims at minimizing both financial costs and CO_2 emissions. Both load consumption and DG output are considered uncertain, which is represented through the use of a scenario set on which the expected costs of production and losses are computed. A genetic algorithm is then used to find the Pareto front, i.e. the set of non-dominated solutions to this bi-objective problem. The problem of the security constrained optimal power flow (SCOPF) is implemented with a scenario-approach in [19]. This paper aims at performing a day-ahead security planning, i.e. find an optimal combination of preventive and corrective actions such that, in every possible load and renewable generation scenario, there exists a feasible solution for every postulated contingency.

6.1.3 Risk handling policy

Regardless of the way uncertainty is modelled, there exist different ways to handle the risk associated with uncertainty, either in the constraints or in the objective function.

Constraints

The most conservative way of handling the risk of constraint violation is to adopt a robust approach where the solution of the problem should be feasible for every possible event and for every possible scenario (in the limits of the model). Bearing this in mind, the N-1 criterion, very common in power systems planning and operation, may be seen as particular case of a robust approach: it forces the solution to be feasible in the case of an outage of any one system asset (generator, line, transformer,...). However, it does not ensure a safe operating point in the case of two or more simultaneous outages. The N-1 criterion is widely used when considering the security planning of power systems, i.e. their ability to face contingencies.
Another way of dealing with constraint violation is to adopt a chance-constrained approach, as explained above. By setting a tolerance on the constraints violation probabilities, it generally allows to reduce the solution costs that would otherwise be higher in order to cope with rare or extreme events. This policy is common in the field of power quality for example, where the standards read "X should be in the interval $[\underline{X}, \overline{X}]$ with a probability larger than or equal to $(1 - p)$".

Objective function

The risk handling policy is also illustrated by the objective function [44]. In particular, three different policies can be distinguished. Let x be the vector of decision variables, Ω and $\omega \in \Omega$ the uncertainty space and the vector of random variables respectively and $C(y, \omega)$ the total cost of the solution as a function of decision variables and random variables. The following descriptions are largely based on [44]. First, we could aim at minimizing the expectation of the total cost on the considered uncertainty set (either scenario based or analytically determined), which can be considered as a neutral policy in terms of risk handling.

$$\min_{y} \mathbb{E}_{\omega \in \Omega}[C(y, \omega)]$$

Then, a more optimistic policy would be to minimize the total cost in the most favorable scenario, i.e.

$$\min_{y} \min_{\omega \in \Omega} C(y, \omega)$$

The opposite, risk-averse policy consists in minimizing the cost of the solution under every possible scenario.

$$\min_{y} \max_{\omega \in \Omega} C(y, \omega)$$

Finally, the objective might be to choose a solution that minimizes the additional cost with respect to the risk-averse policy solution y^*_{RA} in every possible scenario.

$$\min_{y} \max_{\omega \in \Omega} (C(y, \omega) - C(y^*_{RA}, \omega))$$

The choice of a risk policy depends on the type of problem. As stated in [44], the 'risk neutral policy' does not actually account for risk and may imply decisions that represent a high risk should the worst case scenario happen. If the anticipated consequence of the worst-case scenario is critical, then a risk-averse policy might be more adapted. In the present case, we are dealing with a long term planning problem. The main risk at this time scale would be to have a structural lack of capacity (distribution or generation) if the loading conditions are more severe than forecast. However, this type of problem may be mitigated closer to real-time operation by monitoring the evolution of loading conditions and taking adequate actions. Furthermore, a risk-averse approach at this time scale might imply significantly larger investment costs that would be justified only for a small fraction of time. Hence, we choose a 'risk-neutral' policy in the present context.

6.1.4 Illustration of uncertainty in power systems problems

As mentioned in the introduction to this chapter, various sources of uncertainty affect power systems: load an intermittent generation forecast errors and distribution and generation assets outages. Another source of uncertainty lies in the values of network parameters as well. For example, the real impedance value of a particular cable might differ from the datasheet value.
We list hereunder various power systems related problem types depending on the network type (Medium Voltage (MV), Low Voltage (LV) or Microgrid (MG)), the type of uncertainty that affects them and the available tools to deal with these uncertainty sources. These problems may be divided into three broad categories: economic problems, technical problems and security/reliability problems.

Problem type	Network type	Uncertainty type	Method
Economic UC, OPF, Investment Planning	MV,LV,MG	Load & generation forecast	Stochastic Optimization CC Optimization RO
Security Security Planning, SCOPF	MV,MG	Load & generation forecast outages	Scenario approach RO CC Optimization
Technical Operational planning	MV,LV,MG	Load & generation forecast outages parameter errors	Probabilistic load flow Scenario approach

Table 6.1: Uncertainty in power systems related problems

6.2 Load related uncertainty consideration in the autonomous microgrid planning

Thus far, the different formulations of the autonomous microgrid planning presented in chapter 4 considered deterministic load consumption values p_{it}^C and q_{it}^C. We now want to consider the intrinsic uncertainty related to load forecast. Henceforth, we thus denote load consumption by random variables $\widetilde{p_{it}^C}$ and $\widetilde{q_{it}^C}$. A random variable x is expressed as the sum of an expected value ($\overline{x}$) and a zero-mean random variable (Δ_x). At this point, we make no assumption yet on the probability distribution of these random variables.

$$\widetilde{p_{it}^C} = \overline{p_{it}^C} + \Delta_{p_{it}^C} \tag{32}$$

$$\widetilde{q_{it}^C} = \overline{q_{it}^C} + \Delta_{q_{it}^C} \tag{33}$$

As explained in the previous section, these are independent variables of the problem.
In the deterministic formulations of the problem, generator's active and reactive output p_{igt}^G and q_{igt}^G were deterministic decision variables. However, in the stochastic case, the active nodal power balance equations should hold for every possible realization of random variables, i.e. (idem for reactive power):

$$\sum_{g \in \mathcal{G}} \widetilde{p_{ig}^G} - \widetilde{p_i^C} = \sum_{(i,j) \in \mathcal{E}} \widetilde{p_{ijt}} \tag{34}$$

In (**34**), generation output and line flow variables are written with the tilde symbol (˜) to emphasize that they become random variables too. More precisely, they are

dependent variables of the problem as they must vary accordingly to independent variables variations, i.e. load consumption variations, for (**34**) to hold. This equation can be separated in average terms and variational terms:

$$\sum_{g\in\mathcal{G}} \overline{p_{ig}^{G}} - \overline{p_{i}^{C}} = \sum_{(i,j)\in\mathcal{E}} \overline{p_{ijt}} \tag{35}$$

$$\sum_{g\in\mathcal{G}} \Delta_{p_{ig}^{G}} - \Delta_{p_{i}^{C}} = \sum_{(i,j)\in\mathcal{E}} \Delta_{p_{ijt}} \tag{36}$$

6.3 Chance-constrained formulation of the autonomous microgrid planning problem

In section 6.1.2, we mentioned that analytical approaches could be more interesting in terms of computational burden and representation of a realistic risk-handling policy. In particular, the chance-constrained optimization framework offers the advantage of explicitly modelling operational margins on physical quantities such as currents and voltages while avoiding a costly scenario sampling.
As stated in [85], a chance constraint may be generically expressed as

$$\int_{\Omega} f(y(\omega))\mathbb{P}(\omega)d\omega \leqslant \epsilon \tag{37}$$

In this expression, $\Omega \in \mathbb{R}^m$ is the uncertainty space where the vector of m random variables ω takes values. The function $y(\omega)$ represents the amplitude of the constraint violation in function of the realization of random variables, f is a risk weighting function that can be used to penalize different constraint violation amplitudes differently, $\mathbb{P}$ is a multivariate probability distribution of (possibly correlated) random variables ω .
The choice of the weighting function reflects the risk policy. In the simplest form, it is a Heaviside function (i.e. null for the negative orthant and equal to one for the positive orthant), which means that all violations ($y \geqslant 0$) are penalized the same way. Using a linear weighting function corresponds to limiting the expected violation of constraints to a certain threshold ϵ [85].

Let us now consider the first planning model proposed in chapter 4, i.e. (NC-JPM) . In this model, constraints (**1.2**)-(**1.5**) are the power flow equations, representing Kirchhoff's laws. Hence, they must apply at any time, regardless of the variation

in load consumption. Constraints (**1.9**)-(**1.13**) and (**1.17**)-(**1.19**) ensure that the network is radial and that there is no asset divesting. They do not include any operational variable, which is why they remain deterministic constraints, as well as (**1.14**). Remaining constraints relate to equipment limits: (**1.6**) for the maximal thermal rating of the lines, (**1.15**) and (**1.16**) for the active and reactive power capability of generators and (**1.7**)-(**1.8**) for the voltage limits. These constraints do not reflect the physical nature of AC power flows, they are engineering constraints that seek to ensure a safe operation of all system parts and maximize their lifetime, whether they be distribution and generation equipment or customer electrical appliances. As mentioned above, the system operator is willing to accept some violations up to a certain threshold in order to avoid additional system upgrade costs to cope with rare events. Violations of line thermal ratings and voltage levels does not necessarily impede the continuity of the power supply, but a generation capacity shortage will require a partial load shedding to reach a balance between power consumption and production. The formulation of (**1.6**),(**1.15**),(**1.7**) as chance constraints is done as follows (this can be done similarly for (**1.16**) and(**1.8**)) :

$$\mathbb{P}(\widetilde{p_{ijt}}^2 + \widetilde{q_{ijt}}^2 - \sum_{l\in\mathcal{L}}(\lambda_{ijly}\overline{S}_l)^2 \geqslant 0) \leqslant \epsilon_{line} \tag{38}$$

$$\mathbb{P}(\widetilde{p^G_{igt}} - \rho_{igy} \geqslant 0) \leqslant \epsilon_{gen} \tag{39}$$

$$\mathbb{P}(\widetilde{v_{it}} - \underline{v} \geqslant 0 \;||\; \widetilde{v_{it}} - \overline{v} \geqslant 0) \leqslant \epsilon_v \tag{40}$$

Chance constraints (**38**), (**39**) and (**40**) correspond to the generic expression(**37**) where the weighting function $f(.)$ is the Heaviside function. Left-hand terms $\left(p^2_{ijt} + q^2_{ijt} - \sum_{l\in\mathcal{L}}(\lambda_{ijly}\overline{S}_l)^2\right)$, $(p^G_{igt} - \rho_{igy})$, $(v_{it} - \underline{v})$ and $(v_{it} - \overline{v})$ represent constraint violations, i.e. the y term in (**38**). To find a closed-form expression of these chance constraints , we need an analytical formulation for $y(\omega)$ to determine its probability distribution as a function of random variables ω distribution.
First, we need to express the generator control policy. In power systems, frequency control is implemented such that an imbalance between production and consumption is compensated by a subset of generators committed to this task in exchange for remuneration. The control law is affine in the total unbalance observed in the system [11], with α_{igt} the participation factor of the technology g generator located at node i at timestep t. It is considered as a decision variable for what follows.

$$\widetilde{p^G_{igt}} = \overline{p^G_{igt}} + \alpha_{igt}\sum_{i\in\mathcal{V}}\Delta_{p^C_{it}} \tag{41}$$

Using (**41**), (**39**) may be rewritten

$$\mathbb{P}(\overline{p_{igt}^G} + \alpha_{igt} \sum_{i \in \mathcal{V}} \Delta_{p_{it}^C} - \rho_{igy} \geqslant 0) \leqslant \epsilon_{gen} \tag{42}$$

Let us now assume that random variables $\Delta_{p_{jt}^C}$ are normally distributed and uncorrelated, i.e. $\Delta_{p_{jt}^C} \sim \mathcal{N}(0, \sigma_{jt}^C) \forall j \in \mathcal{V}$. Then, (**42**) is equivalent to $\mathbb{P}(X \geqslant 0) \leqslant \epsilon_{gen}$ with $X \sim \mathcal{N}(\mu_X, \sigma_X)$ a normally distributed random variable, μ_X being equal to $\overline{p_{igt}^G} - \rho_{igy}$ and σ_X being equal to $\alpha_{igt}\sqrt{\sum_{j \in \mathcal{V}} (\sigma_{jt}^C)^2}$. It follows from the above that

$$\mathbb{P}(X \geqslant 0) = \mathbb{P}(\frac{X - \mu_X}{\sigma_X} \geqslant \frac{-\mu_X}{\sigma_X}) = 1 - \mathbb{P}(\frac{X - \mu_X}{\sigma_X} \leqslant \frac{-\mu_X}{\sigma_X}) = 1 - \Phi(\frac{-\mu_X}{\sigma_X})$$

In this expression, Φ stands for the cumulative distribution function of a standard normal variable. Then, (**42**) may be further developed into

$$\mathbb{P}(X \geqslant 0) \leqslant \epsilon_{gen} \Leftrightarrow -\frac{\mu_X}{\sigma_X} \geqslant \Phi^{-1}(1 - \epsilon_{gen}) \Leftrightarrow \sigma_X \Phi^{-1}(1 - \epsilon_{gen}) \leqslant -\mu_X$$

In this expression, Φ^{-1} denotes the inverse function of CDF. We replace now σ_X and μ_X by their expression to get the final expression of the generator capacity chance constraint

$$\alpha_{igt}\ \Phi^{-1}(1 - \epsilon_{gen}) \sqrt{\sum_{j \in \mathcal{V}} (\sigma_{jt}^C)^2} + \overline{p_{igt}^G} \leqslant \rho_{igt} \tag{12.12}$$

In a chance-constrained version of the planning problem, constraint (**12.12**) would replace constraint (**1.15**). It has to be noted that (**12.12**) remains linear in the decision variables α_{igt}, $\overline{p_{igt}^G}$ and ρ_{igt} which is desirable for computational tractability.

We now want to find similar suitable expressions for (**38**) and (**40**). When developing (**39**) into the closed-form expression (**12.12**), we used the affine generator control policy (**41**) to obtain a relationship between uncertainty sources, i.e. random load fluctuations and generator output fluctuations. Similarly, we should find a relationship between these random load fluctuations and line flow and voltage fluctuations respectively.

For line flows, (**3.1**) gives a relationship between line flows and bus injections. However, if we want to isolate the flow on a particular line as a function of different bus injections, we have to reverse the equation, which is neither necessarily feasible nor unique given that the bus injection vector and the branch flow vector do not have the same dimension, hence this system matrix is generally non-square (which is the case for radial networks with n nodes and $n - 1$ branches).

We can overcome this difficulty by using the DC approximation as in [6],[85] and [11]. This allows to write (**43**). In this expression, we have $\hat{p_{ij}}$ [card($\mathcal{E}$) $\times$ 1] the vector of all line flows, $\hat{P}$ [$(n-1) \times 1$] the vector of all bus power injections (except bus 1), B_f [card($\mathcal{E}$) $\times$ n] the branch admittance matrix and B_{bus} [$n-1 \times n-1$] the nodal admittance matrix.

$$\hat{p_{ij}} = B_f \begin{bmatrix} B_{bus}^{-1} \hat{P} \\ 0 \end{bmatrix} \tag{43}$$

$$B_{bus}^{(i,j)} = \begin{cases} \sum\limits_{j \neq i} \sum\limits_{l \in \mathcal{L}} \lambda_{ijl} b_l & i = j, \quad i \in \{1, ..., n-1\} \\ -\sum\limits_{l \in \mathcal{L}} \lambda_{ijl} b_l & i \neq j, \quad i, j \in \{1, ..., n-1\} \end{cases} \tag{44}$$

$$B_f(e,i) = \begin{cases} \sum\limits_{l \in \mathcal{L}} \lambda_{ijl} b_l & i \text{ is the sending node of branch } e, \ i \in \{1, ..., n\}, e \in \mathcal{E} \\ -\sum\limits_{l \in \mathcal{L}} \lambda_{ijl} b_l & i \text{ is the sending node of branch } e, \ i \in \{1, ..., n\}, e \in \mathcal{E} \end{cases} \tag{45}$$

Equation (**43**) is used in [6],[85] and [11] as B_f and B_{bus} are constant matrices given as an input to the OPF problem. In the present planning problem, they are no longer constant but depend on line investment decision variables λ_{ijl} as it can be seen from definitions (**44**) and (**45**). Furthermore, (**43**) implies the inversion of B_{bus}, now a function of λ_{ijl}, which cannot be done in a standard form mathematical program.

These observations preclude the choice of chance-constrained programming for the inclusion of uncertainty in the planning problem.

6.4 Robust formulation of the autonomous microgrid planning problem

Parts of this section are based on: B. Martin, E. De Jaeger, and F. Glineur. A robust convex optimization framework for autonomous network planning under load uncertainty. In *2017 IEEE Manchester PowerTech*, pages 1–6, 2017

6.4.1 Notations

A. Sets

$\mathcal{PP}$	Set of problematic load power consumption patterns regarding engineering constraints
$\mathcal{S}$	Set of scenarios
VC	Set of violated constraints
PS	Set of patterns to be added to the scenario set at the current iteration

B. Parameters

$n_S = \textbf{card}(\mathcal{S})$	Number of considered scenarios
$p_{it}^{C,min}$, $p_{it}^{C,max}$	Lower and upper bounds for active power consumption at node i at timestep t
$p_{it}^{G,ref}$, $q_{it}^{G,ref}$	Reference active and reactive power production values obtained from the joint planning problem on the average consumption scenario t
$q_{it}^{C,min}$, $q_{it}^{C,max}$	Lower and upper bounds for reactive power consumption at node i at timestep t
A_{it}^{G}	Indicates which constraints the generation capacity adversarial problem is trying to violate.
A_{ijt}^{TH}	Indicates which constraints the line thermal rating adversarial problem is trying to violate.
e_i	Integer between 1 and n attributed to a node to represent its eccentricity in the complete graph of vertices $\mathcal{V}$, from the maximum eccentricity node (value 1) to the least eccentricity node (value n)

LF	Loss factor (>1), upper bound on the ratio of total produced power over total consumed power
n_{scen}^{max}	Maximal number of scenarios added at each iteration of the robust optimization
C^{ENS}	Cost of Energy Not Supplied in case of load shedding

C. Variables

$p_{it}^{C,var}, q_{it}^{C,var}$	Active and reactive power consumption at node i at timestep t
$p_{it}^{shed}, q_{it}^{shed}$	Active and reactive load shedding at node i at timestep t
$p_{it}^{res}, q_{it}^{res}$	Active and reactive power generated by the fictitious reserve generator
RES_{iy}	Binary variable indicating the presence of a fictitious reserve generator at node i during year y
NFR_t	Binary variable indicating the Need For Reserve at timestep t

6.4.2 State of the art

A robust optimization (RO) approach to a problem including random variables should deliver a solution that is feasible for every possible realization of these random variables. Such problems are difficult to solve and are generally NP-hard . Indeed, considering continuous random variables leads to a continuous uncertainty space which in turn leads to an infinite number of constraints to consider in the RO problem [17]. In [17], the authors propose a finite constraint sampling scheme to overcome this problem. They show that the probability of constraint violations rapidly decreases with the number of samples. They also provide an upper bound on the number of samples needed to obtain a predefined level of confidence concerning constraint enforcement, which allows to efficiently solve the problem to arbitrary accuracy. In [64] and [96], the authors propose another method to reduce the set of constraints to a finite size. They show that for a problem with a polytopic uncertainty set Ω and convex constraints of the form $g(x) \leqslant 0$, the body of these constraints will always be maximal on the vertices of Ω. To enforce such constraints for all $\boldsymbol{\omega} \in \Omega$, it is thus sufficient to enforce them on every vertex of Ω. Nonetheless, even in the simple case where Ω is an hyper-rectangular set, the number of vertices is equal to 2^{n^Ω} which rapidly becomes intractable with a growing number of random variables n^Ω.
Consequently, we adopt the approach developed in [19] which has been used for security planning under uncertainty in transmission networks [18]. This approach

consists in computing a subset of the vertices of Ω, i.e. a set of scenarios to incorporate in the RO problem, sufficient to guarantee constraint enforcement on the whole uncertainty set Ω. The approach is adversarial, as defined in [43], i.e. based on the successive and iterative computation of an adversarial problem where the infeasibility (i.e. violation) of the constraints is maximized in order to find problematic scenarios to add to the RO problem and a corrective problem where we try to remove these infeasibilities thanks to remedial actions.

6.4.3 Modelling hypotheses

In this chapter, we consider that the load uncertainty set is rectangular. This means that all load power consumption values are uncorrelated and no hypotheses are made on their probability distribution. This is formally expressed as follows:

$$\Omega = \{\boldsymbol{\omega} \in \mathbb{R}^{n^\Omega} \ : \omega_i \in \left[\omega_i^L; \omega_i^U\right] \ \forall i \in 1, ..., n^\Omega\} \tag{46}$$

In the above expression, ω_i^L and ω_i^U represent the lowest and highest values respectively that can be taken by the i-th random variable ω_i.
This simple uncertainty space formulation is chosen as the main focus is on the robust optimization procedure rather than the uncertainty modelling. However, it is not restrictive. As a matter of fact, it is shown in section 6.4.7 that this may easily extended to any multivariate and correlated probability distribution.

6.4.4 General working principle

As explained in section 6.3, constraints representing the physics of power flows should hold for every microgrid operating point in order to guarantee a physical solution. However, engineering constraints related to the limits of the various assets are dictated by safety considerations rather than physical laws. For example, the thermal rating of a line represents the maximal admissible power that may flow through that line without damaging it. A larger power could flow through that line at the expense of a premature ageing or an excessive sag due to an excessive thermal heating.
In the adversarial robust approach developed hereafter, a distinction is made between physical and engineering constraints. While the former should always be satisfied, we are looking for the values of the loads random power consumption such that the latter are violated. The general working principle is illustrated in 1. In this algorithm, $\mathcal{S}$ represents the set of scenarios on which the planning problem is solved, $\mathcal{PP}$ the set of problematic patterns and k the iteration counter. Solving the problem on a set of power consumption scenarios instead of a single operating point implies that physical and engineering constraints are replicated for every consumption scenario which makes the problem more computationally challenging.

The working principle is the following: for a given microgrid investment solution, we are looking for the load consumption patterns that violate engineering constraints. For every such pattern, if it not possible to find a suitable generation redispatch that allows engineering constraints to be satisfied, then the pattern is considered as problematic and added to $\mathcal{PP}$. These problematic patterns are added as load consumption scenarios and the planning problem is solved again on this augmented set of load consumption scenarios. This procedure is repeated until no additional problematic consumption pattern is found.

Algorithm 1: Robust planning procedure - schematic representation

```
Initialize 𝒮
while First iteration OR problematic patterns found at previous iteration do
    Unfix investment variables
    Solve the joint planning problem on 𝒮
    Fix investment variables
    for every engineering constraint do
        Solve adversarial problem and find current worst consumption
          pattern P_cur
        if Constraint violation > 0
            Fix power consumption pattern
            Solve corrective problem
        end if
        if constraint violation >0 & P_cur ∉ 𝒫𝒫
            𝒫𝒫 ← 𝒫𝒫 ∪ P_cur
        end if
    end for
    𝒮 ← 𝒮 ∪ 𝒫𝒫
end while
```

In this work, the only engineering constraints that have been considered to compute problematic consumption patterns are the generation capacity and line thermal rating constraints. Voltage limits have not been taken into account for this procedure, however the approach presented in this chapter may easily be extended to include them.

6.4.5 Planning model adaptation for robust optimization

The robust planning procedure presented in the previous section relies on solving five different problems:

(i) The robust joint planning problem
(ii) Generation capacity adversarial problems
(iii) Generation capacity corrective problems
(iv) Line thermal rating adversarial problems
(v) Line thermal rating corrective problems

This section details the models corresponding to these different problems.

Robust joint planning problem

This problem is very similar to the deterministic joint planning model (CDF-JPM-OA) , with the following exceptions:

(i) Operational variables and parameters are now indexed over the scenario set $\mathcal{S}$ as well with the subscript $s \in \mathcal{S}$: p_{ijts}, q_{ijts}, l_{ijts}, w_{its}, p^G_{igts}, q^G_{igts}, p^C_{its} and q^C_{its}
(ii) Constraints including the aforementioned variables and parameters are thus also indexed over $\mathcal{S}$. As mentioned above, this multiplies the number of such constraints by $n_S = |S|$ which makes the problem more computationally intensive.
(iii) The objective of the deterministic planning problem (**7.1**) is slightly modified into (**47**) . As a matter of fact, the energy production cost is not computed on a single operating point anymore but is expressed as an expected fuel cost computed over $\mathcal{S}$. The different scenarios are considered as equiprobable for the expected value computation, which is coherent with the uniform distribution of random variables that we consider.

$$\sum_{i\in\mathcal{V},g\in\mathcal{G}}\left(\gamma_{ig1}C^B_{gf}+\rho_{ig1}C^B_{gv}+\sum_{y\geqslant 2}\frac{1}{(1+d)^{y-1}}[(\gamma_{ig,y}-\gamma_{ig,y-1})C^B_{gf}+(\rho_{ig,y}-\rho_{ig,y-1})C^B_{gv}]\right)$$
$$+\sum_{(i,j)\in\mathcal{E}}D_{ij}\left(\omega_{ij1}C^{BL}_{f}+\sum_{l\in\mathcal{L}}\lambda_{ijl1}C^{BL}_{lv}+\sum_{y\geqslant 2}\frac{1}{(1+d)^{y-1}}[(\omega_{ig,y}-\omega_{ig,y-1})C^{BL}_{lf}\right.$$
$$\left.+(\lambda_{ijl,y}-\lambda_{ijl,y-1})C^{BL}_{lv}]\right)+\frac{1}{n_S}\sum_{i\in\mathcal{V},g\in\mathcal{G},t\in\mathcal{T},s\in\mathcal{S}}\frac{1}{(1+d)^{t\ \mathrm{div}\ H}}\frac{8760}{H}\left(\gamma_{igy}C^P_{gf}+p_{gits}C^P_{gv}\right) \quad \textbf{(47)}$$

Generation adversarial problem

The generation adversarial problem consists in finding the consumption patterns $p_{it}^{C,var}$, $q_{it}^{C,var}$ that maximize the violation of the selected generation capacity constraints for the current investment solution. Hence, investment variables are fixed in this problem.

Rather than dropping the generation capacity constraints and maximizing their violation, load shedding term are introduced in active and reactive power balance equations (**13.2**) and (**13.3**). The objective of (G-AP) is then formulated as the maximization of the sum of active and reactive load shedding for the selected constraints (these are determined by the parameter A_{it}^{G}). In this problem, generators active and reactive power production values are fixed to their optimal value obtained from the previous planning problem solved on the average consumption scenario. Otherwise, other things being equal, the solver would find it advantageous to artificially put power production variables to 0 so that (**13.2**) and (**13.2**) enforce larger values of shedding terms which in turn would improve the objective value. The resulting consumption pattern might thus not be a really problematic one.

New constraints are also added in the model. Eqs. (**13.4**) and (**13.5**) represent the bounds on random load consumption variables while eqs. (**13.6**) and (**13.7**) limit the load shedding at a node to the power consumption of this node to avoid artificially large values of load shedding not related to truly problematic consumption patterns. The remainder of the constraints are the same as those presented in the (CDF-JPM-OA) model, i.e. losses constraints (**13.9**)-(**13.12**), voltage constraints (**13.13**)-(**13.14**), line thermal rating constraints (**13.15**) and current constraints (**13.16**).

Model 13 Generation adversarial problem (G-AP)

Fixed: $\omega_{ijy}, \lambda_{ijly}, \gamma_{igy}, \rho_{igy}, p_{igt}^{G}, q_{igt}^{G}$

Variable: $p_{it}^{shed}, q_{it}^{shed}, p_{it}^{C,var}, q_{it}^{C,var}, p_{ijt}, q_{ijt}, l_{ijt}, w_{it}$

Maximize:

$$\sum_{i\in\mathcal{V},t\in\mathcal{T}} A_{it}^{G}(p_{it}^{shed} + q_{it}^{shed}) \tag{13.1}$$

Subject to:

$$\sum_{g\in\mathcal{G}} p_{igt}^{G} + p_{it}^{shed} - p_{it}^{C,var} = \sum_{(i,j)\in\mathcal{E}} p_{ijt} \qquad \forall i \in \mathcal{V}, t \in \mathcal{T} \tag{13.2}$$

$$\sum_{g\in\mathcal{G}} q_{igt}^{G} + q_{it}^{shed} - q_{it}^{C,var} = \sum_{(i,j)\in\mathcal{E}} q_{ijt} \qquad \forall i \in \mathcal{V}, t \in \mathcal{T} \tag{13.3}$$

$$p_{it}^{C,min} \leqslant p_{it}^{C,var} \leqslant p_{it}^{C,max} \qquad \forall i \in \mathcal{V}, t \in \mathcal{T} \quad \textbf{(13.4)}$$

$$q_{it}^{C,min} \leqslant q_{it}^{C,var} \leqslant q_{it}^{C,max} \qquad \forall i \in \mathcal{V}, t \in \mathcal{T} \quad \textbf{(13.5)}$$

$$0 \leqslant p_{it}^{shed} \leqslant p_{it}^{C,var} \qquad \forall i \in \mathcal{V}, t \in \mathcal{T} \quad \textbf{(13.6)}$$

$$0 \leqslant q_{it}^{shed} \leqslant q_{it}^{C,var} \qquad \forall i \in \mathcal{V}, t \in \mathcal{T} \quad \textbf{(13.7)}$$

$$\left\langle p_{ijt}^2 + q_{ijt}^2 \leqslant w_{it} l_{ijt} \right\rangle^{OA} \qquad \forall (i,j) \in \mathcal{E}, t \in \mathcal{T} \quad \textbf{(13.8)}$$

$$-(1-\lambda_{ijly}) r_l D_{ij} \frac{\overline{S}_\Lambda^2}{\underline{v}^2} \leqslant p_{ijt} + p_{jit} - r_l D_{ij} l_{ijt} \leqslant D_{ij} \max_l (r_l \overline{S}_l^2) \frac{1}{\underline{v}^2} (1-\lambda_{ijly}) \qquad \forall (i,j) \in \mathcal{E}, l \in \mathcal{L}, y \in \mathcal{Y} \quad \textbf{(13.9)}$$

$$-(1-\lambda_{ijly}) x_l D_{ij} \frac{\overline{S}_\Lambda^2}{\underline{v}^2} \leqslant q_{ijt} + q_{jit} - x_l D_{ij} l_{ijt} \leqslant D_{ij} \max_l (x_l \overline{S}_l^2) \frac{1}{\underline{v}^2} (1-\lambda_{ijly}) \qquad \forall (i,j) \in \mathcal{E}, l \in \mathcal{L}, y \in \mathcal{Y} \quad \textbf{(13.10)}$$

$$p_{ijt} + p_{jit} \geqslant 0 \qquad \forall (i,j) \in \mathcal{E}, t \in \mathcal{T} \quad \textbf{(13.11)}$$

$$q_{ijt} + q_{jit} \geqslant 0 \qquad \forall (i,j) \in \mathcal{E}, t \in \mathcal{T} \quad \textbf{(13.12)}$$

$$\begin{aligned}(1-\lambda_{ijly})[\underline{v}^2 - \overline{v}^2 - 2D_{ij}\overline{S}_\Lambda(r_l + x_l) - D_{ij}^2(r_l^2 + x_l^2)\frac{\overline{S}_\Lambda^2}{\underline{v}^2}] \\ \leqslant w_{jt} - w_{it} + 2D_{ij}(r_l p_{ijt} + x_l q_{ijt}) - D_{ij}^2(r_l^2 + x_l^2) l_{ijt} \\ \leqslant (1-\lambda_{ijly})[\overline{v}^2 - \underline{v}^2 + 2D_{ij}\overline{S}_\Lambda(r_l + x_l)]\end{aligned}$$

$$\forall (i,j) \in \mathcal{E}, t \in \mathcal{T}, y \in \mathcal{Y} : y = t \text{ div } H + 1 \quad \textbf{(13.13)}$$

$$\underline{v}^2 \leqslant w_{it} \leqslant \overline{v}^2 \qquad \forall i \in \mathcal{V}, t \in \mathcal{T}, \quad \textbf{(13.14)}$$

$$\left\langle p_{ijt}^2 + q_{ijt}^2 \leqslant \left(\sum_{l \in \mathcal{L}} \lambda_{ijly} \overline{S}_l \right)^2 \right\rangle^{OA} \qquad \forall (i,j) \in \mathcal{E}, t \in \mathcal{T}, y \in \mathcal{Y} : y = t \text{ div } H + 1 \quad \textbf{(13.15)}$$

$$l_{ijt} = l_{jit} \qquad \forall (i,j) \in \mathcal{E}, t \in \mathcal{T} \quad \textbf{(13.16)}$$

Generation corrective problem

If the (G-AP) objective value is positive, a corrective problem is solved to see if a suitable generation redispatch is able to alleviate the constraints violation. Hence, the consumption pattern is now fixed and the generator active and reactive production variables are unfixed. The objective is now to minimize the violation of the generation capacity constraints (hence the sum of load shedding terms). The constraints are the same as in (G-AP) to the sole exception of constraints (**13.4**) and (**13.5**) that are not considered here because $p_{it}^{C,var}$ and $q_{it}^{C,var}$ are fixed.

Model 14 Generation corrective problem (G-CP)

Fixed: $\omega_{ijy}, \lambda_{ijly}, \gamma_{igy}, \rho_{igy}, p_{it}^{C,var}, q_{it}^{C,var}$

Variable: $p_{it}^{shed}, q_{it}^{shed}, p_{igt}^{G}, q_{igt}^{G}, p_{ijt}, q_{ijt}, l_{ijt}, w_{it}$

Minimize:

$$\sum_{i \in \mathcal{V}, t \in \mathcal{T}} p_{it}^{shed} + q_{it}^{shed} \tag{14.1}$$

Subject to: (**13.2**)-(**13.3**), (**13.6**)-(**13.16**)

Line thermal rating adversarial problem

The objective of this problem is to find problematic patterns regarding line thermal rating constraints, i.e. consumption profiles that lead to violations of these constraints. To express this violation, we might work with the currents or the power flows. In the former case, the objective of apparent power maximization could be expressed equivalently by the maximization of the sum of line currents squared amplitudes $\sum_{(i,j):i<j} l_{ijt}$. In the latter case, it could be expressed with the sum of apparent powers or squared apparent powers on the different lines, i.e. $\sqrt{p_{ijt}^2 + q_{ijt}^2}$ (non-linear objective function) or $p_{ijt}^2 + q_{ijt}^2$ (quadratic objective function). The linear current-based formulation should be preferred over the flow-based formulations that are either quadratic or non-linear. However, we do not use this current-based formulation either in the present case as the OA is quite inaccurate regarding current amplitude computation. As a matter of fact, lots of adversarial problems are to be solved during the robust optimization procedure. Hence, a relatively low OA relaxation degree is chosen ($\kappa = 3$) in order to ease the computational burden of the individual adversarial problems.

The objective is thus expressed as the maximization of the sum of active and reactive losses on the selected lines (**15.1**). It has the advantage of remaining linear while being proportional to the squared current amplitude and consequently the squared

apparent power amplitude. A salient feature of this choice is that the solver tries to maximize the losses on the selected lines by artificially injecting too much power p_{ijt} on the sending end of the line (if i is the sending node, $p_{ijt} \geqslant 0$) for a given amount of power p_{jit} at the receiving end (if j is the receiving node, $p_{jit} \leqslant 0$) , hence creating artificially larger losses $p_{ijt}+p_{jit}$ and thus a better objective value. This non-physical feature is due to the fact that the losses are proportional to the squared current amplitude (**15.7**)-(**15.8**), and larger losses implie larger current amplitudes as well on the lines. Yet, the relaxed SOC constraint (**15.6**) only gives a lower bound on l_{ijt} but no upper bound. The solver is thus allowed to choose artificially large current amplitudes (i.e. that do not match the constitutive equation $p_{ijt}^2 + q_{ijt}^2 = w_i l_{ijt}$ at the receiving end) in order to get higher objective values. This differs from what is presented in section 4.4.2 where the losses minimization objective makes it more profitable to put l_{ijt} at its lower bound value.

In the present adversarial problem, active and reactive power consumptions are allowed to vary within their lower and upper bounds (**15.4**) and (**15.5**). Eqs. (**15.15**) - (**15.16**) limit the power production levels to their reference optimal value obtained from the average scenario in the planning problem and eqs. (**15.17**)- (**15.18**) limit the sum of generators power outputs with the sum of loads power consumptions, multiplied by a loss factor representing the losses on the network. Since the load consumption might be higher than in the average scenario, the generator production level might be insufficient due to (**15.15**) - (**15.16**). Hence, a single fictitious reserve generator (**15.19**) is introduced in the network for this adversarial problem in order to supply additional power if need be.

Eq.(**15.20**) ensures the fictitious reserve generator is located on a node where a real generator exists and (**15.21**) places it on the node with the least possible eccentricity. In the same way as for real generators, the fictitious reserve generator output is limited by eqs. (**15.22**)-(**15.27**) in order to avoid an artificially larger power production that would create fictitious losses on lines. Firstly, eqs. (**15.22**)-(**15.23**) ensures that the fictitious reserve power is produced at the node where the reserve generator is located and does not produce more than the total maximal consumption of the microgrid.

Then, constraints (**15.24**)-(**15.25**) model both situations where reserve active power generation is needed or not. If the total difference between consumption and production, affected by a loss factor, is negative, then NFR should be equal to 0 for (**15.25**) to be satisfied, M being a large enough constant. This forces the reserve active power generation to be zero in constraint (**15.24**). If the random consumptions exceed the reference production level, then NFR must be equal to 1 in order to allow non-zero reserve active power generation in (**15.24**). In this situation, the

reserve production should not exceed the difference between the total consumption and production weighed by the loss factor. Eqs. (**15.26**)- (**15.27**) represent the same constraints for reserve reactive power generation.
The remaining constraints of (TH-AP) correspond to the regular constraints of the planning problem (CDF-JPM-OA) .

Model 15 Line thermal rating adversarial problem (TH-AP)

Fixed: $\omega_{ijy}, \lambda_{ijly}, \gamma_{igy}, \rho_{igy}$

Variable: $p^G_{igt}, q^G_{igt}, p^{C,var}_{it}, q^{C,var}_{it}, p_{ijt}, q_{ijt}, l_{ijt}, w_{it}, p^{res}_{it}, q^{res}_{it}, RES_i, NFR$

Maximize:

$$\sum_{i\in\mathcal{V},t\in\mathcal{T}} A^{TH}_{ijt}(p_{ijt}+p_{jit}+q_{ijt}+q_{jit}) \tag{15.1}$$

Subject to:

$$\sum_{g\in\mathcal{G}} p^G_{igt}+p^{res}_{it}-p^{C,var}_{it}=\sum_{(i,j)\in\mathcal{E}} p_{ijt} \qquad \forall i\in\mathcal{V},t\in\mathcal{T} \tag{15.2}$$

$$\sum_{g\in\mathcal{G}} q^G_{igt}+q^{res}_{it}-q^{C,var}_{it}=\sum_{(i,j)\in\mathcal{E}} q_{ijt} \qquad \forall i\in\mathcal{V},t\in\mathcal{T} \tag{15.3}$$

$$p^{C,min}_{it}\leqslant p^{C,var}_{it}\leqslant p^{C,max}_{it} \qquad \forall i\in\mathcal{V},t\in\mathcal{T} \tag{15.4}$$

$$q^{C,min}_{it}\leqslant q^{C,var}_{it}\leqslant q^{C,max}_{it} \qquad \forall i\in\mathcal{V},t\in\mathcal{T} \tag{15.5}$$

$$\left\langle p^2_{ijt}+q^2_{ijt}\leqslant w_{it}l_{ijt}\right\rangle^{OA} \qquad \forall (i,j)\in\mathcal{E},t\in\mathcal{T} \tag{15.6}$$

$$-(1-\lambda_{ijly})r_l D_{ij}\frac{\overline{S}^2_\Lambda}{\underline{v}^2}\leqslant p_{ijt}+p_{jit}-r_l D_{ij}l_{ijt}\leqslant D_{ij}\max_l(r_l\overline{S}^2_l)\frac{1}{\underline{v}^2}(1-\lambda_{ijly}) \qquad \forall (i,j)\in\mathcal{E},l\in\mathcal{L},y\in\mathcal{Y} \tag{15.7}$$

$$-(1-\lambda_{ijly})x_l D_{ij}\frac{\overline{S}^2_\Lambda}{\underline{v}^2}\leqslant q_{ijt}+q_{jit}-x_l D_{ij}l_{ijt}\leqslant D_{ij}\max_l(x_l\overline{S}^2_l)\frac{1}{\underline{v}^2}(1-\lambda_{ijly}) \qquad \forall (i,j)\in\mathcal{E},l\in\mathcal{L},y\in\mathcal{Y} \tag{15.8}$$

$$p_{ijt}+p_{jit}\geqslant 0 \qquad \forall (i,j)\in\mathcal{E},t\in\mathcal{T} \tag{15.9}$$

$$q_{ijt}+q_{jit}\geqslant 0 \qquad \forall (i,j)\in\mathcal{E},t\in\mathcal{T} \tag{15.10}$$

$$\begin{aligned}(1-\lambda_{ijly})[\underline{v}^2-\overline{v}^2-2D_{ij}\overline{S}_\Lambda(r_l+x_l)-D^2_{ij}(r^2_l+x^2_l)\frac{\overline{S}^2_\Lambda}{\underline{v}^2}]\\ \leqslant w_{jt}-w_{it}+2D_{ij}(r_l p_{ijt}+x_l q_{ijt})-D^2_{ij}(r^2_l+x^2_l)l_{ijt}\\ \leqslant(1-\lambda_{ijly})[\overline{v}^2-\underline{v}^2+2D_{ij}\overline{S}_\Lambda(r_l+x_l)]\\ \forall (i,j)\in\mathcal{E},t\in\mathcal{T},y\in\mathcal{Y}:y=t\ \text{div}\ H+1\end{aligned} \tag{15.11}$$

$$\underline{v}^2 \leqslant w_{it} \leqslant \overline{v}^2 \qquad \forall i \in \mathcal{V}, t \in \mathcal{T}, \quad \textbf{(15.12)}$$

$$p_{ijt} = 0, \quad q_{ijt} = 0 \quad \forall (i,j) \in \mathcal{E}, t \in \mathcal{T}, y \in \mathcal{Y} : \omega_{ijy} = 0, \; y = t \text{ div } H + 1 \quad \textbf{(15.13)}$$

$$l_{ijt} = l_{jit} \qquad \forall (i,j) \in \mathcal{E}, t \in \mathcal{T} \quad \textbf{(15.14)}$$

$$0 \leqslant p^G_{igt} \leqslant p^{G,ref}_{igt} \qquad \forall i \in \mathcal{V}, g \in \mathcal{G}, t \in \mathcal{T}, y \in \mathcal{Y} : y = t \text{ div } H + 1 \quad \textbf{(15.15)}$$

$$|q^G_{igt}| \leqslant |q^{G,ref}_{igt}| \qquad \forall i \in \mathcal{V}, g \in \mathcal{G}, t \in \mathcal{T} \quad \textbf{(15.16)}$$

$$\sum_{i \in \mathcal{V}, g \in \mathcal{G}} p^G_{igt} \leqslant LF \sum_{i \in \mathcal{V}} p^{C,var}_{it} \qquad \forall t \in \mathcal{T} \quad \textbf{(15.17)}$$

$$\sum_{i \in \mathcal{V}, g \in \mathcal{G}} q^G_{igt} \leqslant LF \sum_{i \in \mathcal{V}} q^{C,var}_{it} \qquad \forall t \in \mathcal{T} \quad \textbf{(15.18)}$$

$$\sum_{i \in \mathcal{V}} RES_{iy} = 1 \qquad \forall y \in \mathcal{Y} \quad \textbf{(15.19)}$$

$$RES_{iy} \leqslant \sum_{g \in \mathcal{G}} \gamma_{igy} \qquad \forall i \in \mathcal{V}, y \in \mathcal{Y} \quad \textbf{(15.20)}$$

$$\frac{\sum_{g \in \mathcal{G}} \gamma_{igy} e_i}{|\mathcal{G}|} \leqslant \sum_{j \in \mathcal{V}} RES_{jy} e_j \qquad \forall i \in \mathcal{V}, y \in \mathcal{Y} \quad \textbf{(15.21)}$$

$$0 \leqslant p^{res}_{it} \leqslant RES_{iy} \sum_{j \in \mathcal{V}} p^{C,max}_{jt} \qquad i \in \mathcal{V}, t \in \mathcal{T}, y \in \mathcal{Y} : y = t \text{ div } H + 1 \quad \textbf{(15.22)}$$

$$0 \leqslant q^{res}_{it} \leqslant RES_{iy} \sum_{j \in \mathcal{V}} q^{C,max}_{jt} \qquad i \in \mathcal{V}, t \in \mathcal{T}, y \in \mathcal{Y} : y = t \text{ div } H + 1 \quad \textbf{(15.23)}$$

$$\sum_{i \in \mathcal{V}} p^{res}_{it} \leqslant M \times NFR \qquad \forall t \in \mathcal{T} \quad \textbf{(15.24)}$$

$$\sum_{i \in \mathcal{V}} p^{res}_{it} \leqslant \sum_{i \in \mathcal{V}, g \in \mathcal{G}} LF \; (p^{C,var}_{it} - p^{G,ref}_{igt}) + M(1 - NFR) \qquad \forall t \in \mathcal{T} \quad \textbf{(15.25)}$$

$$\sum_{i \in \mathcal{V}} q^{res}_{it} \leqslant M \times NFR \qquad \forall t \in \mathcal{T} \quad \textbf{(15.26)}$$

$$\sum_{i \in \mathcal{V}} q^{res}_{it} \leqslant \sum_{i \in \mathcal{V}, g \in \mathcal{G}} LF \; (q^{C,var}_{it} - q^{G,ref}_{igt}) + M(1 - NFR) \qquad \forall t \in \mathcal{T} \quad \textbf{(15.27)}$$

Line thermal rating corrective problem

As for generation capacity constraints, a corrective problem is solved in the case where the line thermal rating constraints are violated. In this corrective problem, the random load consumptions are fixed to their values from the adversarial problem and the generator outputs may be redispatched within their allowed operating range (**16.2**)-(**16.3**) in order to try to relieve the line thermal rating violations. Line thermal rating constraints are reintroduced in the problem, with an additional term

δ_{ijt} that allows the violation of these constraints. This term is limited to non-zero values only for existing lines in the current planning solution to avoid power flows on non-existing lines (**16.5**), M being a large enough constant. The objective is to minimize the sum of these δ terms. Hence, for this fixed consumption pattern, if there exists a solution satisfying engineering constraints, the δ terms do not need to be non-zero and the solver will put them at 0 in order to minimize the objective value. If no generation redispatch exists such that $\sum_{(i,j)\in\mathcal{E},t\in\mathcal{T}} \delta_{ijt} = 0$, then the line thermal rating violation in the current consumption pattern cannot be relieved.
A penalty term is introduced in the objective to discourage the use of the fictitious reserve generator ($C^{penalty}$ being a large penalty cost parameter). As a matter of fact, the solver might use reserve power generation to relieve line thermal rating violation but this is not a desirable output of the corrective problem as we want to check whether the current planning solution (lines and *real* generators) are able to handle the current consumption pattern in a way that satisfies all engineering constraints. If the objective of the problem is larger than zero, it means that the current planning solution is not able to deal with the current consumption pattern, hence this pattern is considered as problematic.

Model 16 Line thermal rating corrective problem (TH-CP)

Fixed: $\omega_{ijy}, \lambda_{ijly}, \gamma_{igy}, \rho_{igy}, p_{it}^{C,var}, q_{it}^{C,var}$

Variable: $p_{igt}^{G}, q_{igt}^{G}, p_{ijt}, q_{ijt}, l_{ijt}, w_{it}, p_{it}^{res}, q_{it}^{res}, RES_i, NFR$

Minimize:

$$\sum_{(i,j)\in\mathcal{E},t\in\mathcal{T}} \delta_{ijt} + \sum_{i\in\mathcal{V},t\in\mathcal{T}} C^{penalty}(p_{it}^{res} + q_{it}^{res}) \quad \textbf{(16.1)}$$

Subject to: (**15.2**)-(**15.3**), (**15.6**)-(**15.12**), (**15.14**), (**15.19**)-(**15.27**)

$$0 \leqslant p_{igt}^{G} \leqslant \rho_{igy} \qquad \forall i \in \mathcal{V}, g \in \mathcal{G}, t \in \mathcal{T}, y \in \mathcal{Y} : y = t \text{ div } H + 1 \quad \textbf{(16.2)}$$

$$|q_{igt}^{G}| \leqslant p_{igt}^{G} \tan(\cos^{-1}(\overline{PF}_g)) \qquad \forall i \in \mathcal{V}, g \in \mathcal{G}, t \in \mathcal{T} \quad \textbf{(16.3)}$$

$$\left\langle p_{ijt}^2 + q_{ijt}^2 \leqslant (\sum_{l\in\mathcal{L}} \lambda_{ijly}\overline{S}_l + \delta_{ijt})^2 \right\rangle^{OA} \qquad \forall (i,j) \in \mathcal{E}, t \in \mathcal{T}, y \in \mathcal{Y} : y = t \text{ div } H + 1 \quad \textbf{(16.4)}$$

$$0 \leqslant \delta_{ijt} \leqslant \omega_{ijy} M \qquad \forall (i,j) \in \mathcal{E}, t \in \mathcal{T}, y \in \mathcal{Y} : y = t \text{ div } H + 1 \quad \textbf{(16.5)}$$

Detailed algorithm for the robust microgrid planning

The detailed flowchart for the robust planning algorithm is presented on Fig. 6.1. For brevity's sake, we only present the procedure for the generation capacity constraints. To account for both types of constraints in the robust optimization, the steps of the algorithms enclosed in the dashed rectangle have to be transposed for thermal rating constraints and must be executed just after them.

The procedure begins with the initialization of the scenario set with the sole average consumption pattern. Then, the planning problem is solved a first time and the *Robust* binary variable is set to 1. Then the adversarial problem is successively solved for every single generation capacity constraint by setting all entries of the A_{it}^{G} matrix to 0 except the one corresponding to the considered constraints, which can result in three different outcomes in function of the set of violated constraints $\mathcal{VC}$ in the optimal solution of the adversarial problem. First, if there is no violated constraint, then, the algorithm directly goes to the next constraint. Then, if the current considered constraint is the only one to be violated, the algorithm fixes the load consumption pattern to its current optimal value and solves the corrective problem. If several constraints are violated by the adversarial problem, all the entries of A_{it}^{G} corresponding to these constraints are set to 1 and the adversarial problem is solved again before solving the corrective problem.

If the objective of this corrective problem is 0, then the current microgrid solution is able to relieve the constraint violation and the current consumption pattern is not considered as problematic. Otherwise, the *Robust* variable is set to 0 as there exists at least one consumption pattern such that the current microgrid solution does not satisfy all engineering constraints. Then, we add this pattern to $\mathcal{PP}$ if it does not belong to it yet. When all generation capacity constraints have been considered, if no problematic consumption pattern has been found at the current iteration (hence, Robust $= 1$) , the algorithm terminates and the current microgrid solution is considered as robust for the load consumption uncertainty range. Otherwise (Robust $= 0$), the problematic consumption patterns that were not yet added to the scenario set are sorted by decreasing order of constraint violation amplitude and the n_{scen}^{max} first patterns are added to the scenario set, which terminates the iteration. The next iteration begins by solving the planning problem again on the augmented scenario set.

The reason for which only a subset of the most problematic patterns are added at each iteration is that we want to keep the size of the planning problem as small as possible. By adding only the worst patterns, we expect to hedge against the constraints violations of less problematic patterns as well. Hence, there is a trade-off between the number of scenarios added per iteration and the number of planning problems that need to be solved. If the former is too small, the number of scenarios accounted for is low and it is likely that problematic patterns will be found at the

next iteration, which will lead to another iteration, hence a new planning problem to solve. However, if too many scenarios are added at once, the size of the planning problem to be solved at the next iteration might become too large and the problem might be computationally intractable.

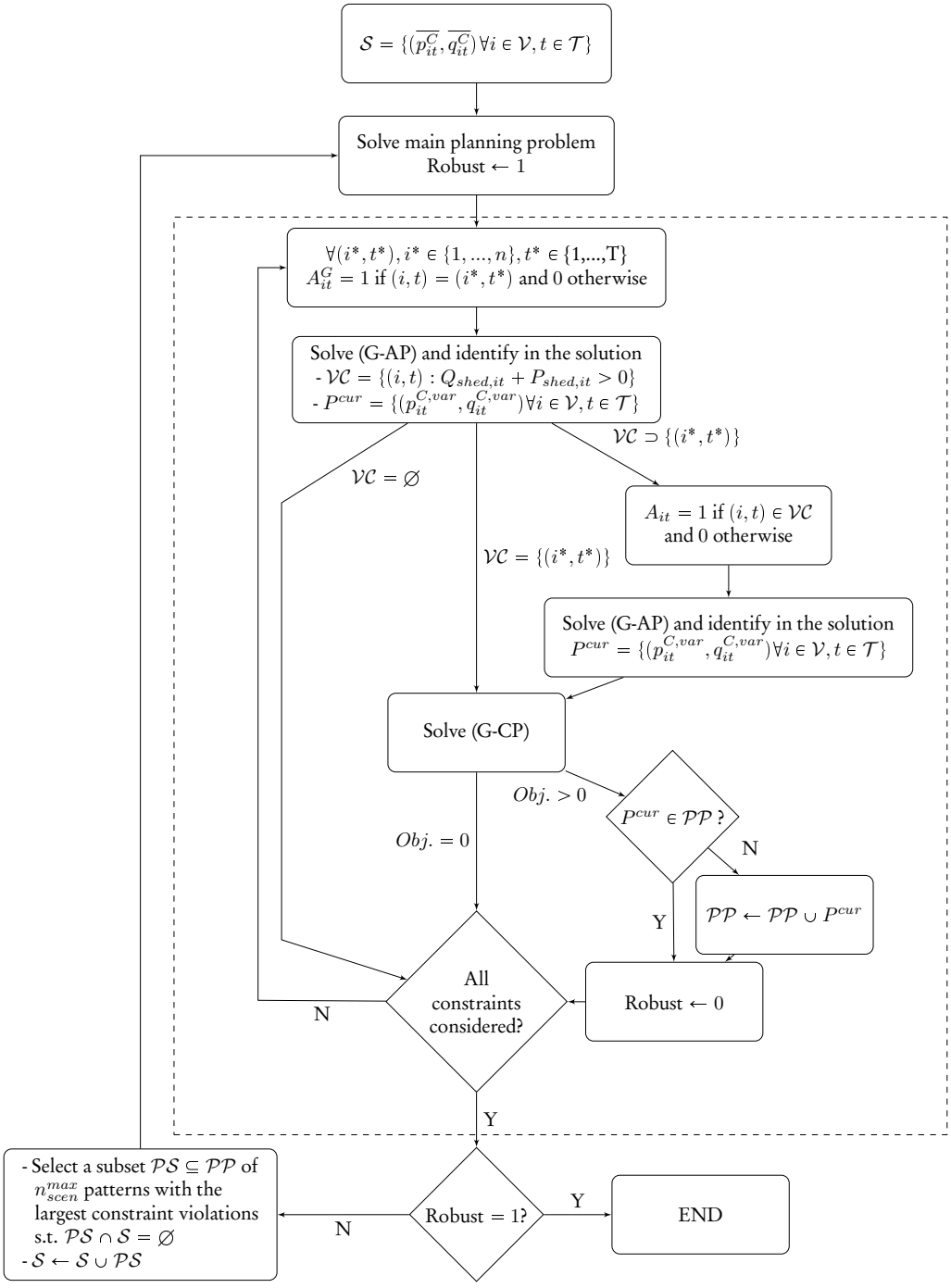

Fig. 6.1: Flowchart of the robust planning algorithm for the case of generation infeasibility

6.4.6 Results

Parameters

The robust approach presented above is applied to the first of the four microgrids presented in chapter 4 with the same parameters (see tables 4.2, 4.3 and 4.4). Specific robust optimization parameter values chosen for this test case are detailed in table 6.2

$p_{it}^{C,min}$, $p_{it}^{C,max}$	$[pu]$	$0.5\ p_{it}^{C}$, $2\ p_{it}^{C}$
$q_{it}^{C,min}$, $q_{it}^{C,max}$	$[pu]$	$0.5\ q_{it}^{C}$, $2\ q_{it}^{C}$
n_{scen}^{max}	[/]	4
LF	[/]	1.1
C^{ENS}	[MU/kWh]	1.5

Table 6.2: Robust optimization parameters values

Comparison of the deterministic and robust solutions

The robust solution is compared to the deterministic solution presented in chapter 4 on Fig. 6.2. As before, generators locations are marked with red dots and thin and thick blue lines represent *Mole* and *Gopher* line sections respectively.
The first observation is that there are three generators in the robust investment solution while there is only one in the deterministic solution. Furthermore, there are fewer *Gopher* line sections in the robust solution than in the deterministic one. This can be explained by the presence of a larger number of decentralized generators that allow to generate power nearer from consumption points, hence achieving a better balance of power flows on the different line sections of the microgrid. Voltage drops and power flows are thus reduced on critical sections, allowing for smaller conductors.

Comparison of system costs

The deterministic solution is not able to cope with all consumption scenarios determined in the robust approach. Yet, we want to compare total system costs (investment and operational expenses) of both deterministic and robust solutions on an equal basis. Hence, we have to simulate the operation of the microgrid obtained from the deterministic solution on the set of scenarios obtained in the robust approach. We introduce load shedding in power flow equations similarly to eqs. (**13.2**)

and (**13.3**) to determine the amount of load shedding needed to find a feasible operating points in every scenario. The cost of Energy Not Served (ENS) due to load

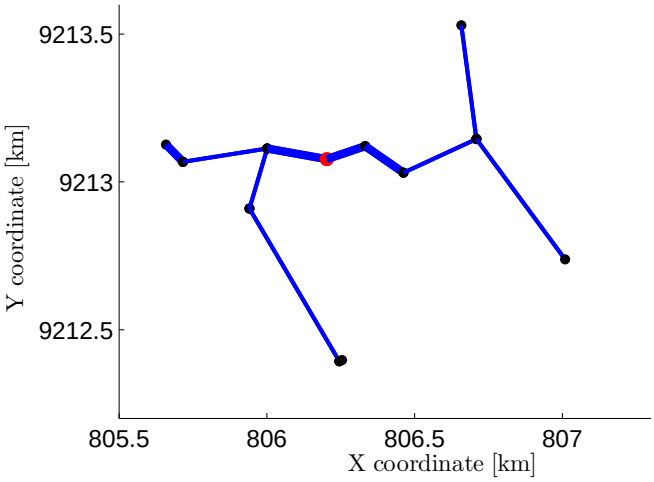

(a) Investment solution for the deterministic approach on Microgrid 1

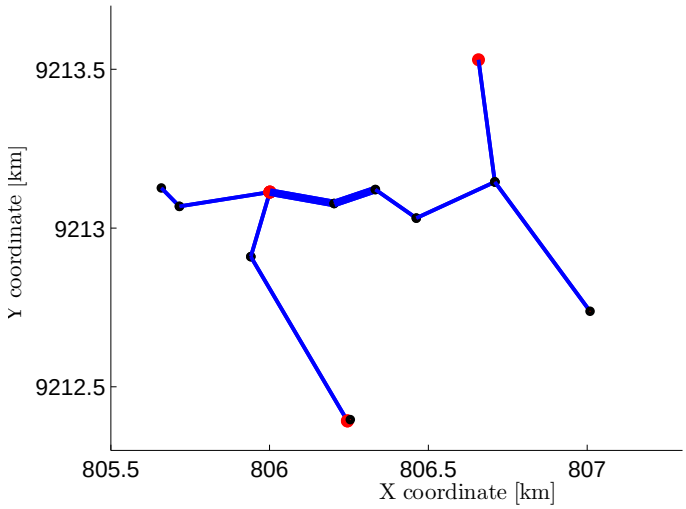

(b) Investment solution for the robust approach on Microgrid 1

Fig. 6.2: Comparison of investment solutions from deterministic and robust approaches

shedding is fixed at $[1.5MU/kWh]$ [42].
An OPF is solved for every scenario by fixing investment variables to their values from the deterministic solutions. The objective function to minimize in this OPF is the sum of generation costs and load shedding costs (**48**). Note that active and reactive load shedding are penalized in the same way.

$$\frac{1}{n_S} \sum_{i\in\mathcal{V}, g\in\mathcal{G}, t\in\mathcal{T}, s\in\mathcal{S}} \frac{1}{(1+d)^{t \text{ div } H}} \frac{8760}{H} \left(\gamma_{igy} C^P_{gf} + p_{gits} C^P_{gv} + C^{ENS}(p^{shed}_{its} + q^{shed}_{its})\right) \tag{48}$$

Finally, contrary to what is presented in chapter 4, all 24 hourly timesteps of the day are considered.

Costs are broken down into the different categories for the robust and the deterministic solutions respectively on Fig. 6.3. A logarithmic scale is used as the costs cover several different orders of magnitude. First, it can be seen that the line investment costs are nearly the same for both solutions with a difference of about one percent. As a matter of fact, both network have the same layout and only differ in the size of some line sections. Then, the generation investment cost is three times larger in the robust solution than in the deterministic one as there are three generators in the former and only one in the latter. This implies that the O& M costs are 50 % larger for the robust solution as there are more assets to maintain.
The main difference between both solutions costs lies in the fuel costs. Indeed, these are 2.5 times larger in the robust solution than in the deterministic one. This is due to the fact that generator start-up and stop is not modelled in this work as it would require additional binary variables that would make the problem even more computationally challenging .In the current test case, this simplified generator operation modelling is not problematic for the deterministic solution that includes a single generator as it has to be continuously in operation. However, when several generators are present, as in the robust solution, it is not necessarily needed to operate all units simultaneously and some of them can be turned off to avoid no-load costs. In the present case, units are considered to be permanently online which means that this no load-cost has to be paid for each generator at every timestep irrespective of its power production. This is illustrated on Fig. 6.4. On this graph, the red dotted line represents the generator hourly cost in function of the output power (considered constant over an hour), with a no load cost of about 0.5 [MU/h]. The superimposed histogram represents the distribution of generator setpoints over time. The first three blue bars represent the three generators of the robust solution while the orange bar represents the single generator of the deterministic solution. We can observe that the three generators of the robust solution are more often operated at low setpoints than the generator from the deterministic solution. This means that the cost of a generated kilowatt hour is proportionally higher than in the determinis-

tic solution, which explains the higher fuel costs of the robust solution on Fig. 6.3. With a proper modelling of generator start-up and stop, this fuel cost difference between robust and deterministic solutions should vanish.
The last cost category concerns the Energy Not Supplied (ENS). By definition of the robust solution, it should not allow any load shedding, hence the ENS cost is zero for this solution. The deterministic solution requires to shed load during peak power conditions for the critical consumption scenarios as the single generator is not able to cover the whole consumption in these conditions. However, the load shedding is very low in this test case and the cost of ENS is low as well, around $10^3[MU]$.

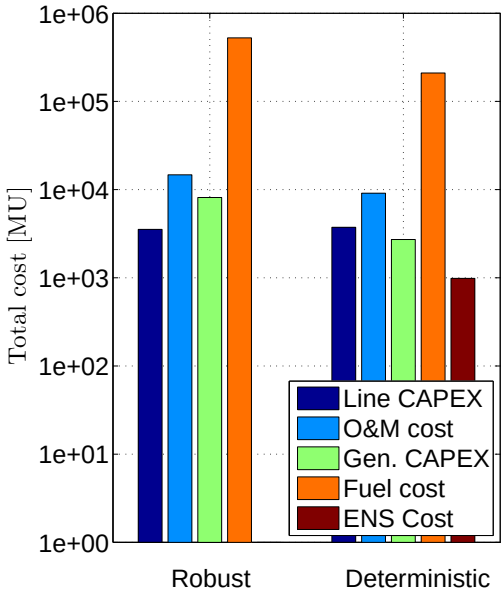

Fig. 6.3: Comparison of the different cost categories for the deterministic and robust solutions on a logarithmic scale

Computational analysis

The computational features of the robust approach applied to the current test case are summarized in Table 6.3. The runtime is about 1.5×10^4[s], which is three times more than in the deterministic case. The problem is solved within 2 iterations, which means that the planning problem has to be solved twice, with a larger set of constraints on the second iteration as new scenarios are added to the problem. On one side, a total of 1056 line thermal rating adversarial problems are solved, none of them giving rise to a problematic consumption pattern. On the other side, generation capacity constraints adversarial problems highlight 191 problematic consump-

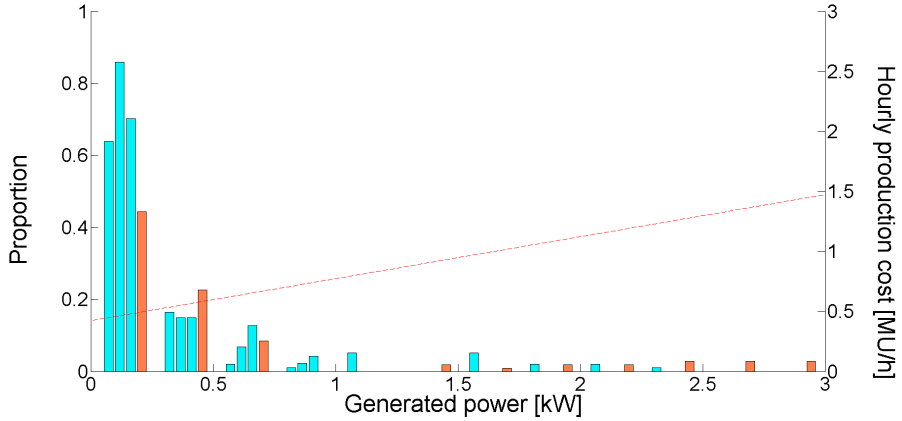

Fig. 6.4: Red dotted line : hourly generation cost (right y-axis) - Blue bars: histogram of the three generators setpoints for the robust solution (left y-axis) - Orange bars: histogram of the generator setpoints for the deterministic solution (left y-axis)

tion patterns by solving 2302 problems (including adversarial and corrective problems). It is observed in the current test case that adding only the 4 most problematic consumption patterns as scenarios of the planning problem is enough to ensure a feasible microgrid operating point for the considered load consumption uncertainty range. This is a really interesting feature as including all 191 patterns would make the problem more computationally challenging if not intractable.

Runtime [s]	1.5×10^4
Iterations	2
Thermal rating adv. problems	1056
Generation capacity adv. and corr. problems	2302
Problematic patterns	191
Added scenarios	4

Table 6.3: Computational features of the robust test case

6.4.7 Extension to chance constrained programming and general probability distributions

As mentioned in the beginning of this section, the proposed method can also be used with probabilistic modelling, i.e. when we consider that the joint distribution function of random variables is known (variables may be correlated in general). Indeed, let us consider the vector of random variables $\omega \in \Omega$ and the joint density function $p(\omega)$. If we define the two vectors of parameters $\overline{\omega}^L$ and $\overline{\omega}^U$, the probability that $\overline{\omega}^L \leqslant \omega \leqslant \overline{\omega}^U$ is then expressed as the following integral:

$$\mathbb{P}(\overline{\omega}^L \leqslant \omega \leqslant \overline{\omega}^U) = \int_{\overline{\omega}^L}^{\overline{\omega}^U} p(\omega) d\omega \tag{49}$$

As mentioned in [64], this allows to formulate chance-constrained optimization as robust optimization. Indeed, the chance-constrained paradigm consists of finding the extremum of an objective function $f(x)$ while allowing constraints $h(x) \leqslant 0$ to be violated with a small probability ϵ:

$$\begin{aligned} &\sup_x f(x) \\ &s.t. \quad \mathbb{P}\big(h(x,\omega) \leqslant 0\big) \geqslant 1-\epsilon \quad \forall \omega \in \Omega \end{aligned} \tag{50}$$

This can be reformulated in a robust way on a subspace of Ω such that the probability that random variables belong to this subspace is equal to $1-\epsilon$. Note that the rectangular uncertainty interval defined by constraint (**51**) can be computed offline.

$$\begin{aligned} &\sup_x f(x) \\ &\quad s.t. \quad h(x,\omega) \leqslant 0 \\ &\qquad \overline{\omega}^L \leqslant \omega \leqslant \overline{\omega}^U \\ &\qquad \int_{\overline{\omega}^L}^{\overline{\omega}^U} p(\omega) d\omega = 1-\epsilon \end{aligned} \tag{51}$$

6.5 Discussion and perspectives

In this chapter, a robust optimization procedure has been developed for the autonomous microgrid planning problem. We showed that the increase in computational complexity was controlled. As a matter of fact, the runtime of the robust approach is only three times larger than in the deterministic case, considering that

two planning problems and thousands of adversarial and corrective problems have to be solved during this period. This is made possible by the scenario selection scheme. Indeed, it allows to only include a small subset of the problematic consumption patterns in the planning problem. The inclusion of these patterns implicitly ensures that a feasible operating point exists for other problematic patterns as well and avoids adding too many constraints to the planning problem.

A first axis of improvement would be to only add constraints modelling problematic timesteps instead of problematic patterns to reduce the computational burden. Indeed, at the moment, we identify a whole consumption pattern (i.e. the values of random load consumption variables for every considered timestep) that maximizes the constraints violation for a given microgrid. Yet, constraint violations only occur on a small susbset of these timesteps. We could thus reduce the number of constraints added to the planning problem by considering only this subset of the timesteps.

Another desirable feature for a robust microgrid planning would be to consider reliability issues. Indeed, we did not consider any microgrid component failure in the presented approach. This would require to include additional scenarios representing the various components conditions (available or subject to an outage) and their frequency of occurrence, depending on the reliability policy, e.g. planning under N-1 criterion. It has to be further investigated whether or not the additional scenarios could increase the computational burden to a point where it would become intractable.

Renewable energy sources are not considered in this chapter as we focused on load uncertainty. However, the presented robust approach is directly transposable to generation related uncertainty if the uncertainty range of RES generation is known. Binary generator investment variables still represent the fact that a generator is located at a certain node or not and the output of a RES generator is not a decision variable anymore but a random variable. The adversarial problem then consists in looking within the RES uncertainty range for the production patterns that are the most problematic regarding engineering constraints.

Finally, we showed that the robust procedure could be seen as a reformulation of a chance constrained optimization and allowed to account for correlated and multivariate probability distributions. Using the described procedure in a chance-constrained way, with a given ϵ tolerance, consists in solving a robust planning problem on a subset of the total uncertainty set such that the probability that random variables take values within this subset is larger than or equal to $(1 - \epsilon)$.

Conclusion 7

This thesis addressed the problem of autonomous microgrid investment planning in a rural electrification context. In a first phase, we presented a dynamic programming approach to the network planning. However, this approach proved to be already computationally challenging for the sole network planning problem. We thus chose to tackle the problem through convex optimization. First, we formulated it as a non-convex and mixed-integer optimization problem. Due to the inherent computational complexity of this problem class, we developed a hierarchy of deterministic convex relaxations and we studied their respective performances in terms of runtime, power flow modelling accuracy and solution adequacy. Then, we investigated in more depth the power flow modelling accuracy of the tightest relaxation among the proposed hierarchy, i.e. the Convex DistFlow relaxation. We finally extended the deterministic models by proposing a robust approach in order to integrate load-related uncertainty in the planning process.
In this concluding chapter, we highlight the contributions of the present work, we identify some of its shortcomings and we propose areas of improvement for further research as well as potential applications.

7.1 Contributions

We begin this section by summarizing the main contributions of the thesis.

Summary of contributions

1. To our knowledge, this work is the first to tackle the joint planning of generation and distribution in autonomous microgrids from a mathematical optimization perspective.
2. We presented a hierarchy of convex formulations for this problem that leverage the recent advances in power flows modelling
3. We built this hierarchy in a modular way, from the simplest formulations to the richest ones. We clearly identified the successive steps in formulating a set of planning problems including growing accuracy relaxations of power flow equations.
4. We investigated in depth how these models performed in terms of runtime, modelling accuracy and feasibility of the solutions. We could highlight the direct relation between the latter two, and the cost of modelling accuracy in terms of runtime.
5. We proposed a robust planning approach allowing to account for the uncertainty related to load and intermittent renewable power production. The increase in computational burden was shown to be controlled.

We now provide elements of a response to the open questions exposed in the introduction to this document by making use of the results we obtained.

How does the accuracy of power flow modelling, and more precisely the use of convex relaxations of power flow equations , impact the quality of planning solutions?

We observed that the power flow modelling accuracy was of paramount importance regarding the adequacy of solutions. As a matter of fact, the CDF-OA model was the only one to deliver solutions that were feasible for all loading conditions. On the other hand, solutions of other, less accurate models, were found to be infeasible for up to 20% of considered timesteps in the test cases. We also observed that the most binding constraints were related to the voltage level, which was expected in a

rural context with long lines and sparse population. Yet, weaker formulations either omit voltages (NF-IA/OA) or compute them with significant inaccuracy as 75% of node voltages presented relative errors larger than 10% in the different test cases for models TH-IA/OA and TH-L-IA/OA. In contrast, we showed that the CDF-OA relaxation could be made as accurate as wanted, at the expense of a larger computational burden. For these two reasons, it can be strongly argued that the adequacy of a planning solution largely depends on the underlying optimization model accuracy in this rural electrification context. Hence, when considering a mathematical optimization framework, CDF relaxation-based or comparable accuracy approaches should be retained for microgrid investment planning problems.

Is it possible to devise scalable and accurate joint planning methods that leverage the strength of mathematical optimization?

In the present work, we identified a clear trade-off between scalable and less accurate methods (NF-IA/OA, TH-IA/OA, TH-L-IA/OA) and an accurate but less scalable model (CDF-OA). The latter has been found difficult to solve for real-world size problems. As this question needs further investigation, we formulate improvement suggestions related to this matter in the following section. They offer real perspectives for the improvement of the problem's computational tractability.

How to account for the uncertainty inherent to the planning of autonomous microgrids in a scalable way?

We could show that a robust optimization approach integrating load-related uncertainty represented a reasonable increase in computational burden with respect to the deterministic version. We also showed how the proposed approach could easily be extended to account for the RES generation intermittency or to formulate the satisfaction of engineering constraints in a chance-constrained way, which is in line with the usual power system operation practice. Nonetheless, we neither investigated how reliability issues could be integrated in this approach nor determined how it would affect the computational tractability. Yet, reliability issues are important in power systems, particularly in microgrids where they determine the technical and financial viability of the system. This last point thus needs to be the object of further investigations.

7.2 Research perspectives

Scalability

As mentioned in the previous section, accurate power flow representations are necessary to deliver adequate planning solutions. Yet, we showed that the Convex DistFlow relaxation - the only considered formulation to exhibit sufficient accuracy - could not scale for moderate size problems. Hence, the following paragraph sets out suggestions for future research, with a view to extending the scope of application of the proposed planning model to larger size cases.
In this work, we put the emphasis on the trade-off between the accuracy and the feasibility of planning solutions. Nonetheless, these planning solutions may also be classified along a third axis: optimality. Indeed, we stated in the introduction to this work that distribution and generation planning should be performed simultaneously as the opposite would be suboptimal. However, the combinatorial nature of the problem - due to integer investment variables - implies that the size of the discrete solution space grows exponentially with the size of the problem. This combinatorial explosion inherent to discrete problems is known as the curse of dimensionality. This is true regardless of the power flow representation. Yet, the CDF formulation has three times more constraints involving integer variables than other formulations, which greatly complicates the problem. To counter the curse of dimensionality, we could give up a bit of optimality for tractability by considering two separate and consecutive subproblems: feeder routing and sizing on one side, and generation siting and sizing on the other side. Considering a set of n nodes, the number of spanning trees is n^{n-2} and the number of generator siting options is 2^n (each node may or may not host a generator). Considering both decision types simultaneously amounts to a total number of possible configurations of $n^{n-2} \times 2^n$ while setting those two decision types apart amounts to two consecutive problems with a respective number of n^{n-2} and 2^n possible combinations. For a 20 node network, this represents around 2.7×10^{29} and $(2.6 \times 10^{23} + 1 \times 10^6)$ combinations respectively. The separate consideration of distribution and generation planning problems thus offers really interesting perspectives regarding the reduction of the solution space size. The joint planning problem could then be tackled in an iterative way with the following steps:

1. Perform network planning considering a single generator located at its centre that is able to cover the whole load
2. Solve generation planning problem on the network found at step 1)
3. Solve a new network planning problem considering the generator siting and sizing determined at step 2)
4. Iterate through steps 2) and 3) until convergence of the global distribution and generation planning solution

This type of method should be compared to the simultaneous planning method to quantify the loss in optimality (i.e. solution cost increase) and the impact on the runtime. Whether the latter justifies the former remains an open question.
The results we obtained in the present work with the simultaneous approach show that the optimal network layout either corresponds to the Minimum Spanning Tree (MST) or is close to it. Yet, without considering line sizing aspects, the MST layout is likely to be the optimal solution to the sole network planning problem as it minimizes the total length of lines. Hence, it does not seem unreasonable to think that solving network and generation planning separately might not drastically change the global planning solution compared to the simultaneous planning approach.

In a similar vein, decomposition approaches mentioned in chapter 4 also offer interesting improvement perspectives in terms of computational tractability. In the present work, we already implemented such an approach by using the Benders decomposition, which allowed us to find solutions to the CDF-OA model for the considered test cases. As a matter of fact, the classical branch-and-bound algorithm did not converge when using the CDF-OA model, even for these small test-cases. We did not fine-tune the Benders decomposition algorithm, letting all integer variables in the master problem and continuous ones in the subproblems. There may be potential for improvement regarding the parametrisation of this method. Other decomposition approaches based on duality exist, such as lagrangian decomposition methods. It remains to be seen whether such methods can offer significant improvements in computational tractability in the present context. However it has been shown that these methods notably outperformed conventional B&B algorithms of commercial solvers in the context of unit commitment [40]. They could thus be successfully applied to the joint planning problem to make it more scalable.

Reliability

Reliability aspects were not considered in this work. However, a planning tool should incorporate them in order to deliver a solution adequate for forecast conditions as well as contingency conditions. Incorporating distribution and generation assets failures in the planning is computationally challenging as it adds complexity to an already difficult problem. For example, planning according to the $N-1$ criterion requires to build a system able to cope with the failure of every single system component (line, generator). The Security-constrained Optimal Power Flow (SCOPF) integrates this criterion by replicating the problem constraints for every system component failure. In [19], the adversarial procedure - on which the robust planning method proposed in chapter 6 is based - is reproduced for every contingency., In these two examples, the $N-1$ criterion represents a huge increase in computational

complexity. Furthermore, such approaches deliver solutions with high redundancy which makes them more expensive. In a rural electrification context where capital scarcity is likely to occur, it might not be possible to implement such solutions. In this case, less conservative reliability criteria may be more adapted to find a trade-off between cost and security of supply.

7.3 Applications

Distribution systems expansion planning

The tools developed in this work can be directly applied to the expansion planning of distribution systems in central grids. As a matter of fact, a distribution network may be modelled in the exact same way as a microgrid. The transmission or sub-transmission network is then represented by its Thé venin equivalent at the connection point between both networks.
Using the tools developed in this work for distribution system planning is particularly relevant in the current context. As a matter of fact, a strong will to increase the renewables share in the energy mix and incentivising policies from governments have led to a dramatic increase in the amount of Decentralized Generation (DG) units connected at the distribution level. These distribution grids historically transferred energy from the transmission grid to the final user in a unidirectional way, which was achieved through a top-down, tree-like architecture. Yet, when they inject their power on the grid, DG units can significantly change, if not reverse, the PF patterns. Distribution grid planning must thus now account for decentralized generation as it is the case for microgrids.
Hence, a DSO could use a joint planning approach as developed in this work to simultaneously determine needed line reinforcements or expansion and decide on optimal DG locations within the existing network.

Large-scale rural electrification

The Michiquillay district (Peru) presented in chapter 4 has been the object of a large-scale study that aimed at determining the best way to electrify 6700 households. The REM/RNM tool used in this study is able to choose between the three following modes of electrification: grid expansion, microgrid or standalone systems. In a second phase, it can be used to design the individual microgrids or the grid extensions. The planning method developed in this work is neither intended nor able to identify the optimal modes of electrification on such a large scale. However, it has shown to be able to deliver adequate solutions for the planning of moderate-size microgrids. Hence, it should rather be seen as a detailed design tool.

Simplified approaches such as REM/RNM or the NF-IA/OA planning models presented in chapter 4 thus remain necessary to make decisions on a larger scale. They should be used in complementarity with more detailed tools, such as the planning method developed in this work, to address the problem of rural electrification in all its aspects.

List of Figures

List of Tables

List of models

Acronyms

AC	Alternating Current
ACA	Ant Colony Algorithm
AIS	Artificial Immune Systems
B&B	Branch-and-Bound
BIM	Bus Injection Model
CAPEX	Capital Expenditures
CC	Chance-Constrained
DC	Direct Current
DFIG	Doubly Fed Induction Generator
DG	Distributed Generation
DP	Dynamic Programming
DSM	Demand Side Management
DSO	Distribution System Operator
EA	Evolutionary Algorithms
GA	Genetic Algorithm
IA	Inner Approximation
ICA	Imperialist Competitive Algorithm
ICE	Internal Combustion Engine
IEEE	Institute of Electrical and Electronics Engineers
IEA	International Energy Agency
KCL	Kirchhoff's Current Law
LV	Low Voltage
LP	Linear Program
MILP	Mixed-Integer Linear Program
MINLP	Mixed-Integer Non-Linear Program
MST	Minimum Spanning Tree
MU	Monetary units
MV	Medium Voltage
NC	Non-Convex
NL	Non-Linear
NP	Nondeterministic Polynomial
RES	Renewable Energy Sources
OA	Outer Approximation

OPEX	Operational Expenditures
OPF	Optimal Power Flow
PCC	Point of common coupling
PF	Power Flow
PSO	Particle Swarm Optimization
PU	Per Unit
PV	Photovoltaïc
QC	Quadratic Convex
RO	Robust Optimization
SA	Simulated Annealing
SCADA	Supervisory Control And Data Acquisition
SDG	Sustainable Development Goals
SDP	Semi-Definite Program
SOCP	Second Order Cone Program
TSO	Transmission System Operator
UC	Unit Commitment
WT	Wind turbine

Bibliography

[1] HOMER - Hybrid Renewable and Distributed Generation System Design Software. https://www.homerenergy.com/, 01/02/2018.

[2] S. Albert. *Solving mixed integer linear programs using branch and cut algorithm*. PhD thesis, North Carolina State University, 2006.

[3] M.-C. Alvarez-Herault. *Architecture des reseaux de distribution du futur en presence de production decentralisee*. PhD thesis, Institut National Polytechnique de Grenoble - INPG, 2009.

[4] M. C. Alvarez-Herault, R. Caire, B. Raison, N. HadjSaid, and W. Bienia. Optimizing traditional urban network architectures to increase distributed generation connection. *International Journal of Electrical Power & Energy Systems*, 35(1):148–157, 2012.

[5] M.-C. Alvarez-Hérault. *ARCHITECTURES DES RÉSEAUX DE DISTRIBUTION DU FUTUR EN PRÉSENCE DE PRODUCTION DÉCENTRALISÉE*. PhD thesis, Institut National Polytechnique de Grenoble - INPG, 2009.

[6] G. Andersson, M. Vrakopoulou, J. Lygeros, and K. Margellos. Probabilistic guarantees for the N-1 security of systems with wind power generation. In *Proceedings of PMAPS 2012*, Istanbul, 2012.

[7] X. Bai, H. Weihua, K. Fujisawa, and Y. Wang. Semidefinite programming for optimal power flow problems. *International Journal of Electrical Power & Energy Systems*, 30:383–392, 2008.

[8] World Bank. State of electricity access report. 2017.

[9] M. E. Baran and F. F. Wu. Optimal capacitor placement on radial distribution systems. *IEEE Transactions on Power Delivery*, 4(1):725–734, 1989.

[10] A. Ben-Tal and A. Nemirovski. On polyhedral approximations of the second-order cone. *Mathematics of Operations Research*, 26(2):193–205, 2001.

[11] D. Bienstock, M. Chertkov, and S. Harnett. Chance-Constrained Optimal Power Flow: Risk-Aware Network Control under Uncertainty. *SIAM Review*, 56(3):461–495, 2014.

[12] M. Bierlaire. Optimisation en nombres entiers, Slides du cours 'Recherche opérationnelle'. 2010, Ecole Polytechnique Fédérale de Lausanne.

[13] K. Bithas and P. Kalimeris. A Brief History of Energy Use in Human Societies. In *Revisiting the Energy-Development Link*, pages 5–10. Springer International Publishing, Cham, 2016.

[14] J. A. Bondy and U. S. R. Murty. *Graph theory, volume 244 of Graduate Texts in Mathematics*. Springer, New York, 2008.

[15] N. Boulaxis and M. Papadopoulos. Optimal feeder routing in distribution system planning using dynamic programming technique and GIS facilities. *IEEE Transactions on Power Delivery*, 17(1):242–247, 2002.

[16] S. P. Boyd and L. Vandenberghe. *Convex optimization*. Cambridge University Press, 2004.

[17] G. Calafiore and M. Campi. The Scenario Approach to Robust Control Design. *IEEE Transactions on Automatic Control*, 51(5):742–753, 2006.

[18] F. Capitanescu, S. Fliscounakis, P. Panciatici, and L. Wehenkel. Cautious operation planning under uncertainties. *IEEE Transactions on Power Systems*, 27(4):1859–1869, 2012.

[19] F. Capitanescu and L. Wehenkel. Computation of Worst Operation Scenarios Under Uncertainty for Static Security Management. *IEEE Transactions on Power Systems*, 28(2):1697–1705, 2013.

[20] E. G. Carrano, F. G. Guimaraes, R. H. C. Takahashi, O. M. Neto, and F. Campelo. Electric Distribution Network Expansion Under Load-Evolution Uncertainty Using an Immune System Inspired Algorithm. *IEEE Transactions on Power Systems*, 22(2):851–861, 2007.

[21] E. G. Carrano and L. A. Soares. Data Used in Simulations of Paper Electric Distribution Network Design Using a Problem-Specific Genetic Algorithm. 2006.

[22] E. G. Carrano, L. A. Soares, R. H. Takahashi, R. R. Saldanha, and O. M. Neto. Electric distribution network multiobjective design using a problem-specific genetic algorithm. *Power Delivery, IEEE Transactions on*, 21(2):995–1005, 2006.

[23] G. Celli, F. Pilo, G. Pisano, V. Allegranza, and R. Cicoria. Distribution network interconnection for facilitating the diffusion of distributed generation. In *Electricity Distribution, 2005. CIRED 2005. 18th International Conference and Exhibition on*, pages 1–5. IET, 2005.

[24] J. Clausen. Branch and bound algorithms-principles and examples. *Department of Computer Science, University of Copenhagen*, pages 1–30, 1999.

[25] C. Coffrin, H. Hijazi, and P. Van Hentenryck. Network flow and copper plate relaxations for AC transmission systems. In *Power Systems Computation Conference (PSCC), 2016*, pages 1–8. IEEE, 2016.

[26] C. Coffrin, H. L. Hijazi, and P. Van Hentenryck. DistFlow Extensions for AC Transmission Systems. *arXiv:1506.04773 [cs, math]*, 2015.

[27] C. Coffrin, H. L. Hijazi, and P. Van Hentenryck. The qc relaxation: Theoretical and computational results on optimal power flow. *arXiv preprint arXiv:1502.07847*, 2015.

[28] E. Demirok, S. B. Kj\a er, D. Sera, and R. Teodorescu. Three-phase unbalanced load flow tool for distribution networks. In *Proceedings of the 2nd International Workshop on Integration of Solar Power Systems Energynautics GmbH, Lisbon, Portugal*, pages 12–13, 2012.

[29] D. Dubois. Théorie des possibilités, Séminaire à l'IMT Atlantique. 2012.

[30] Intelligent Energy Europe. MICROGRIDS Promotion of microgrids and renewable energy sources for electrification in developing countries. 2008.

[31] H. Falaghi, M. Ramezani, M.-R. Haghifam, and K. R. Milani. Optimal selection of conductors in radial distribution systems with time varying load. In *Electricity Distribution, 2005. CIRED 2005. 18th International Conference and Exhibition on*, pages 1–4. IET, 2005.

[32] H. Falaghi, C. Singh, M.-R. Haghifam, and M. Ramezani. DG integrated multistage distribution system expansion planning. *International Journal of Electrical Power & Energy Systems*, 33(8):1489–1497, 2011.

[33] M. Farivar, C. R. Clarke, S. H. Low, and K. M. Chandy. Inverter VAR control for distribution systems with renewables. In *2011 IEEE International Conference on Smart Grid Communications (SmartGridComm)*, pages 457–462, 2011.

[34] M. A. Farrag, M. M. El-Metwally, and M. S. El-Bages. A new model for distribution system planning. *International Journal of Electrical Power & Energy Systems*, 21(7):523–531, 1999.

[35] C. Field, J. Campbell, and D. Lobell. Biomass energy: the scale of the potential resource. *Trends in Ecology & Evolution*, 23(2):65–72, 2008.

[36] R. Fourer, D. Gay, and B. Kernighan. Ampl: a modeling language for mathematical programming. *Duxbury Press*, 2002.

[37] S. Ganguly, N. C. Sahoo, and D. Das. Multi-objective particle swarm optimization based on fuzzy-Pareto-dominance for possibilistic planning of electrical distribution systems incorporating distributed generation. *Fuzzy Sets and Systems*, 213:47–73, 2013.

[38] S. Ganguly, N. C. Sahoo, and D. Das. Multi-objective planning of electrical distribution systems using dynamic programming. *International Journal of Electrical Power & Energy Systems*, 46:65–78, 2013.

[39] S. Ganguly, N. C. Sahoo, and D. Das. Recent advances on power distribution system planning: a state-of-the-art survey. *Energy Systems*, 4(2):165–193, 2013.

[40] C. Gerard. Coordinated operation of electric power transmission and distribution systems. Master thesis, Université catholique de Louvain, 2017.

[41] F. Glineur. *Topics in Convex Optimization: Interior-Point Methods, Conic Duality and Approximations*. PhD thesis, Faculté Polytechnique de Mons, 2001.

[42] A. Gonzales-Garcia, R. Amatya, R. Stoner, and I. Perez-Arriaga. Evaluation of universal access to modern energy services in Peru Case study of scenarios for Electricity Access in Cajamarca. Low-cost energy technologies for Universal Access. Working Paper Enel Foundation. 2016.

[43] B. L. Gorissen, h. Yanıkoğlu, and D. den Hertog. A practical guide to robust optimization. *Omega*, 53(Supplement C):124–137, 2015.

[44] E. Haesen. *Multi-Objective Optimization of the Integration of Stochastic Distributed Energy Resources in Electricity Grids*. PhD thesis, Katholieke Universiteit Leuven, 2009.

[45] S. Haffner, L. Pereira, L. Pereira, and L. Barreto. Multistage Model for Distribution Expansion Planning With Distributed Generation - Part I: Problem Formulation. *IEEE Transactions on Power Delivery*, 23(2):915–923, 2008.

[46] S. Haffner, L. Pereira, L. Pereira, and L. Barreto. Multistage Model for Distribution Expansion Planning with Distributed Generation - Part II: Numerical Results. *IEEE Transactions on Power Delivery*, 23(2):924–929, 2008.

[47] N. Hatziargyriou, H. Asano, R. Iravani, and C. Marnay. Microgrids. *IEEE Power and Energy Magazine*, 5(4):78–94, 2007.

[48] IEA. Energy Access Outlook 2017: From Poverty To Prosperity. 2017.

[49] IEC. IEC 60050 - International Electrotechnical Vocabulary. http://www.electropedia.org/, 01/02/2018.

[50] R. Jabr. Radial Distribution Load Flow Using Conic Programming. *IEEE Transactions on Power Systems*, 21(3):1458–1459, 2006.

[51] J.-M. Jancovici. Combien suis-je un esclavagiste? https://jancovici.com/transition-energetique/l-energie-et-nous/combien-suis-je-un-esclavagiste/, 01/02/2018.

[52] N. Janssens and E. De Jaeger. *Réseaux d'énergie électrique - Notes de cours*. 2009.

[53] B. M. Kalesar and A. R. Seifi. Fuzzy load flow in balanced and unbalanced radial distribution systems incorporating composite load model. *International Journal of Electrical Power & Energy Systems*, 32(1):17–23, 2010.

[54] B. M. Kalesar and A. R. Seifi. Optimal substation placement and feeder routing in distribution system planning using genetic algorithm. *Elixir International journal of Electrical Enggineering*, pages 3908–3915, 2011.

[55] E. Klotz and A. M. Newman. Practical guidelines for solving difficult mixed integer linear programs. *Surveys in Operations Research and Management Science*, 18(1–2):18–32, 2013.

[56] D. Kumar, S. R. Samantaray, and G. Joos. A reliability assessment based graph theoretical approach for feeder routing in power distribution networks including distributed generations. *International Journal of Electrical Power & Energy Systems*, 57:11–30, 2014.

[57] T. Lambert, P. Gilman, and P. Lilienthal. Micropower system modeling with HOMER. *Integration of alternative sources of energy*, 1, 2006.

[58] J. Lasserre. Global Optimization with Polynomials and the Problem of Moments. *SIAM Journal on Optimization*, 11(3):796–817, 2001.

[59] A. Latiers, F. Glineur, B. Martin, and E. De Jaeger. On Decentralized Control of Small Loads and Energy Rebound within Primary Frequency Control. 2016.

[60] V. Li. The Local Reference Electrification Model: comprehensive decision-making tool for the design of rural microgrids,. Master thesis, Massachusetts Institute of Technology, 2016.

[61] H. Liang, H. Liu, and M. Fan. Optimal Planning of Microgrid applied in Remote Rural Area. In *Proceedings of the CIGRE Symposium 2012*, 2012.

[62] S. H. Low. Convex Relaxation of Optimal Power Flow, Part II: Exactness. *IEEE Transactions on Control of Network Systems*, 1(2):177–189, 2014.

[63] C. Lueken, P. M. S. Carvalho, and J. Apt. Distribution grid reconfiguration reduces power losses and helps integrate renewables. *Energy Policy*, 48:260–273, 2012.

[64] K. Margellos, P. Goulart, and J. Lygeros. On the Road Between Robust Optimization and the Scenario Approach for Chance Constrained Optimization Problems. *IEEE Transactions on Automatic Control*, 59(8):2258–2263, 2014.

[65] B. Martin, E. De Jaeger, F. Glineur, and A. Latiers. A dynamic programming approach to multi-period planning of isolated microgrids. In *Advances in Energy System Optimization*, pages 123–137. Springer, 2017.

[66] B. Martin, P. De Rua, E. De Jaeger, and F. Glineur. Loss reduction in a windfarm participating in primary voltage control using an extension of the Convex DistFlow OPF (Forthcoming). In *20th Power Systems Computation Conference*, Dublin, 2018.

[67] B. Martin, B. Feron, A. Monti, E. De Jaeger, and F. Glineur. Peak shaving: a planning alternative to reduce investment costs in distribution systems? *Submitted to Energy Systems*, 2018.

[68] B. Martin, E. D. Jaeger, and F. Glineur. Comparison of convex formulations for the joint planning of microgrids. *CIRED - Open Access Proceedings Journal*, 2017(1):2174–2178, 2017.

[69] B. Martin, E. D. Jaeger, and F. Glineur. A robust convex optimization framework for autonomous network planning under load uncertainty. In *2017 IEEE Manchester PowerTech*, pages 1–6, 2017.

[70] G. P. McCormick. Computability of global solutions to factorable nonconvex programs: Part I — Convex underestimating problems. *Mathematical Programming*, 10(1):147–175, 1976.

[71] S. Melkote and M. S. Daskin. Capacitated facility location/network design problems. *European journal of operational research*, 129(3):481–495, 2001.

[72] S. Mhanna, G. Verbic, and A. Chapman. Tight LP Approximations for the Optimal Power Flow Problem. *arXiv preprint arXiv:1603.00773*, 2016.

[73] D. K. Molzahn and I. A. Hiskens. Moment-based relaxation of the optimal power flow problem. In *Power Systems Computation Conference (PSCC), 2014*, pages 1–7. IEEE, 2014.

[74] D. K. Molzahn and I. A. Hiskens. A Survey of Relaxations and Approximations of the Power Flow Equations. Invited submission to "Foundations and Trends in Electric Energy Systems. 2017.

[75] G. G. Moshi, C. Bovo, A. Berizzi, and L. Taccari. Optimization of Integrated Design and Operation of Microgrids Under Uncertainty. In *Power Systems Computation Conference (PSCC), 2016*, Genoa, 2016.

[76] G. Muñoz-Delgado, J. Contreras, and J. M. Arroyo. Joint Expansion Planning of Distributed Generation and Distribution Networks. *IEEE Transactions on Power Systems*, PP(99):1–12, 2014.

[77] H. Nagarajan, E. Yamangil, R. Bent, P. Van Hentenryck, and S. Backhaus. Optimal Resilient transmission Grid Design. In *Power Systems Computation Conference (PSCC), 2016*, pages 1–7. IEEE, 2016.

[78] J. Nahman and J. Spirić. Optimal planning of rural medium voltage distribution networks. *International Journal of Electrical Power & Energy Systems*, 19(8):549–556, 1997.

[79] N. Newham. Power System investment planning using stochastic dual dynamic programming. 2008.

[80] O. Palizban, K. Kauhaniemi, and J. M. Guerrero. Microgrids in active network management—Part I: Hierarchical control, energy storage, virtual power plants, and market participation. *Renewable and Sustainable Energy Reviews*, 36:428–439, 2014.

[81] F. Pilo, S. Jupe, C. Abbey, A. Baitch, B. Bak-Jensen, C. Carter-Brown, G. Celli, K. El Bakari, M. Fan, P. Georgilakis, T. Hearne, L. Ochoa, G. Petretto, and J. Taylor. Planning and optimization methods for active distribution systems. 2013.

[82] I. Ramirez-Rosado and J. Dominguez-Navarro. New Multiobjective Tabu Search Algorithm for Fuzzy Optimal Planning of Power Distribution Systems. *IEEE Transactions on Power Systems*, 21(1):224–233, 2006.

[83] R. Ranjan, B. Venkatesh, and D. Das. A new algorithm for power distribution system planning. *Electric Power Systems Research*, 62(1):55–65, 2002.

[84] S. N. Ravadanegh and R. G. Roshanagh. On optimal multistage electric power distribution networks expansion planning. *International Journal of Electrical Power & Energy Systems*, 54:487–497, 2014.

[85] L. Roald, S. Misra, M. Chertkov, S. Backhaus, and G. Andersson. Chance Constrained Optimal Power Flow with Curtailment and Reserves from Wind Power Plants. *arXiv preprint arXiv:1601.04321*, 2016.

[86] B. Ruben, A. Cross, D. Strickland, M. Aten, and R. Ferris. Meshing radial networks at 11kv. In *Innovative Smart Grid Technologies (ISGT Europe), 2011 2nd IEEE PES International Conference and Exhibition on*, pages 1–8. IEEE, 2011.

[87] D. Schnitzer, D. S. Lounsbury, and J. Carvallo. Microgrids for Rural Electrification: A critical review of best practices based on seven case studies. United Nations Foundation. 2014.

[88] A. H. Seddighi and A. Ahmadi-Javid. Integrated multiperiod power generation and transmission expansion planning with sustainability aspects in a stochastic environment. *Energy*, 86:9–18, 2015.

[89] J. Shi, Y. Qiao, Y. Wang, J. Wen, J. Tong, and J. Zhang. The planning of distribution network containing distributed generators based on mixed integer linear programming. In *2015 5th International Conference on Electric Utility Deregulation and Restructuring and Power Technologies (DRPT)*, pages 449–453, 2015.

[90] N. Shor. Quadratic optimization problems. *Soviet Journal of Computer and Systems Sciences*, 25, 1987.

[91] A. Soroudi and M. Ehsan. A possibilistic–probabilistic tool for evaluating the impact of stochastic renewable and controllable power generation on energy losses in distribution networks—A case study. *Renewable and Sustainable Energy Reviews*, 15(1):794–800, 2011.

[92] G. Stefopoulos, A. P. Meliopoulos, and G. J. Cokkinides. Advanced probabilistic power flow methodology. *15th PSCC, Liege*, pages 22–26, 2005.

[93] J. A. Taylor. *Convex optimization of power systems*. Cambridge University Press, 2015.

[94] J. A. Taylor and F. S. Hover. Lift-and-project relaxations of AC microgrid distribution system planning. In *Proceedings of the 2011 Grand Challenges on Modeling and Simulation Conference*, pages 187–191. Society for Modeling & Simulation International, 2011.

[95] F. Vallée, Z. De Grève, F. Pilo, and G. Celli. Tutorial 5 : Probabilistic methods in modern electricity distribution systems. 2015, CIRED 2015, Lyon.

[96] A. Venzke, L. Halilbasic, U. Markovic, G. Hug, and S. Chatzivasileiadis. Convex Relaxations of Chance Constrained AC Optimal Power Flow. *arXiv preprint arXiv:1702.08372*, 2017.

[97] Wikipedia. Dependent and independent variables. https://en.wikipedia.org/wiki/Dependent_and_independent_variables, 2017/11/01.

[98] L. A. Wolsey and G. L. Nemhauser. *Integer and Combinatorial Optimization*. John Wiley & Sons, 2014.

[99] L. A. Zadeh. Fuzzy sets as a basis for a theory of possibility. *Fuzzy Sets and Systems*, 100, Supplement 1:9–34, 1999.

[100] M. Zdrallek, C. Oerter, H. Brunner, R. Calone, Y. Chollot, H. Englert, D. Kronman, P. Mallet, C. Mota Pinto, H. Müller, D. Openshaw, J. Partanen, and F. Pilo. CIRED WG Smart Grids - Final Report. 2013.

[101] I. Ziari, G. Ledwich, and A. Ghosh. Optimal integrated planning of MV–LV distribution systems using DPSO. *Electric Power Systems Research*, 81(10):1905–1914, 2011.

[102] A. Zidan, M. F. Shaaban, and E. F. El-Saadany. Long-term multi-objective distribution network planning by DG allocation and feeders' reconfiguration. *Electric Power Systems Research*, 105:95–104, 2013.

[103] R. D. Zimmerman. *Comprehensive distribution power flow: modeling, formulation, solution algorithms and analysis*. PhD thesis, Cornell University, 1995.

[104] R. D. Zimmerman, C. E. Murillo-Sanchez, and R. J. Thomas. MATPOWER: Steady-State Operations, Planning, and Analysis Tools for Power Systems Research and Education. *IEEE Transactions on Power Systems*, 26(1):12–19, 2011.